INFORMATION TO USERS

This manuscript has been reproduced from the microfilm master. UMI films the text directly from the original or copy submitted. Thus, some thesis and dissertation copies are in typewriter face, while others may be from any type of computer printer.

The quality of this reproduction is dependent upon the quality of the copy submitted. Broken or indistinct print, colored or poor quality illustrations and photographs, print bleedthrough, substandard margins, and improper alignment can adversely affect reproduction.

In the unlikely event that the author did not send UMI a complete manuscript and there are missing pages, these will be noted. Also, if unauthorized copyright material had to be removed, a note will indicate the deletion.

Oversize materials (e.g., maps, drawings, charts) are reproduced by sectioning the original, beginning at the upper left-hand corner and continuing from left to right in equal sections with small overlaps.

Photographs included in the original manuscript have been reproduced xerographically in this copy. Higher quality 6" x 9" black and white photographic prints are available for any photographs or illustrations appearing in this copy for an additional charge. Contact UMI directly to order.

ProQuest Information and Learning
300 North Zeeb Road, Ann Arbor, MI 48106-1346 USA
800-521-0600

UMI®

Downloaded from SHAREOK. Persistent Handle URL: https://hdl.handle.net/11244/495

UNIVERSITY OF OKLAHOMA

GRADUATE COLLEGE

Search for Magnetic Monopoles Possibly Produced by $p\bar{p}$ Collisions at the Tevatron Collider

A Dissertation

SUBMITTED TO THE GRADUATE FACULTY

In partial fulfillment of the requirements
for the degree of

Doctor of Philosophy

by

WEI LUO
Norman, Oklahoma
2002

UMI Number: 3056946



UMI Microform 3056946

Copyright 2002 by ProQuest Information and Learning Company.
All rights reserved. This microform edition is protected against unauthorized copying under Title 17, United States Code.

ProQuest Information and Learning Company
300 North Zeeb Road
P.O. Box 1346
Ann Arbor, MI 48106-1346

© Copyright by WEI LUO 2002
All Rights Reserved

Search for Magnetic Monopoles Possibly Produced by $p\bar{p}$ Collisions at the Tevatron Collider

A Dissertation APPROVED FOR THE
DEPARTMENT OF PHYSICS AND ASTRONOMY

BY

George Kalbfleisch 8/5/02
George Kalbfleisch

Kimball Milton
Kimball Milton

Phillip Gutierrez
Phillip Gutierrez

Gregory Parker
Gregory Parker

James Hawthorne
James Hawthorne

To Xiu, Haoyang and Alan

Acknowledgments

The magnetic monopole search conducted at the University of Oklahoma includes a lot of hands-on work, complicated programming and data analysis, and deep theoretical arguments, as well as a group of people. First and foremost, I would like to thank my advisor Professor George Kalbfleisch for letting me be involved in this project. His intuitive insight into physics, expertise in experimentation, and guidance were always helpful and greatly appreciated. I feel privileged to have him as my advisor and to be able to learn from his example.

Secondly, I thank Professor Kimball Milton for his help in the theoretical aspect of this research. From his instruction, I have realized that magnetic monopoles, if they exist, would have significant effects on the current quantum field theory. I also thank him for always being willing to help whenever I had questions.

Professor Phillip Gutierrez should be given special thanks, not only because he serves on my committee, but because I took courses with him almost every semester. I learned particle physics from him and, importantly, also learned from him how to make a presentation in English.

My gratefulness extends to Professor Gregory Parker for giving me advice and help whenever I needed them.

I thank Professor James Hawthorne for letting me sit in his Philosophy of Science class where I learned how philosophers look at science.

I am very grateful to Professor Mike Strauss, a member of the monopole search, for his advice on both my teaching and research. I learned teaching from him, not just when I worked as a teaching assistant for him, but whenever I asked him questions. His

comments on my presentations were very helpful. Two other members in the monopole search group should be also thanked. Dr. Eric Smith helped me in using computers and programming. Dr. Leonard Gamberg helped me learn about the theory of magnetic monopoles.

I also thank Professor Pat Skubic and Professor Eric Abraham for their supervising me as a teaching assistant. I took a Mathematical Methods of Physics course with Professor Ronald Kantowski. Besides helping me whenever I asked him, his teaching was humorous and interesting. Professor Chung Kao is thanked for his help.

Thanks also go to Joel Young and Adrienne Wade for their help with apparatus design, making, and set-up, as well as trouble shooting. Two graduate students, Tao Zheng and Isaac Hall, and two undergraduate students, Sho Miyashita and Wade Bullington, participated in operation of experiment and data analysis. Undergraduate students, Michael Nguyen, David Stewart, Benjamin Schlecht, Doney and Roney Abraham were involved in data analysis.

I thank the U.S. Department of Energy for funding this research, the Departments of Physics and Astronomy and of Aerospace and Mechanical Engineering, and the Physics Machine Shop for support, and Fermilab and the DØ and CDF collaborations for the samples. S. Murphy, M. Longo of the University of Michigan, T. Nicols, M. Kuchnir, and H. Haggerty of Fermilab, should be thanked for their help.

I thank Dr. Horst Severini and Dr. Andy Feldt for helping me with solving computer problems.

I also want to take this chance to thank my American friends: John and Judy Korhonen for their hospitality and for giving me a lot of help when I first came to the United States; Nella White, Bill and Pam Kennedy for their caring about my study, my family, and correcting my English. From them, I have learned about American culture,

especially, American human touch.

The greatest thanks should be given to my family: my wife Xiu who has sacrificed her own career in behalf of my study; and my two wonderful sons, Haoyang and Alan who give me a lot of encouragement and joy. This family's support and love are important reasons for me to complete my study.

Contents

Chapter 1	Introduction	1
Chapter 2	The Theories of Magnetic Monopoles	6
	2.1 Monopoles in Maxwell's equations	6
	2.2 Dirac Monopoles	8
	2.3 Monopoles in Gauge Field Theories	15
Chapter 3	The Production of Magnetic Monopoles	23
	3.1 The Problem with the Theory of Magnetic Monopoles	23
	3.2 Quark Parton Model	27
	3.3 Quark Parton Distributions	31
	3.4 Drell-Yan Process for $m\bar{m}$ Production	34
Chapter 4	Monopole Stopping and Trapping in the DØ and CDF Detectors	40
	4.1 Energy Loss of Magnetic Monopoles	40
	4.2 The DØ Detector	44
	4.3 Energy Loss in the DØ Detector	45
	4.4 The CDF Detector	48
	4.5 Energy Loss in CDF Detector	51
	4.6 Binding Energy in Monopole Samples	53
Chapter 5	The Apparatus for Detection of Magnetic Monopoles	59
	5.1 The Outline of Monopole Detector	59
	5.2 Monopole Signature	62
	5.3 Fundamentals of SQUIDs	66
	5.4 Cryogenics	72
	5.5 Noise	79
	5.6 Stabilizing, Reducing, and Homogenizing the Ambient Magnetic Field	84
	5.7 Calibration of the Detector and Monopole Signal	87
Chapter 6	Analysis and Results	95
	6.1 The Strategy of Analysis	95
	6.2 Data Acquisition and Analysis	96
	6.3 DØ Samples and Results	105

6.4 CDF Samples and Results 113
6.5 Discussions and Conclusions 128
Bibliography 135
Appendix 141

Abstract

Magnetic monopoles can be used to explain the quantization of electric charge, and are predicted by gauge field theory. If monopoles exist, they could have been produced by the proton-antiproton collisions at the Tevatron collider—the highest energy accelerator existing in the world, and trapped in the CDF and DØ detectors. We took Al, Be, and Pb samples from the Tevatron and used the induction technique with SQUIDs (Superconducting Quantum Interference Devices) to detect monopoles in the samples. We did not find monopoles, but we have set new limits for the monopole mass and the relavant cross section based on a Drell-Yan model and Monte Carlo calculation.

Chapter 1

Introduction

In 1600, W. Gilbert first realized [1] that a magnet always has two poles (north and south) existing together. It was not known till the 19th century that electricity and magnetism were related. In 1820, Oersted [2] discovered that an electric current produced magnetism. This led to Ampere's theory [3] that magnetism of materials or a magnetic field originates from small electric current loops. In other words, magnetism is different from electricity in existence since it is not independent. Magnetism is just a "by-product", being generated by electric currents. It is entirely a relativistic effect. As a result, fundamental magnetic charges or monopoles did not exist. This was described by the asymmetry between electricity and magnetism exposed in Maxwell's equations. [4] However, the asymmetry of Maxwell's equations has stimulated physicists to symmetrize them by introducing magnetic monopoles. In 1896, Poincaré [5] calculated the motion of a charged particle in the presence of a single magnetic monopole. (This was result of mysterious observation of the motion of cathode rays in the presence of a long magnetic needle.) A few years later, Thomson [6] showed that a static system consisting of a magnetic monopole and an electric charge possessed an angular momentum.

The new era of magnetic monopole theories started in 1931, when Dirac [7] incorporated the magnetic monopole into the framework of quantum mechanics. He introduced magnetic monopoles which are associated with singularities (strings) in the electromagnetic potential, and showed that the existence of magnetic charge implies that electric charge be quantized. According to Dirac, the electric charge e and the magnetic charge g satisfy the quantized relation in rationalized unit system

$$\frac{eg}{4\pi} = \frac{n}{2}\hbar c, n = \pm 1, \pm 2, ...(\hbar c = 1 \text{in natural unit system}) \qquad (1.1)$$

In 1948, Dirac [8] generalized this idea and confirmed the consistency of quantum theory with magnetic monopoles. The monopole introduced by Dirac is called "Dirac monopole".

In the early 1970's, it was realized that the electric charge is naturally quantized in those unified theories of the fundamental interactions in which electromagnetism is embedded in a spontaneously broken non-Abelian gauge theory. In 1974, 't Hooft and Polyakov [9] showed that such unified theories imply the existence of magnetic monopoles and their properties, e.g., mass, are calculable. The monopole mass in these theories is estimated to be about 10^4GeV (by electroweak theory) and 10^{16}GeV (by GUT—grand unified theory).

Although the theories above predict the existence of the magnetic monopole, no complete quantum field theory of magnetically charged particles have been formulated yet. One of the problems is that we are not allowed to use perturbation theory because the string singularity in the theory is unobservable. In the absence of a perturbative quantum theory of monopoles, we are forced to use model calculations. We will discuss this later.

The fact that no complete theory of magnetic charge has been formulated does not prevent people from seeking magnetic monopoles since the most important thing regarding magnetic monopoles is to ascertain if they exist. There are several types of monopole searches. The first is the accelerator search—a search for monopoles produced by high energy collisions. This is suitable for a low mass monopole search that is performed at every new accelerator that opens up a new energy region. In 1959, Bradner *et al.*[10] used p beam at 6 GeV to strike an aluminum target, trying to produce

monopoles; and he set the cross section limit for monopoles with charge $n = 1$ ($1g$) as $\sigma \leq 2.0 \times 10^{-35}$ cm^2 (20 pb) and the mass up to $m \leq 1$ GeV. In 1987, Price *et al.*[11] used $p\bar{p}$ collision in the Tevatron (1800 GeV) and set the cross section limit as $\sigma \leq 3.0 \times 10^{-32}$ cm^2 (30 nb) with mass up to $m \leq 800$ GeV and magnetic charge $n \geq 1$. Later in 1990, they [12] improved the cross section limit to $\sigma \leq 1.2 \times 10^{-33}$ cm^2. Also, Bertani *et al.* [13] set the cross section limit as $\sigma \leq 2.0 \times 10^{-34}$ cm^2 (200 pb) with the mass up to 850 GeV. This was the best result for a direct search (in which monopoles are explicitly produced). In 1993, Pinfold *et al.* [14] performed a monopole search using e^+e^- collision at LEP and set the cross section limit as $\sigma \leq 3.0 \times 10^{-37}$ cm^2 (0.3 pb) with mass up to 45 GeV and magnetic charge $n = 1$, and the cross section limit as $\sigma \leq 3.0 \times 10^{-37}$ cm^2 (0.3 pb) with mass up to 41.6 GeV and magnetic charge $n = 2$. The most recent indirect search (monopoles as virtual intermediate states) was performed by the DØ collaboration [15] in 1998. They set the mass limits for monopoles as $m \geq 610$ GeV, with spin 0 and $n = 1$; and $m \geq 870$ GeV, with spin 1/2 and $n = 1$; and $m \geq 1580$ GeV, with spin 1 and $n = 1$. However, these limits are strongly model dependent and violate unitarity. [16] So far no events have been found in this way.

The second type of search is in cosmic rays—a search for monopoles existing in the Universe. This is suitable for a search for GUT monopoles of huge mass. In 1951, Malkus [17] used a solenoidal accelerator and emulsion technique to detect monopoles in the cosmic rays. This was the first monopole search and he set the monopole flux limit as $f \leq 2.0 \times 10^{-11}$cm^{-2}sr^{-1}s^{-1}. In 1975, Price *et al.*[18] used plastics technique and claimed one event for monopole with $f = 1.0 \times 10^{-1}$ cm^{-2}sr^{-1}s^{-1} , $m \geq 200$ GeV and $n > 2$, which interpretation was shot down by Alvarez [19]. Later in 1982, Cabrera [20] used the induction technique developed by Alvarez *et al* [21] and claimed one event for monopole with $f \leq 4.0 \times 10^{-11}$ cm^{-2}sr^{-1}s^{-1} and $n = 1$. In 1986, Caplin *et al.* [22] also claimed one event for monopole with $n = 1$. However, more events were never seen and these cases are no longer considered as monopole events. In 1991, Orito *et el.* [23]

reduced the flux limit to $f \leq 3.2 \times 10^{-16}$ cm^{-2}sr^{-1}s^{-1} and set the mass limit as $m \geq 10^{10}$ GeV for $n = 1$, for monopole velocities β ($= V/c$) > 0.05. The newest cosmic ray search was performed by MACRO collaboration in 1997 [24] . They set the flux limit as $f < 0.61 \times 10^{-15}$ cm^{-2}sr^{-1}s^{-1} for $n = 1$, and $1.0 \times 10^{-4} < \beta < 1.0 \times 10^{-3}$.

The third way is a matter search. These experiments measure monopole signals in materials such as moon rock, sea water, and meteorites. In 1963, Goto *et al.* [25] tried to extract monopoles from a magnetite outcrop and a stony-iron meteorite, and set the monopole density as $d < 2.0 \times 10^{-3}$/gram. The most recent search of this type was performed by Jeon and Longo [26] in 1995. They applied the induction technique to measure meteorites and set the monopole density limit as $d < 6.9 \times 10^{-6}$/gram for $n > 1/3$.

Another way to set limits is based on astrophysics. In 1970, Parker [27] set the flux limit as $f < 10^{-16}$ cm^{-2}sr^{-1}s^{-1} with $n = 1$ based on the galactic magnetic field analysis. Later in 1993, Adams *et al.* [28] set the flux limit as $f \leq 10^{-16}$cm^{-2}sr^{-1}s^{-1} and the mass limit as $m \leq 10^{17}$ GeV by considering the evolution of the galactic field. In 1999, Freese and Krasteva [29] gave the newest flux limit as $f < 1.3 \times 10^{-22}$cm^{-2}sr^{-1}s^{-1} by analyzing catalysis of nucleon decay [30] in a faint white dwarf.

The experiment presented here [31] is a search for low mass Dirac-type monopoles produced by $p\bar{p}$ collisions at the Tevatron collider at the Fermi National Accelerator Laboratory for an integrated luminosity which has been extended by a factor of 10,000 over the last search of Bertani [13]. If magnetic monopoles have a mass less than 10^0 TeV, they must have been produced by $p\bar{p}$ collisions observed by the DØ and CDF experiments over last a few years, and they should have been trapped in the materials comprising the detectors. We have searched for monopoles bound in these materials including the Be beam pipes, Al drift chamber supports and Pb pieces of the DØ and CDF detectors. We applied the induction method of Alvarez *et al* [20] by using a

detector similar to the Jeon-Longo apparatus.[25] The monopole samples are passed through two superconducting loops that are connected to two DC-SQUIDs (Superconducting Quantum Interference Devices), and the signals induced by the magnetic charge of any magnetic monopoles in the samples can be measured by the SQUIDs. Based on the experimental data and using the Drell-Yan production model, [32] we set new limits for the monopole mass and the relevant cross section.

Chapter 2

The Theory of Magnetic Monopoles

2.1 Magnetic Monopoles in Maxwell's Equations

We know that Maxwell's equations in vacuum in Gaussian units are given by

$$\nabla \bullet \mathbf{E} = 4\pi\rho_e, \tag{2.1}$$

$$\nabla \times \mathbf{B} = \frac{1}{c}\frac{\partial \mathbf{E}}{\partial t} + \frac{4\pi}{c}\mathbf{J}_e, \tag{2.2}$$

$$\nabla \bullet \mathbf{B} = 0, \tag{2.3}$$

$$-\nabla \times \mathbf{E} = \frac{1}{c}\frac{\partial \mathbf{B}}{\partial t}. \tag{2.4}$$

The electric field **E** and the magnetic field **B** are asymmetric in the equations in the presence of ρ_e and $\mathbf{J}_e$. When we introduce magnetic monopoles, we have a magnetic charge density ρ_m and a magnetic current $\mathbf{J}_m$, which are analogous to electric charges and currents ρ_e and $\mathbf{J}_e$. Then Maxwell's equations can be written as:

$$\nabla \bullet \mathbf{E} = 4\pi\rho_e, \tag{2.5}$$

$$\nabla \times \mathbf{B} = \frac{1}{c}\frac{\partial \mathbf{E}}{\partial t} + \frac{4\pi}{c}\mathbf{J}_e, \tag{2.6}$$

$$\nabla \cdot \mathbf{B} = 4\pi\rho_m, \tag{2.7}$$

$$-\nabla \times \mathbf{E} = \frac{1}{c}\frac{\partial \mathbf{B}}{\partial t} + \frac{4\pi}{c}\mathbf{J}_m. \tag{2.8}$$

It can be easily shown from (2.7) and (2.8) that

$$\begin{aligned} 0 = -\nabla \cdot \nabla \times \mathbf{E} &= \frac{1}{c}\frac{\partial \nabla \cdot \mathbf{B}}{\partial t} + \frac{4\pi}{c}\nabla \cdot \mathbf{J}_m \\ &= \frac{1}{c}\frac{\partial (4\pi\rho_m)}{\partial t} + \frac{4\pi}{c}\nabla \cdot \mathbf{J}_m \\ &= \frac{4\pi}{c}\left(\frac{\partial (\rho_m)}{\partial t} + \nabla \cdot \mathbf{J}_m\right) \end{aligned}$$

or

$$\frac{\partial (\rho_m)}{\partial t} + \nabla \cdot \mathbf{J}_m = 0. \tag{2.9}$$

Similarly, we can obtain independently from (2.5) and (2.6)

$$\frac{\partial (\rho_e)}{\partial t} + \nabla \cdot \mathbf{J}_e = 0. \tag{2.10}$$

The equations (5.9) and (5.10) show that both electric charge and magnetic charge are independently conserved.

Also, the modified Maxwell's equations are symmetric under the duality transformations

$$\mathbf{E} \rightarrow \mathbf{B},\ \mathbf{B} \rightarrow -\mathbf{E},\ \mathbf{J}_e \rightarrow \mathbf{J}_m,\ \mathbf{J}_m \rightarrow -\mathbf{J}_e, \rho_e \rightarrow \rho_m, \rho_m \rightarrow -\rho_e. \tag{2.11}$$

Symmetrizing Maxwell's equations was one purpose of introducing magnetic monopoles

although the terms ρ_m and $\mathbf{J}_m$ can be used in practical calculations without asserting the existence of magnetic charge. [33] In 1931, Dirac thought that the quantization of the electric charge was a much stronger reason to consider magnetic monopoles.[7]

2.2 Dirac Monopole

Non-integrable Phase and Electromagnetic Field

We follow Dirac's original paper. [7] Consider a particle whose motion is represented by wave function $\Psi(\mathbf{r},t)$. We can express it in the form

$$\Psi(\mathbf{r},t) = \rho(\mathbf{r},t)e^{i\gamma(\mathbf{r},t)}. \tag{2.12}$$

In quantum mechanics, only the modulus of wave function is completely determined while the phase is not uniquely determined. We assume that the phase change between two different points is path dependent so different paths give different values, and the phase change around a closed curve need not vanish. This is the non-integrability of phase.

Now we express Ψ as a product

$$\Psi = \psi e^{i\beta}, \tag{2.13}$$

where ψ is a wave function similar to Ψ but determined in both amplitude and phase, and β is the uncertain phase factor. The uncertainty of β requires that β should not be a function of r,t with a definite value at each point, but β must have definite derivatives

$$\boldsymbol{\kappa} = \nabla\beta \tag{2.14}$$

at each point. They do not satisfy the conditions of integrability $\partial\kappa_x/\partial y = \partial\kappa_y/\partial x$, etc.,

which means that $\partial\kappa_x/\partial y$ and $\partial\kappa_y/\partial x$ are not continuous everywhere.

The change in phase around a closed curve C will be, by Stokes' theorem,

$$\oint_C \boldsymbol{\kappa} \cdot d\mathbf{l} = \iint_S \nabla \times \boldsymbol{\kappa} \cdot d\mathbf{S}, \tag{2.15}$$

where S is a surface bounded by C. Now we take the derivative of Ψ, and we obtain

$$-i\hbar\frac{\partial}{\partial x}\Psi = e^{i\beta}\left(-i\hbar\frac{\partial}{\partial x} + \hbar\kappa_x\right)\psi. \tag{2.16}$$

It indicates that if Ψ satisfies any equation, involving momentum and energy operators $\mathbf{p}$ and E, ψ will satisfy the corresponding equation in which $\mathbf{p}$ and E have been replaced by $p + \hbar\kappa_x$, and $E - \hbar\kappa_0$. Thus $\boldsymbol{\kappa}$ is associated with an electromagnetic field whose potentials are

$$\mathbf{A} = \frac{\hbar c}{e}\boldsymbol{\kappa}, \phi = -\frac{\hbar c}{e}\kappa_0, \tag{2.17}$$

and the electric and magnetic fields $\mathbf{E}$ and $\mathbf{B}$ are determined by

$$\nabla \times \boldsymbol{\kappa} = \frac{e}{\hbar c}\mathbf{B}, \nabla\kappa_0 - \frac{\partial \boldsymbol{\kappa}}{\partial t} = \frac{e}{\hbar}\mathbf{E}. \tag{2.18}$$

Thus, for a spacelike surface S bounded by C,

$$\iint_S \nabla \times \boldsymbol{\kappa} \cdot d\mathbf{S} = \frac{e}{\hbar c}\iint_S \mathbf{B} \cdot d\mathbf{S} = \frac{e}{\hbar c}\Phi, \tag{2.19}$$

where Φ is the flux going through the curve C. This equation shows that a change in

phase around a closed curve is equivalent to a magnetic flux going through the curve.

Quantization Condition

Dirac considered an exceptional case where the wave function vanishes. As the wave function is complex, the vanishing condition is determined by two combined equations. One of the solutions to the equations gives a line in the 3-dimensional space, along which the wave function vanishes. This line was called a *nodal line* or *string* by Dirac. If the wave function vanishes, its phase has no meaning. So the string is just a singularity of the phase. As a result, the change in phase around an infinitely small curve which encircles a string must be $2\pi n$. Here n is a positive or negative integer, and it is a characteristic of magnetic charge. Then, the change in phase around a finite curve is the sum of $2\pi n$ and the flux going through the surface bounded by the curve:

$$\Delta\beta = 2\pi n + \frac{e}{\hbar c}\iint \mathbf{B} \cdot d\mathbf{S}. \tag{2.20}$$

Now we consider a closed surface, so there is no boundary and $\Delta\beta$ must be zero. Moreover, if the string has an end inside the closed surface, $2\pi n$ will not cancel on the surface. In this case,

$$2\pi n + \frac{e}{\hbar c}\oint \mathbf{B} \cdot d\mathbf{S} = 0, \tag{2.21}$$

or

$$\oint \mathbf{B} \cdot d\mathbf{S} = 2\pi n \frac{\hbar c}{e}. \tag{2.22}$$

Therefore, the total flux crossing a closed surface surrounding the end point is $2\pi n \frac{\hbar c}{e}$. Since the end point of the string is the source of this flux, it can be thought as a magnetic

monopole with magnetic charge g. Therefore,

$$4\pi g = 2\pi n \frac{\hbar c}{e}, \tag{2.23}$$

i.e.,

$$ge = \frac{n}{2}\hbar c \text{ in Gaussian units,} \tag{2.24}$$

or

$$\frac{ge}{4\pi} = \frac{n}{2} \text{ in rationalized units.} \tag{2.25}$$

This is the Dirac quantization condition.

The Dirac quantization condition has shown that both electric and magnetic charge should be quantized. The value of the magnetic charge unit can be determined by taking $n = 1$ and having e be the electric charge unit:

$$g = \frac{e}{2\alpha} = 68.5e, \tag{2.26}$$

which is very big compared to e.

The String Problem

With the monopole being introduced, the string singularity of the magnetic vector potential is also introduced. Without a monopole, the magnetic field **B** is determined by the potential **A**

$$\mathbf{B} = \nabla \times \mathbf{A}, \tag{2.27}$$

and satisfies

$$\nabla \cdot \mathbf{B} = \nabla \cdot \nabla \times \mathbf{A} = 0. \tag{2.28}$$

In the presence of magnetic charge, it seems that no such potential exists because

$$\nabla \cdot \nabla \times \mathbf{A} = \nabla \cdot \mathbf{B} = 4\pi\rho_m \neq 0. \tag{2.29}$$

However, we can keep the magnetic potential if we tolerate a string singularity of the potential. For a point charged monopole at the origin, the magnetic charge density can be described by a delta function.

$$\nabla \cdot \mathbf{B} = 4\pi g\delta(\mathbf{r}). \tag{2.30}$$

Then, we define a new magnetic field

$$\mathbf{B}_s = \mathbf{B} + \mathbf{h}, \tag{2.31}$$

where $\mathbf{h}$ is zero except on string, and can be expressed in terms of a string singularity along a path L from the origin (monopole) to infinity:

$$\mathbf{h}(\mathbf{r}) = -4\pi g \int_L \delta(\mathbf{r} - \mathbf{r}')d\mathbf{r}', \tag{2.32}$$

which leads to

$$\nabla \cdot \mathbf{h}(\mathbf{r}) = -4\pi g\delta(\mathbf{r}). \tag{2.33}$$

Therefore, we can define the potential $\mathbf{A}$ by

$$\mathbf{B}_s = \nabla \times \mathbf{A}(\mathbf{r}), \tag{2.34}$$

which satisfies

$$\nabla \bullet (\nabla \times \mathbf{A}) = \nabla \bullet \mathbf{B}_s = 0 \tag{2.35}$$

everywhere.

$\mathbf{B}_s$ can be realized by the magnetic field from an infinitely long and thin solenoid (string) placed along the negative z-axis with its positive pole (with strength g) at the origin:

$$\mathbf{B}_s = \frac{g}{r^2}\hat{\mathbf{r}} + 4\pi g\theta(-z)\delta(x)\delta(y)\hat{\mathbf{z}}, \tag{2.36}$$

and the magnetic field of a monopole is given by

$$\mathbf{B} = \frac{g}{r^2}\hat{\mathbf{r}} = \nabla \times \mathbf{A} - 4\pi g\theta(-z)\delta(x)\delta(y)\hat{\mathbf{z}}. \tag{2.37}$$

The potential $\mathbf{A}(\mathbf{r})$ of the solenoid can be written, with the conventional definitions of polar and azimuthal angles, as

$$\mathbf{A}(\mathbf{r}) = \frac{g}{r}\left(\frac{1-\cos\theta}{\sin\theta}\right)\hat{\boldsymbol{\Phi}}, \tag{2.38}$$

which is singular on the negative z-axis.

It should be mentioned that the Dirac string is unobservable and therefore it is unphysical. This is because the path L is completely arbitrary; reorienting L is a kind of gauge transformation. This nonobservability can be shown by letting a particle of charge e move along a closed loop trajectory around a string containing magnetic flux $\Phi = 4\pi g$.

Then there is a change in phase of the wave function of the particle, which will be by Stokes's theorem

$$\Delta\alpha = e\oint \mathbf{A}\cdot d\mathbf{l} = e\int \mathbf{B}\cdot d\mathbf{S} = 4\pi eg. \tag{2.39}$$

This phase change should be observed by the Aharonov-Bohm effect [34] if eg is not equal to $n/2$, and therefore the string could be observed. However, the Dirac quantization condition just makes eg be $n/2$, and thus makes it unobservable. If the Dirac string is unobservable, the string at different positions must give physically equivalent results. As a matter of fact, a string can be moved from one position to another by a gauge transformation. Therefore, the Dirac string is just a gauge artifact and unphysical.[35][36][37][38]

The fact that the string is unphysical requires that the physics should be independent of the string. Thus, a realistic quantum theory of monopoles should give string independent results. Nevertheless, quantum theories are built using a Hamiltonian or Lagrangian which contains a magnetic potential. In this case, the string singularity will be included in the theory of magnetic monopoles and may lead to string-dependent physical results such as string-dependent cross section when perturbative calculations are employed. It can be shown, however, that a quantum theory of magnetic charge is string independent using nonperturbative methods. It should be mentioned here that Gamberg and Milton, following on earlier works of Schwinger [39][40][41] and Zwanziger [42], have formulated a quantum field theory of magnetic charge and given a string independent cross section using the eikonal approximation.[37]

Dyons

It is possible that a magnetic monopole carries an electric charge in addition to its magnetic charge. Schwinger called such an object a dyon. Suppose that there exist two

dyons with magnetic and electric charges (g_1, e_1) and (g_2, e_2), Dirac's quantization condition will take the form, in rationalized units, [39][40][41]

$$\frac{e_1 g_2 - e_2 g_1}{4\pi} = \begin{pmatrix} n/2, & \text{unsymmetric} \\ n, & \text{symmetric} \end{pmatrix}, \tag{2.40}$$

where n is an integer. "Symmetric" and "unsymmetric" refer to the presence and absence of dual symmetry in the solutions of Maxwell's equations, i.e., whether the string is infinite or semi-infinite. For a pair of particles consisting of a pure electron and a monopole, i.e., $e_1 = e$, $e_2 = 0$, $g_1 = 0$, $g_2 = g$, we get

$$\frac{e_1 g_2 - e_2 g_1}{4\pi} = \frac{eg}{4\pi} = \begin{pmatrix} n/2, & \text{unsymmetric} \\ n, & \text{symmetric} \end{pmatrix}, \tag{2.41}$$

which gives the Dirac quantization condition for the semi-infinite string (unsymmetric). But for the symmetric case, the value of magnetic charge number, n, will be doubled in terms of the Dirac quantization condition. So the minimum value of n for the smallest magnetic charge or the magnetic charge unit corresponding to the charge of an electron, e, will be 1, or, 2. However, n could be 3, or, 6, if we consider the charge of a quark, $\frac{1}{3}e$, as the electric unit charge. Therefore, we will study the cases for $n = 1, 2, 3, 6$.

2.3 Magnetic Monopoles in Gauge Field Theory

Magnetic monopoles can be generated from a classical topologically stable solution of a non-Abelian gauge field theory by gauge symmetry breaking. We will follow Cheng and Li's approach.[43]

The 't Hooft-Polyakov Monopole [9]

This is the simplest model for magnetic monopoles in gauge theories. We start with a scalar field theory which possesses soliton solutions. Write the Lagrangian for an $SO(3)$ field, ϕ_i, $i = 1,2,3$,

$$L = \frac{1}{2}(\partial_\mu \phi_i)^2 - V(\phi), \tag{2.42}$$

with

$$V(|\phi|) \geq 0. \tag{2.43}$$

The energy for a given configuration for the scalar field is

$$E = \int d^3r \Big[\frac{1}{2}(\partial_0 \phi_i)^2 + \frac{1}{2}(\nabla \phi_i)^2 + V(\phi) \Big]. \tag{2.44}$$

Now we minimize $V(\phi)$ with ϕ being determined by

$$M_0 = \{\phi = \eta; \eta^2 = a^2\}, \tag{2.45}$$

where a is a constant. All points on M_0 are equivalent to each other by $SO(3)$ transformations. If there is a finite energy solution, we must have

$$V(\eta) = 0, \tag{2.46}$$

and

$$\phi_i^\infty(\hat{\mathbf{r}}) = \lim_{R\to\infty} \phi(R\hat{\mathbf{r}}) \in M_0, \tag{2.47}$$

where $\hat{\mathbf{r}}$ is a radial unit vector. Topologically, the spatial infinities form a two-sphere S^2

$$S^2 = \{\hat{r} : \hat{r} = 1\}, \tag{2.48}$$

which has the same topology as M_0. Thus, we can map S^2 to M_0 to get a non-trivial topology

$$\phi_i^\infty = \eta_i = a\hat{r}_i \tag{2.49}$$

If ϕ_i^∞ were not constant on the sphere, $\nabla\phi$ would go like r^{-1} as $r \to \infty$. So the energy E would diverge.

Now we introduce the gauge field, and write the Lagrangian with $SO(3)$ or $SU(2)$ symmetry as

$$L = -\frac{1}{4}F^a_{\mu\nu}F^{\mu\nu}_a + \frac{1}{2}(D^\mu\phi)\bullet(D_\mu\phi) - V(\phi), \tag{2.50}$$

where

$$F^a_{\mu\nu} = \partial_\mu A^a_\nu - \partial_\nu A^a_\mu - e\varepsilon^{abc}A^b_\mu A^c_\nu, \tag{2.51}$$

$$(D_\mu\phi)^a = \partial_\mu\phi^a - e\varepsilon^{abc}A^b_\mu\phi^c, \tag{2.52}$$

$$V(\phi) = \frac{\lambda}{4}(\phi\bullet\phi - a^2)^2. \tag{2.53}$$

ϕ is a triplet *Higgs* scalar and λ a positive parameter. $\nabla\phi$ has been replaced by

$$D_i\phi = \nabla\phi + ie(\mathbf{A}_i\bullet\mathbf{T})\phi, \tag{2.54}$$

where T is the $SO(3)$ generator and

$$T^a_{bc} = i\varepsilon^{abc}. \tag{2.55}$$

We arbitrarily choose

$$\phi = (0,0,a) \tag{2.56}$$

to be the ground state configuration, which breaks the symmetry

$$SU(2) \sim SO(3) \rightarrow SO(2) = U(1). \tag{2.57}$$

Corresponding to $U(1)$ symmetry, the electromagnetic field is given by

$$F_3^{0i} = E^i, \quad F_3^{ij} = \varepsilon^{ijk}B^k. \tag{2.58}$$

For a static state of the system without electric field, i.e.,

$$F_3^{0i} = 0, \tag{2.59}$$

we have [9]

$$H = -L, \tag{2.60}$$

and the energy

$$E = \int Hd^3r = \int[\frac{1}{4}F^a_{ij}F^{ij}_a - \frac{1}{2}(D^i\phi)\bullet(D_i\phi) + V(\phi)]d^3r. \tag{2.61}$$

In order to let the energy integral be convergent, we make the following *ansatz*

$$\phi_b = \frac{r^b}{er^2} H(aer), \tag{2.62}$$

$$A_b^i = -\varepsilon_{bij} \frac{r^j}{er^2} [1 - K(aer)], \tag{2.63}$$

$$A_b^0 = 0. \tag{2.64}$$

Then, we obtain

$$D_i \phi_j(r) = H(aer)K(aer) \frac{1}{er^4} (\delta_{ij} r^2 - r_i r_j) + \left[aer \frac{\partial H(aer)}{\partial (aer)} - H(aer) \right] \frac{r_i r_j}{er^4}. \tag{2.65}$$

In the limit $\lambda \longrightarrow 0$, $H(aer)$ and $K(aer)$ have the forms [44]

$$K(aer) = \frac{aer}{\sinh(aer)}, \tag{2.66}$$

$$H(aer) = \frac{aer}{\tanh(aer)} - 1. \tag{2.67}$$

At large distance, we have

$$H(\xi) \rightarrow \xi and K(\xi) \rightarrow 0 \text{ exponentially as } \xi \rightarrow \infty, \tag{2.68}$$

thus we obtain

$$D_i \phi_j(r) \rightarrow \frac{1}{r^2}, \tag{2.69}$$

and

$$F_a^{ij} \sim \frac{1}{er^4}\varepsilon^{ijk}r_a r_k \sim \frac{1}{aer^3}\varepsilon^{ijk}r_k\phi_a. \tag{2.70}$$

Therefore, the energy is finite, and we have the magnetic field at long distance

$$\mathbf{B} \sim -\frac{1}{e}\frac{\mathbf{r}}{r^3}, \tag{2.71}$$

which corresponds to a magnetic monopole with the magnetic charge

$$g = -4\pi/e. \tag{2.72}$$

But it is only true for $\lambda \longrightarrow 0$. The constant e is the electromagnetic coupling constant that is related to the electric charge operator Q by

$$Q = eT_3, \tag{2.73}$$

where T_3 is the third component of the weak isospin operators that are the $SO(3)$ generators. For $T_3 = \frac{1}{2}$, we obtain the unit electric charge $q_0 = \frac{1}{2}e$, and

$$\frac{q_0 g}{4\pi} = -\frac{1}{2}, \tag{2.74}$$

which is the Dirac quantization condition.

Now the lowest energy of the system for a static configuration is given

$$E = \frac{4\pi a}{e}\int_0^\infty \frac{d\xi}{\xi^2}\xi^2\left[\left(\frac{dK}{d\xi}\right)^2 + \frac{1}{2}\left(\xi\frac{dH}{d\xi} - H\right)^2 + \frac{1}{2}(K^2-1)K^2H^2 + \frac{\lambda}{4e^2}(H^2-\xi^2)^2\right]$$
$$= \frac{4\pi a}{e} f\left(\frac{\lambda}{e^2}\right). \tag{2.75}$$

The lowest energy is interpreted as the mass of the monopole. So the monopole mass is given by

$$M = \frac{4\pi a}{e} f\left(\frac{\lambda}{e^2}\right), \tag{2.76}$$

where $f\left(\frac{\lambda}{e^2}\right)$ is the value of the integral and of order of unity. Thus the scale of monopole mass is given by

$$M = M_X/\alpha, \tag{2.77}$$

where $\alpha = e^2/4\pi$, the fine structure constant, and $M_X = ea$, the mass of the vector boson after symmetry breaking, which may be taken as the symmetry breaking scale.

The magnetic monopole based on the finite energy solution is called the 't Hooft-Polyakov monopole. From the above we can see that both a magnetic monopole and charge quantization have resulted from spontaneous symmetry breaking of a non-Abelian simple group to the electromagnetic group $U(1)$. Compared with the Dirac monopole, the 't Hooft-Polyakov monopole has following features:

a. it behaves the same way as the Dirac monopole at long distance;

b. it has a finite core size that is determined by the gauge bosons or scalar particles;

c. its classical mass is of order of the spontaneous symmetry breaking scale, i.e., the

vacuum expectation value of the scalar field.

Monopoles in Grand Unified Theories

The $SU(2) \rightarrow U(1)$ 't Hooft-Polyakov monopole solution can be generalized to stable monopole solutions for any gauge theories in which a simple group G is broken down to a smaller group $H = h \times U(1)$. The grand unified theories usually have a large simple group like $SU(5)$ or $SO(10)$, which would break down to some small groups such as $SU(3)_c \times U(1)_{em}$. Thus we have the 't Hooft-Polyakov monopole for the grand unified theories. The monopole mass is also determined by the vacuum expectation value in such a way that it is of order of M_X/e^2. In the $SU(5)$ model, $M_X \geq 10^{14}$ GeV. Therefore, the GUT monopole masses are of order of 10^{16} GeV, which is out of reach for their production by existing or any conceivable accelerators. However, the GUT monopoles can be primordial and produced in the early Universe and should still be around as cosmic relics. Thus, they will behave as a flux in the cosmic radiation reaching the earth, and they could be detected.

We can also obtain light monopoles if we consider electroweak symmetry breaking. The monopole mass at this scale is $M_W/\alpha \sim 10$ TeV.[45][46] (But this is a controversial topic. See [47][48]) This type of monopole, if it exists, could be seen at future accelerators.

Chapter 3

The Production of Magnetic Monopoles

3.1 The Problem with the Theory of Magnetic Monopole

We are looking for the monopoles produced by proton-antiproton collisions so we need to know the cross section of production and the relationship between the cross section and the monopole mass. Unfortunately, we do not have a practical quantum field theory of magnetic monopoles, which we can use to calculate the cross section. There is a serious problem for constructing a quantum field theory of monopoles, as has been pointed out by Schwinger [40][49]. The problem is that we cannot use perturbative methods to calculate cross section as we do for other particles.

To see the problem, we follow Schwinger's approach and start with the vacuum amplitude for a quantum electrodynamic system with magnetic charge included:

$$< 0_+|0_- >^{J,J^*} = \exp[iW(J,J^*)], \tag{3.1}$$

with

$$W(J,J^*) = \frac{1}{2}\int(dx)[J^\mu(x)A_\mu(x) +^* J^\mu(x)B_\mu(x)], \tag{3.2}$$

where $J^\mu(x)$ and ${}^*J^\mu(x)$ are electric and magnetic sources which for classical point particles can be represented by

$$J^\mu(x) = \sum_e e\int dx_e^\mu \delta(x - x_e), \tag{3.3}$$

$$^*J^\mu(x) = \sum_g g \int dx_g^\mu \delta(x - x_g), \tag{3.4}$$

where x_e and x_g are the coordinates of charge-bearing points. $A_\mu(x)$ and $B_\mu(x)$ are electromagnetic potentials which are related to the fields $F_{\mu\nu}(x)$ and $^*F_{\mu\nu}(x)$, and the string function $f^\mu(x - x')$ by

$$A_\mu(x) = -\int (dx') f^\nu(x - x') F_{\mu\nu}(x') \tag{3.5}$$

$$B_\mu(x) = \int (dx') f^\nu(x - x') {}^*F_{\mu\nu}(x'), \tag{3.6}$$

and

$$^*F_{\mu\nu} = \frac{1}{2} \epsilon_{\mu\nu\sigma\tau} F^{\sigma\tau}. \tag{3.7}$$

If we take a variation in the path of the electric charges, we obtain

$$\begin{aligned} \delta W = \sum_e e\delta \int dx_e^\mu A_\mu(x_e) = \sum_e e \int \frac{1}{2} d\sigma_e^{\mu\nu} (\partial_\mu A_\nu - \partial_\nu A_\mu)(x_e) = \\ \sum_e e \int \frac{1}{2} d\sigma_e^{\mu\nu} F_{\mu\nu}(x_e) - \sum_e eg \int d\sigma^\mu f_\mu(x_e - x_g), \end{aligned} \tag{3.8}$$

where the two-dimensional surfaces are bounded by the initial and varied paths, and we have used

$$F_{\mu\nu} = \partial_\mu A_\nu - \partial_\nu A_\mu + {}^* \left[\int (dx') (f_\mu(x - x') {}^* J_\nu(x') - f_\nu(x - x') {}^* J_\mu(x')) \right]. \tag{3.9}$$

The string function $f_\mu(x)$ satisfies

$$\partial_\mu f^\mu(x) = \delta(x). \tag{3.10}$$

Therefore, for any closed surface that surrounds the origin, we get

$$\oint d\sigma_\mu f^\mu(x) = 1. \tag{3.11}$$

For any open integration surface Σ,

$$\int_\Sigma d\sigma_\mu f^\mu(x) = \begin{pmatrix} 1, \text{ if string passes through } \Sigma \\ 1/2, \text{ if string crosses the boundary of } \Sigma \\ 0, \text{ if string misses } \Sigma \end{pmatrix}. \tag{3.12}$$

Then the requirement that $\exp[iW(J,J^*)]$ be unique requires that the variation satisfy

$$\delta W(J,J^*) = 2\pi n. \tag{3.13}$$

As it can be shown that

$$-\sum_{e,g} eg \int d\sigma^\mu f_\mu(x_e - x_g) = \frac{1}{2}eg, \tag{3.14}$$

and

$$\sum_e e \int \frac{1}{2} d\sigma_e^{\mu\nu} F_{\mu\nu}(x_e) = e \int d\mathbf{S} \cdot \mathbf{B} = e\Phi, \tag{3.15}$$

we obtain

$$\delta W(J,J^*) = \frac{1}{2}eg + e\Phi, \tag{3.16}$$

where $e\Phi$ can be small and ignored. Thus,

$$\frac{1}{2}eg = 2n\pi, \tag{3.17}$$

which is just the quantization condition.

Therefore, the string singularity, the quantization condition, and the gauge invariance in the theory of magnetic monopole, are consistent in quantum field theory. However, the uncertainty of $2\pi n$ for $W(J,J^*)$ is a constant and it makes $\exp[iW(J,J^*)]$ invariant but $W(J,J^*)$ not gauge invariant, so perturbation method is impossible. Thus, the existing perturbative quantum field theory cannot be used for calculating the monopole production cross section. Nonperturbative methods are the only hope. At present, we can only use models to calculate the cross section for monopole production in the absence of a complete quantum field theory of magnetic monopoles.

The Dirac quantization condition and Maxwell's equations show that magnetic monopoles are very similar to electrons: they are quantized and the charge is conserved. In quantum field theory, the action for the interaction between a monopole and an electron mediated by photon exchange is given by [36][40][41], which follows immediately from $W(J,J^*)$ above,

$$W_{int} = \epsilon_{\mu\nu\sigma\tau}\int j^{\mu}(x)\partial^{\nu}f^{\sigma}(x-x')D_{+}(x'-x'')^{*}j^{\beta}(x''), \tag{3.18}$$

where the electric and magnetic currents are $j^{\mu} = e\bar{\psi}\gamma^{\mu}\psi$ and ${}^{*}j^{\mu} = e\bar{\chi}\gamma^{\mu}\chi$, assuming the monopoles have spin–1/2, and D_{+} is the photon propagator. However, we do not know how to calculate the cross section using this interaction because of the string problem. For simplicity, we treat monopoles as point-like particles, and assume they are produced in a one-photon process that is similar to that of electrons or other leptons such as muon pairs. As this action term is string dependent, we will, as we see below, not

attempt to use it to compute the production process. Instead, for the proton-antiproton interaction, we will use Drell-Yan process [32] for $\mu\overline{\mu}$ (muon anti-muon) pair production of hadrons to model $m\overline{m}$ (monopole anti-monopole) pair production of hadrons, including a velocity suppression factor in the amplitude as suggested by the derivative term in W_{int}.

3.2 The Quark Parton Model

The Drell-Yan process is based on the parton model which was proposed by Feynman [50] in the study of inelastic scattering of hadrons. Here we consider an inelastic electron-proton scattering that is shown in Figure 3.1, where there is more than just an electron and proton in the final state.

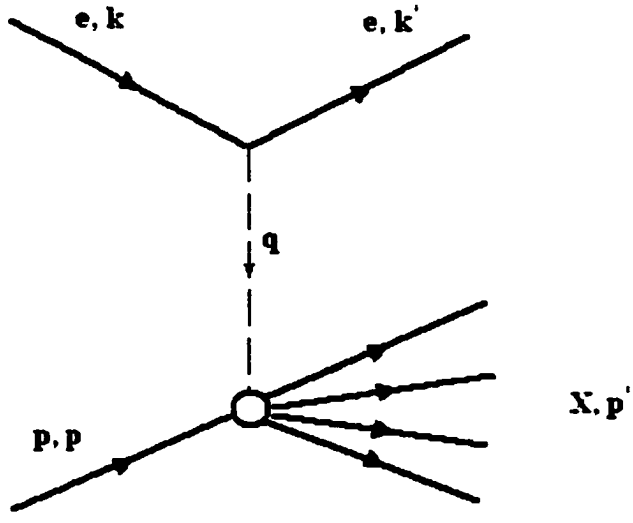


Figure 3.1 Inelastic electron-proton scattering, in one-photon exchange approximation. X represents unobserved hadrons.

We try to calculate the cross section for which only the final electron is observed, which is called the inclusive cross section. This cross section can be factored into a leptonic

tensor $L_{\mu\nu}$ contracted with a tensor $W_{\mu\nu}$ describing the hadron vertex

$$d\sigma \sim L_{\mu\nu}W^{\mu\nu}. \tag{3.19}$$

The leptonic tensor $L_{\mu\nu}$ is defined by (for the unpolarized case)

$$L_{\mu\nu} = \frac{1}{2}\sum_{s}\sum_{s'} \bar{u}(k',s')\gamma_\mu u(k,s)\bar{u}(k,s)\gamma_\nu u(k',s'), \tag{3.20}$$

and takes form

$$L_{\mu\nu} = 2\left[k'_\mu k_\nu + k'_\nu k_\mu + (q^2/2)g_{\mu\nu}\right], \tag{3.21}$$

where $q = k - k'$. In the absence of any information about the hadronic vertex, we may write $W_{\mu\nu}$ in the general form

$$W_{\mu\nu} = V_1 g_{\mu\nu} + V_2 p_\mu p_\nu + V_3(p_\mu q_\nu + q_\mu p_\nu) + V_4(p_\mu q_\nu - q_\mu p_\nu) + V_5 q_\mu q_\nu + V_6 \varepsilon_{\mu\nu\alpha\beta}p^\alpha q^\beta, \tag{3.22}$$

where p_μ is the four-momentum of the proton. Since $L_{\mu\nu}$ is symmetric under interchange of μ and ν, the antisymmetric terms proportional to V_4 and V_6 should be excluded. Considering current conservation requires

$$q^\mu W_{\mu\nu} = 0 = q^\nu W_{\mu\nu}, \tag{3.23}$$

we find that

$$V_3 = -(q \bullet p)V_2/q^2, \tag{3.24}$$

and

$$V_5 = \frac{(q \bullet p)^2 V_2}{q^4} - \frac{V_1}{q^2}, \tag{3.25}$$

thus

$$W^{\mu\nu}(q,p) = (-g^{\mu\nu} + q^\mu q^\nu/q^2)W_1(Q^2,\nu) + [p^\mu - (p \bullet q/q^2)q^\mu] \times [p^\nu - (p \bullet q/q^2)q^\nu]M^{-2}W_2(Q^2,\nu) \tag{3.26}$$

where $W_1 = -V_1$, $W_2 = M^2 V_2$, M is the mass of produced electrons, and

$$Q^2 = -q^2, \tag{3.27}$$

and ν is defined by

$$\nu = q \bullet p/M. \tag{3.28}$$

ν is recognized as the energy transfer in the laboratory frame

$$\nu = (k' - k)^0 = E' - E. \tag{3.29}$$

$W_1(Q^2,\nu)$ and $W_2(Q^2,\nu)$ are known as structure functions of the scalars Q^2 and ν. For elastic scattering, Q^2 and ν are related by

$$Q^2 = 2M\nu. \tag{3.30}$$

But for inelastic scattering, we have the relation

$$2M\nu = Q^2 + W^2 - M^2. \tag{3.31}$$

Here W is the invariant mass of the hadronic final state and is a variable. Therefore,

Q^2 and ν are independent in inelastic scattering.

In 1969, Bjorken [51] predicted that in deep inelastic scattering, the structure functions should *scale*, i.e., become functions of Q^2/ν but not of Q^2 and ν independently. More specifically, if $Q^2 \to \infty$ and $\nu \to \infty$ with $x = Q^2/2M\nu$ fixed, the structure functions will scale as

$$MW_1(Q^2,\nu) \to F_1(x), \nu W_2(Q^2,\nu) \to F_2(x) \tag{3.32}$$

where $F_1(x)$ and $F_2(x)$ are finite, and $F_1(x)$ and $F_2(x)$ satisfy the Callan-Gross relation [52]

$$2xF_1(x) = F_2(x), \tag{3.33}$$

which is a direct consequence of the assumption that the partons are spin-1/2 quarks.

Bjorken scaling can be explained in terms of *elastic* scattering from *free* pointlike constituents [50] of the nucleons. At high Q^2 and ν, the virtual photon is probing very short distance and time scales within the hadron and it interacts *elastically* with small pointlike *free* partons that carry only a certain fraction x of the hadron's energy and momentum. Thus, the structure functions $F_1(x)$ and $F_2(x)$ can be obtained as a sum of the probability functions of the quarks (parton distributions), $f_a(x)$, in the hadron. In inelastic electron-proton scattering, for example, $F_2(x)$ for the proton has the form

$$F_2(x) = \sum_a e_a^2 x f_a(x) = x\left\{\frac{4}{9}[u(x) + \bar{u}(x)] + \frac{1}{9}\left[d(x) + \bar{d}(x) + s(x) + \bar{s}(x)\right] + others\right\}, \tag{3.34}$$

where $u(x)$ is the probability distribution for u quarks in the proton, $\bar{u}(x)$ for u antiquarks, and so on. But this is just a model, and we cannot derive it from QCD.

In principle, the perturbative calculation of the cross section for hadron interactions is not applicable because the interaction becomes strong at large distance. But asymptotic freedom [53] of what we now know as the underlying theory QCD (Quantum Chromodynamics) shows that the interaction between partons is almost negligible within short distances in the hadron. This makes perturbative calculations possible in many cases such as the deep inelastic e-p scattering and the Drell-Yan process. Therefore, we can make use of the parton model to factorize the hadronic cross section into two parts: a long distance factor and a short distance factor. [54] The short distance factor is associated with the subprocess of interactions with parton in the hadron, where we can perform perturbative calculations, while the long distance factor can be absorbed into the parton distribution functions. This is known as *factorization*. Using factorization, we can express the cross section in terms of parton distribution functions convoluted with a perturbatively calculable subprocess cross section: [55]

$$d\sigma_X = \sum_{a,b} \int dx_1 dx_2 f_a(x_1) f_b(x_2) d\hat{\sigma}_{ab\to X} \tag{3.35}$$

where X stands for any produced particles, x_1 and x_2 are the moment fractions of constitutes a and b, respectively, and $\hat{\sigma}_{ab\to X}$ the cross section for the subprocess $ab \to X$.

3.3 Quark Parton Distributions

In general, the parton distributions are functions of x and depend upon Q^2, i.e., $f_a(x, Q^2)$, the Q^2 dependence arising from a QCD correction due to gluon emission by quarks. The Q^2 dependence implies a violation of scaling, which is seen in electron, muon, and neutrino scattering data. [56] The parton distributions can be determined from a global fit to a wide range of deep inelastic and related hard scattering data. The basic procedure is to parametrize $f_a(x, Q^2)$ at a low value of $Q^2 = Q_0^2$ and then compute $f_a(x, Q^2)$ at higher Q^2 by using the renormalization group evolution equation, [57] or Altarelli-Parisi

equation

$$\frac{d}{d\log Q^2} f_a(x,Q^2) = \frac{\alpha_s(Q^2)}{2\pi} \int_x^1 \frac{dz}{z} P_{qq}(x/z) f_a(z,Q^2) + O(\alpha_s^2(Q^2)), \quad (3.36)$$

where $\alpha_s(Q^2)$ is the running coupling constant of QCD, and $P_{qq}(y)$, the splitting function is

$$P_{qq}(y) = \frac{4}{3}\left[\frac{1+y^2}{1-y}\right], \quad (3.37)$$

which is the probability that a quark, having radiated a gluon, is left with the fraction y of its original momentum. The evolution equation shows that the change in the distribution for a quark with momentum fraction x, which absorbs the virtual gluon, is then given by the integral over z of the corresponding distribution for a quark with momentum fraction z, which radiated away (via a gluon) a fraction x/z of its momentum with probability $(\alpha_s(Q^2)/2\pi)P_{qq}(x/z)$. Therefore, given the measured quark distribution $f_a(z,Q^2)$ over the range x to 1, the logarithmic derivative with respect to Q^2, is determined by $\alpha_s(Q^2)$.

The parametrization must be general enough to accommodate all the possible x and quark flavor dependence, but it should not contain too many parameters so that the curve fitting becomes undetermined. In practice, it is common to use a form [54]

$$xq(x,Q) = A_0 x^{A_1}(1-x)^{A_2} P(x) \quad (3.38)$$

where $P(x)$ is a smooth function; x^{A_1} dominates if x is small and $(1-x)^{A_2}$ dominates if x is large.

The first generation of parton distributions, based on leading order evolution and data of the early 1980s, were given by Gluck et al. [58] and others. Second generation global

analyses, based on next to leading order evolution and more recent data, have been carried out by several groups, e.g., [59] Similar efforts have been made by CTEQ collaboration since 1992. [60] They give different parametric forms and are continuing to improve their parametrizations with updated data and new physics processes available.

1. In GRV parametrizations [61], the P functions are given by

$$P(x, Q^2) = 1 + Ax^b + Bx + Cx^{3/2}, \tag{3.39}$$

where $A, B, C,$ and b are functions of Q and vary with different quarks.

2. MRST uses the following P functions [55]

$$P(x, Q^2) = 1 + A\sqrt{x} + Bx, \tag{3.40}$$

where A and B are functions of Q.

3. The CTEQ collaboration uses a simple P function [62]

$$P(x, Q^2) = 1 + Ax^B, \tag{3.41}$$

where A and B are also functions of Q.

The differences between them come from choosing different factorization schemes, emphasizing different partons, and, more importantly, using different data sets. For example, CTEQ used inclusive jet data of CDF and DØ, [63] whereas MRST relied on direct photon production results of WA70 and E706 [64]. The different parametrizations, however, are not very different. The CTEQ and MRST collaborations have given similar quark distribution functions that are shown in Figure 3.2.

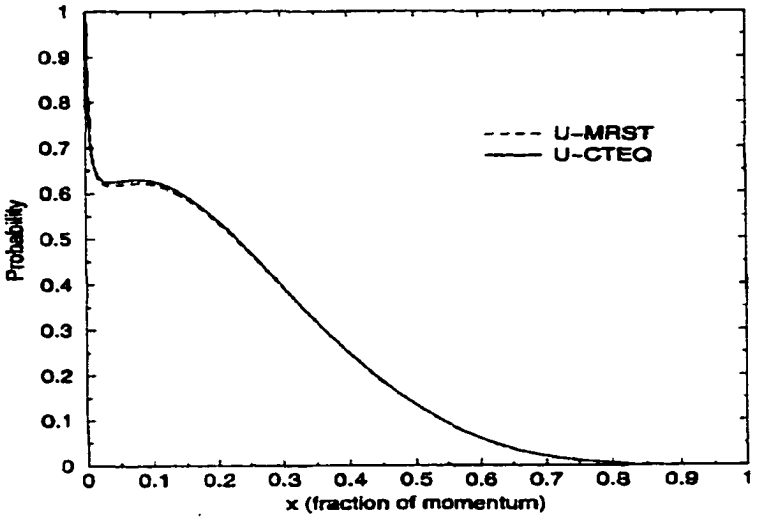


Figure 3.2 A comparison of the U quark distribution, $U(x)$, between CTEQ and MRST parametrizations, which shows that they are approximately the same and should not give very different results. (see Figure 3.4)

3.4 The Drell-Yan Process for $m\bar{m}$ Production

First, we consider the Drell-Yan process for $\mu\bar{\mu}$ production

$$p + \bar{p} \rightarrow \mu + \bar{\mu} + X. \tag{3.42}$$

This process involves a hard scattering subprocess and thus can be described by the parton model. Figure 3.3 shows an incoming proton or anti-proton with momentum P is represented as composed of partons i carrying longitudinal momentum fractions $x_i (0 \leq x_i \leq 1)$. We ignore transversi momenta of the partons since they are small. The subprocess is

$$q + \bar{q} \rightarrow \mu + \bar{\mu}. \tag{3.43}$$

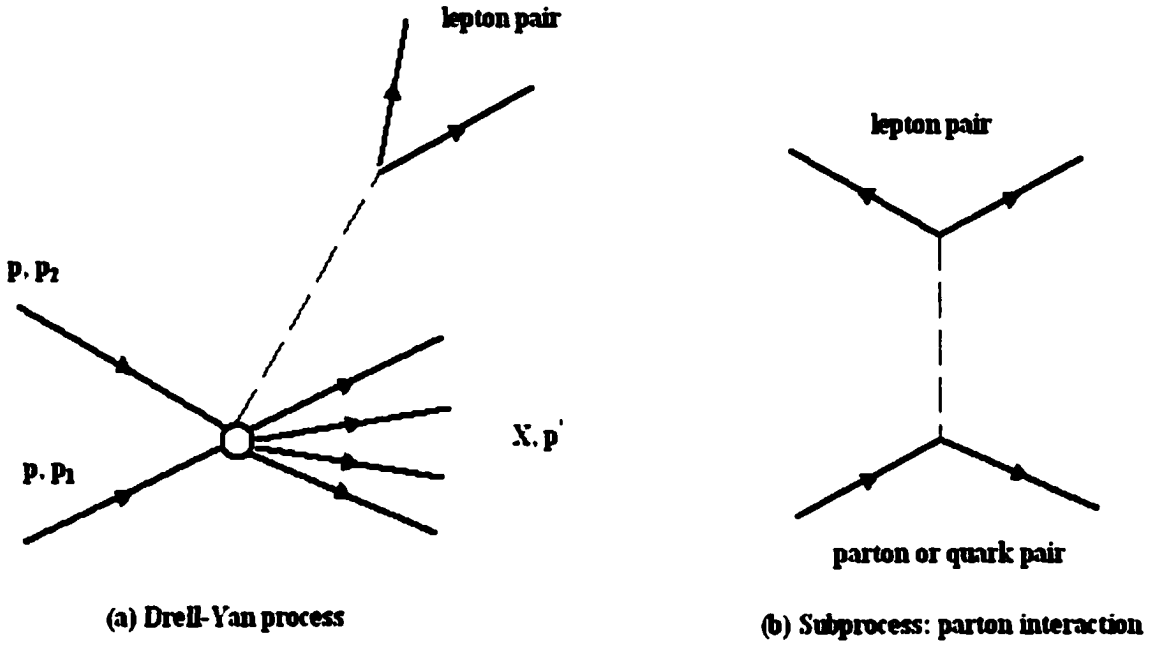


Figure 3.3 Drell-Yan process with the parton subprocess.

The cross section for $p\bar{p}$ collision is obtained from factorization by multiplying the cross section for the subprocess by the quark parton momentum distributions $dx_1 q_a(x_1) dx_2 \bar{q}_a(x_2)$, summing over parton and antiparton types and integrating over x_1 and x_2; also an average must be made over different colors. That is [65][66]

$$\sigma(p\bar{p} \rightarrow \mu\bar{\mu}X) = \sum_a C_a \int dx_1 dx_2 [q_a(x_1)\bar{q}_a(x_2)]\sigma(q_a\bar{q}_a \rightarrow \mu\bar{\mu}), \tag{3.44}$$

where in the leading order approximation

$$\sigma(q_a\bar{q}_a \rightarrow \mu\bar{\mu}) = (4\pi\alpha^2/3q^2)e_a^2, \tag{3.45}$$

and $C_a = 1/3$. Therefore

$$\sigma(p\bar{p} \rightarrow \mu\bar{\mu}X) = \frac{4\pi\alpha^2}{9q^2}\sum_a \int e_a^2[q_a(x_1)\bar{q}_a(x_2)]dx_1dx_2, \tag{3.46}$$

or written in differential form

$$d^2\sigma(p\bar{p} \rightarrow \mu\bar{\mu}X) = \frac{4\pi\alpha^2}{9q^2}\sum_a e_a^2[q_a(x_1)\bar{q}_a(x_2)]dx_1dx_2. \tag{3.47}$$

We can insert a δ function $\delta(q^2 - sx_1x_2)$ according to

$$\int dq^2\delta(q^2 - sx_1x_2) = 1, \tag{3.48}$$

then, fixing q^2 but integrating over x_1 and x_2,

$$\frac{d\sigma}{dq^2} = \frac{4\pi\alpha^2}{9q^4}\int dx_1dx_2x_1x_2\delta(x_1x_2 - \tau)\sum_a e_a^2[q_a(x_1)\bar{q}_a(x_2)], \tag{3.49}$$

where $q^2 = s\tau$. Considering $q^2 = M^2$ (M is the center of mass energy of the muon pair), we can write the differential cross section for the Drell-Yan process by integrating over x_2 as

$$\frac{d\sigma}{dM} = \frac{8\pi\alpha^2}{9M}\int dx_1\sum_a e_a^2\left[q_a(x_1)\bar{q}_a(\frac{q^2}{sx_1})\right]/(x_1s). \tag{3.50}$$

In the case of monopole production

$$p + \bar{p} \rightarrow m + \bar{m} + X, \tag{3.51}$$

in principle, we cannot simply use the Drell-Yan calculation because of the problem with the perturbation theory of magnetic monopoles due to the fixed and large magnetic charge and dependence of the amplitude on the Dirac string. But, heuristically, if we consider the similarity between the Lorentz forces for an electron and a monopole

$$\mathbf{F}_e = e\mathbf{E} + e\boldsymbol{\beta} \times \mathbf{B} \text{ for electron,} \tag{3.52}$$

$$\mathbf{F}_g = g\mathbf{B} - g\boldsymbol{\beta} \times \mathbf{E} \text{ for monopole,} \tag{3.53}$$

and try a replacement in the cross section

$$e \rightarrow \beta g \tag{3.54}$$

then

$$\alpha = \frac{e^2}{4\pi} \rightarrow \beta^2 \frac{g^2}{4\pi} = \beta^2 \frac{e^2}{4\pi\alpha^2} \left(\frac{n}{2}\right)^2 = \beta^2 (68.5n)^2 \alpha. \tag{3.55}$$

This replacement is also approximately valid when people derive the energy loss of a monopole. [67] Moreover, [68] the nonrelativistic result (classical or quantum) for small angle scattering of electrons by monopoles differs from that of charged particle scattering by the same replacement $e \rightarrow \beta g$. In addition, we need to include a β as a phase space factor for the cross section formula. As a result, we roughly expect that the Drell-Yan cross section for monopole production will be significantly reduced by a factor β^3, i.e.,

$$\frac{d\sigma}{dM} = \beta^3(67.5n)^2\frac{8\pi a^2}{9M}\int dx_1 \sum_a e_a^2\left[q_a(x_1)\bar{q}_a(\frac{q^2}{sx_1})\right]/(x_1 s). \qquad (3.56)$$

Although the β^3 correction somewhat compensates for the largeness of g^2, we must emphasize that the Drell-Yan production mechanism proposed here for monopoles is still just a model. There is no solid physical foundation supporting this model. However, this is a reasonable working model, with which a mass limit can be determined based on a conservative cross section below the unitarity limit for $n = 1, 2$. (see Chap.6)

To calculate the cross section for monopoles to be produced by $p\bar{p}$ collisions, we should know the quark distributions in the proton and antiproton. In a proton, there are valence quarks that constitute the proton ($u_v u_v d_v$), and sea quarks that are $q\bar{q}$ pairs virtually produced. Then, the u quark and d quark distributions in a proton can be parametrized by the sum of valence and sea contributions.

$$U = u_v + u_s, \qquad D = d_v + d_s, \qquad \bar{s} = s, \qquad (3.57)$$

while the antiquark $\bar{u}$ and $\bar{d}$ and strange quark s are taken to be pure sea. An antiproton is composed of antiquarks ($\bar{u}_v \bar{u}_v \bar{d}_v$), but the distribution functions are equal to the corresponding quark distributions in a proton, i.e.,

$$\bar{U} = U, \bar{D} = D \qquad (3.58)$$

thus,

$$\sum_a e_a^2[q_a(x_1)\bar{q}_a(x_2)] = \frac{4e^2}{9}[U(x_1)U(x_2) + \bar{u}(x_1)\bar{u}(x_2)] + \frac{e^2}{9}[D(x_1)D(x_2) + \bar{d}(x_1)\bar{d}(x_2)] + \frac{2e^2}{9}[s(x_1)s(x_2)]. \quad (3.59)$$

We have used both CTEQ and MRST parametrizations to work out the cross section calculations for $n = 1$, and obtained roughly the same results which are shown in Figure 3.4. We used CTEQ5 parametrization to complete the Drell-Yan calculations.

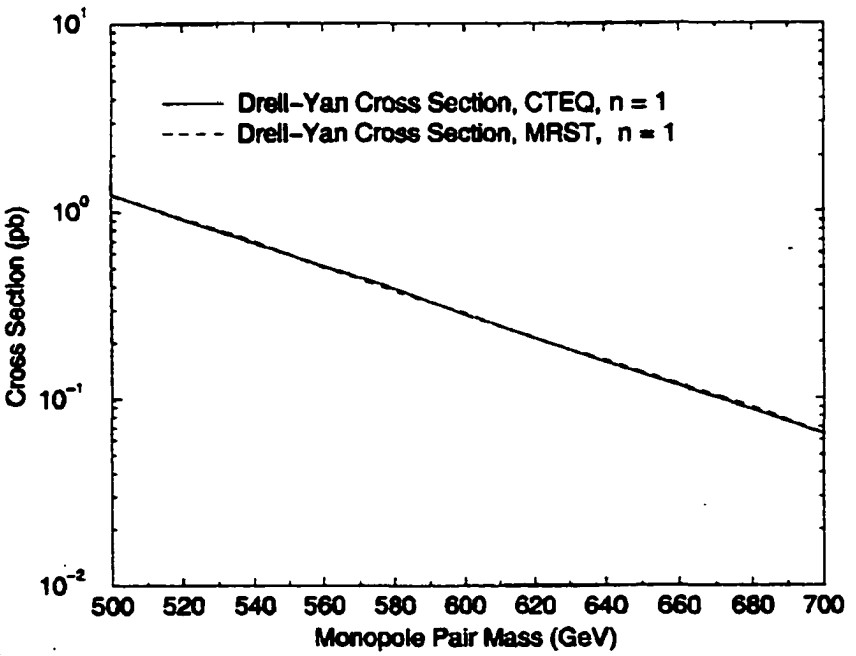


Figure 3.4 CTEQ and MRST obtain almost the same cross section with their own quark distributions.

Chapter 4

Monopole Stopping and Trapping in the DØ and CDF Detectors

4.1 The Energy Loss of Magnetic Monopoles

We first consider the case of electrically charged particles, and then we will extend the analysis to magnetic monopoles. When the charged particles pass through matter, they will have energy loss that is caused by inelastic collisions between the charged particle and the atomic electrons of the materials. The energy loss is represented by a quantity called the stopping power: $\frac{dE}{dx}$, which is the average energy loss per unit path length. Many people have calculated the stopping power. [69] Bohr [70] first calculated the stopping power using classical arguments. He gave the formula

$$-\frac{dE}{dx} = \frac{4\pi z^2 e^2}{m_e V^2} N_e \left(\ln \frac{1.123 m_e V^3}{z e^2 \omega} - \ln(1-\beta^2) - \frac{\beta^2}{2} + R_1 \right), \qquad (4.1)$$

where N_e is the number of electrons per unit volume, m_e the mass of electron, z the charge value of the charged particle in terms of the charge on the electron, V the velocity of the particle, ω the characteristic atomic frequency of the orbital motion of the electron, $\beta = V/c$, and R_1 a small ignorable correction factor (normally, ~ 10^{-4}).

After quantum mechanics was formed, Bethe [71] and Bloch [72] conducted a quantum mechanical calculation of the energy loss. The formula they obtained is

$$-\frac{dE}{dx} = \frac{4\pi z^2 e^4}{m_e V^2} N_e \left(\ln \frac{2m_e V^2}{I} - \ln(1-\beta^2) - \beta^2 \right)$$
$$= \frac{4\pi z^2 e^4}{m_e c^2 \beta^2} N_e \left(\ln \frac{2m_e c^2 \beta^2 \gamma^2}{I} - \beta^2 \right), \qquad (4.2)$$

where I is the excitation potential or ionization potential per electron.

However, Bohr, Bethe and Bloch assumed that the absorbing material is a dilute, cold gas, and that assumption is not true in many cases. Then, a so-called "density effect" must be included. Fermi gave a classical treatment of the density effect, and Fano [73] discussed the quantum mechanical approach. But in most cases, the classical and quantum mechanical approaches are equivalent. As a result, a density correction δ has been added in above formula

$$-\frac{dE}{dx} = \frac{4\pi z^2 e^4}{m_e c^2 \beta^2} N_e \left(\ln \frac{2m_e c^2 \beta^2 \gamma^2}{I} - \beta^2 - \frac{\delta}{2} \right). \qquad (4.3)$$

Sternheimer [74] derived a numerical functional form of δ

$$\delta = \left\{ \begin{array}{c} 0,\ X < X_0 \\ 4.606X + C + a(X_1 - X)^m,\ X_0 < X < X_1 \\ 4.606X + C,\ X_1 < X \end{array} \right\}, \qquad (4.4)$$

where

$$X = \log(\beta\gamma),\ C = -2\ln\left(\frac{I}{\hbar\omega_p}\right) - 1,\ m = 3.0,\ a = -(C + 4.606X_0)/(X_1 - X_0)^m, \qquad (4.5)$$

and the values for C, a, X_0, X_1, and m are given in Table 4.1.

Table 4.1 (a) Parameters used for the density correction [75]

Solids and Liquids:

I	$\|C\|$	X_0	X_1
$I < 100$ eV	$\|C\| < 3.681$	0.2	2.0
$I < 100$ eV	$\|C\| \geq 3.681$	$0.326\|C\| - 1.0$	2.0
$I \geq 100$ eV	$\|C\| < 5.215$	0.2	3.0
$I \geq 100$ eV	$\|C\| \geq 5.215$	$0.326\|C\| - 1.5$	3.0

Table 4.1 (b) Parameters used for the density correction [75]

Gases at STP (T = 0°C and P = 1 atm):

$\|C\|$	X_0	X_1
$\|C\| < 10.0$	1.6	4.0
$10.0 \leq \|C\| < 10.5$	1.7	4.0
$10.5 \leq \|C\| < 11.0$	1.8	4.0
$11.0 \leq \|C\| < 11.5$	1.9	4.0
$11.5 \leq \|C\| < 12.25$	2.0	4.0
$12.25 \leq \|C\| < 13.804$	2.0	5.0
$\|C\| \geq 13.804$	$0.326\|C\| - 2.5$	5.0

The energy losses of magnetic monopoles are caused mainly by the interaction between the electric field of moving monopoles and the atomic electrons of the absorber. Other interactions such as nuclear reactions are extremely rare and can be ignored. [69][76] In principle, the electrical charged particle stopping power calculation can be applied to a magnetic monopole if the monopole features are taken into account. In fact, the energy loss by a magnetically charged particle is approximately obtained from that of an electrically charged particle by the substitution [68]

$$\frac{Ze}{V} \rightarrow \frac{g}{c}, \text{ or } Ze \rightarrow \beta g. \tag{4.6}$$

This is just a classical approach, though. Kasama, Yang, and Goldhaber [77] have used quantum mechanics for an electron moving in the magnetic field of a fixed monopole to obtain the differential scattering cross section; Ahlen [78] has used this cross section to obtain the following expression for monopole stopping power.

$$-\frac{dE}{dx} = \frac{4\pi g^2 e^2}{m_e c^2} N_e \left(\ln \frac{2m_e c^2 \beta^2 \gamma^2}{I_m} + \frac{K(|g|)}{2} - \frac{\delta_m}{2} - \frac{1}{2} - B(|g|) \right), \tag{4.7}$$

where $K(|g|)$ is the Kasama, Yang, and Goldhaber cross section correction:

$$K(|g|) = \left\{ \begin{array}{c} 0.406,\ |g| = \frac{n}{2\alpha} e,\ n = 1 \\ 0.346,\ |g| = \frac{n}{2\alpha} e,\ n = 2,3,6 \end{array} \right\} \tag{4.8}$$

and $B(|g|)$ is the Bloch correction that is determined by the digamma function ψ[79]:

$$B(|g|) = -(\psi(1) - \mathrm{Re}\,\psi(1 + ig\alpha/e)) = \sum_{k=1}^{\infty} \frac{(g\alpha/e)^2}{k^3 + k(g\alpha/e)^2}$$

$$\approx \left\{ \begin{array}{l} 0.248,\ |g| = \frac{n}{2\alpha} e,\ n = 1 \\ 0.672,\ |g| = \frac{n}{2\alpha} e,\ n = 2 \\ 1.022,\ |g| = \frac{n}{2\alpha} e,\ n = 3 \\ 1.685,\ |g| = \frac{n}{2\alpha} e,\ n = 6 \end{array} \right\} \tag{4.9}$$

We cut off the k summation at 1000 and obtain good enough corrections, and the error is $O(10^{-6})$. The above stopping power formula is valid only for the large β range ($\beta > 0.1$). For small β ($\beta < 0.1$), Ahlen and Kinoshita [80] have given a different

formula

$$-\frac{dE}{dx} = \frac{4m_e V_F^2 g^2 e^2}{3\pi\hbar^3 c} N_e \ln\left(\frac{1}{\psi_{\min}^m}\right)\beta \qquad (4.10)$$

In this expression, $\psi_{\min}^m$ is a minimum allowed electron scattering angle, and V_F is the Fermi velocity of the electrons. This expression shows that the monopole stopping power is proportional to β for $\beta < 0.1$.

4.2 The DØ Detector [81]

The Tevatron collider at the Fermi National Accelerator Laboratory is currently the world's highest energy accelerator, colliding anti-protons and protons at a center-of-mass energy of 1.8 TeV. The DØ detector and CDF detector are the two general purpose detectors built to exploit the Tevatron, from (the Run I version of) which we took samples to search for magnetic monopoles. The DØ detector is used to study high mass states and large p_T phenomena, which include the search for the top quark, sensitive tests of the standard model, various studies of perturbative QCD, and searches for new phenomena beyond the standard model.

The material used for monopole samples in the DØ detector was part of the central detector that is composed of tracking and transition radiation detectors. The central detector includes four main parts: (i) the vertex drift chamber (VTX), (ii) the transition radiation detector (TRD), (iii) the central drift chamber (CDC), and (iv) two forward drift chambers (FDC). The VTX, TRD, and CDC cover a large angular region and are arranged in three cylinders concentric with the beams. The FDCs are oriented perpendicular to the beams. Three aluminum cylinders (main and two extensions) surrounded the FDCs, of which the extension cylinders were taken for our monopole samples. Figure 4.1 shows the layout of the detector. Also we took a half meter of the

beryllium beam pipe as a sample since it has the largest solid angle coverage (~ 95%).

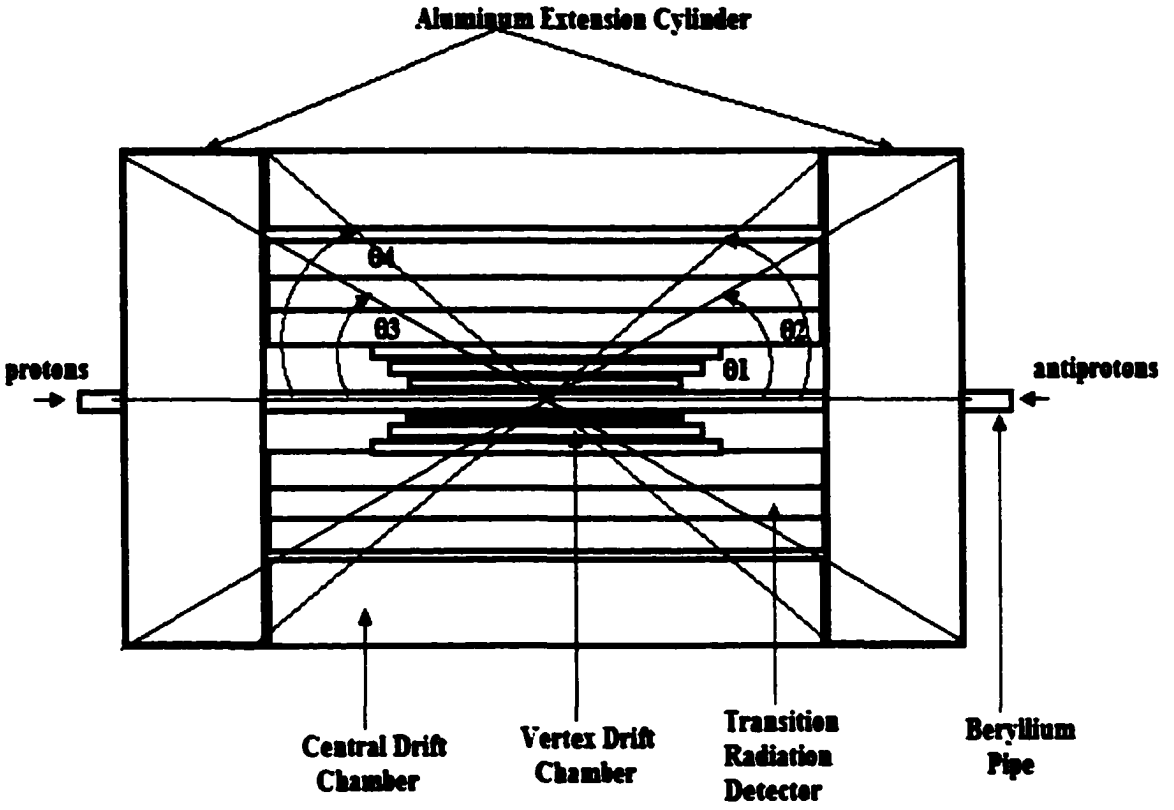


Figure 4.1 The DØ detector. $\theta_1 = 30°, \theta_2 = 40°$, and $\theta_1 = \theta_3, \theta_2 = \theta_4$.

4.3 Energy loss in the DØ Detector

Suppose that magnetic monopole pairs were produced by proton antiproton collisions. They would have gone through the beryllium pipe, VDC, TRD, and CDC if they had enough energy. Moreover, they would have been stopped in the aluminum cylinder if they lost all their kinetic energy when they reached the cylinder. Moreover, they would have been trapped in the cylinder if they were bound to the nuclei of the materials. In that case we would be able to find monopoles in the aluminum cylinder. Therefore, the first thing we need to do is to estimate the energy loss for a monopole going through the

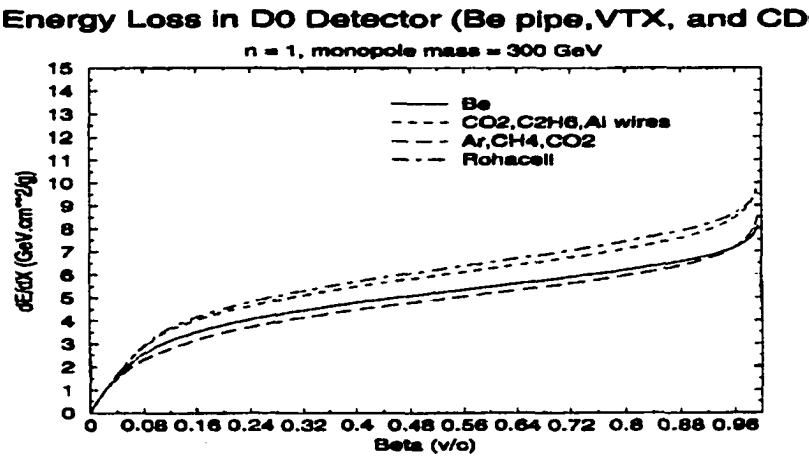
materials in each detector.

The VTX chamber is the innermost tracking detector. It has an inner radius of 3.7 cm and an outer active radius of 16.2 cm. There are a variety of materials inside the VTX: carbon fiber support tubes, sense wires, field and grid wires, and gases such as CO_2 and ethane, etc.. Most of them are negligible, but CO_2 and ethane gases and aluminum field and grid wires were considered for the energy loss of monopoles.

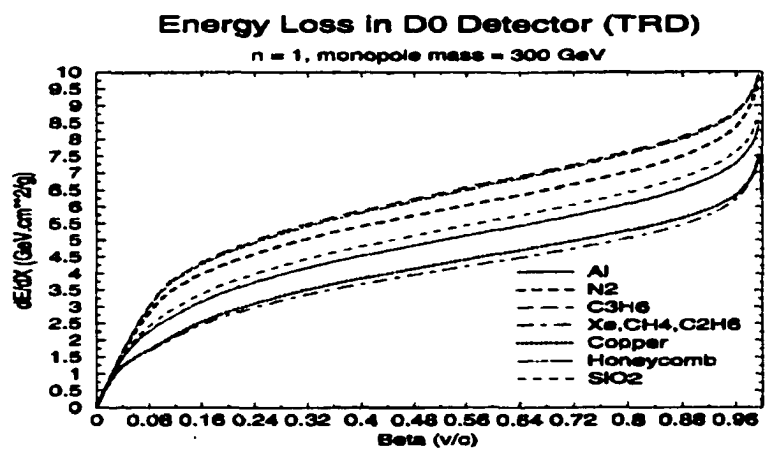
The TRD consists of three separate units, each containing a radiator and an X-ray detection chamber. The radiator section consists of 393 foils of 18 μm thick polypropylene in a volume filled with nitrogen gas. The radiator section is enclosed in a carbon-fiber tube with end flanges made of Rochacell with carbon-fiber skins. The radiator and detector volumes are separated by a pair of 23 μm aluminized mylar windows. Dry CO_2 gas flows through the gap between these two windows to keep the nitrogen in the radiator from leaking into the detector volume and polluting the recirculating chamber gas, a mixture of Xe (91%) / CH_2 (7%) / C_2H_6 (2%). The outer support cylinder of each of the TRD units is a 1.1 cm thick plastic honeycomb with fiber-glass skins.

The CDC is a cylindrical shell of length 184 cm, and its inner and outer radii are 49.5 and 74.5 cm, respectively. It consists of four concentric rings of 32 azimuthal cells per ring. Each cell contains seven 30 μm tungsten sense wires. The chamber is divided into 32 separate identical modules. Each module is made from a set of Rochacell structural members ("shelves") covered with epoxy-coated Kevlar cloth and wrapped with a double layer of 50 μm Kapton. The separate modules are positioned within a single support cylinder. The inner surface is a composite carbon fiber/Rochacell tube. The outer main cylinder is 0.95 cm thick aluminum and serves as the main support for the full CDC. The CDC is operated with Ar(92.5%) CH_4(4%) CO_2(3%) gas and 0.5% H_2O. We use Ahlen's monopole stopping power equations and Sternheimer's parameters

[74] obtain the numerical curves for each material in the detector, which are shown in Figure 4.2.



(a)



(b)

Figure 4.2 (a) (b) Energy loss of magnetic monopoles for the materials in DØ detector. dE/dx is around 5 GeV•cm^2/g for $0.1 < \beta < 0.8$.

The range between the Al sample (1.27 cm thick) and the IR collision point at an angle (35°) with respect to the beam pipe in the DØ detector is about 9.4 g/cm^2. The materials in DØ detector and the corresponding range are listed in Table 4.2.

Table 4.2 The materials and the ranges at angle of 35° in DØ Detector

Detector	Material	Range (g/cm^2) at 35°
	Beryllium pipe	0.16
VTX	C_2H_6&CO_2 gases and Al wire Mixture	0.12
TRD	Al Window	2.18
	N_2 gas	0.01
	Polypropylene	1.12
	Xe, CH_4, C_2H_6 gases	0.02
	Honeycomb	1.99
CDC	Ar, CO_2, CH_4 gases	0.07
	Kapton	0.1
	Rohacell	0.49
	Endplate (Al)	4.18
	G10	1.11
Total		9.4

4.4 The CDF Detector [82]

The CDF dectector consists of a central detector which is made up of the solenoidal magnet, steel yoke, tracking chambers, electromagnetic shower counters, hadron calorimeters and muon chambers, and two identical forward/backward detectors consisting of segmented time-of-flight counters, electromagnetic shower counters, hadron calorimeters, and muon toroidal spectrometers. An elevation view of the forward half of the complete detector is shown in Figure 4.3. The detector is divided into a central detector ($10° < \theta_s < 170°$), which includes the end-plugs which form the pole

pieces for the solenoidal magnet ($10° < \theta_s < 30°$), and the forward/backward regions ($\theta_s < 10°$), where θ_s is the polar angle measured from either the proton or antiproton beam. At angles less than 10° to either beam, particles produced at the interaction point exit the conical hole in the end plug and strike the forward shower counters and hadron calorimeters. The lead plates we used as samples were taken from the forward shower counters.

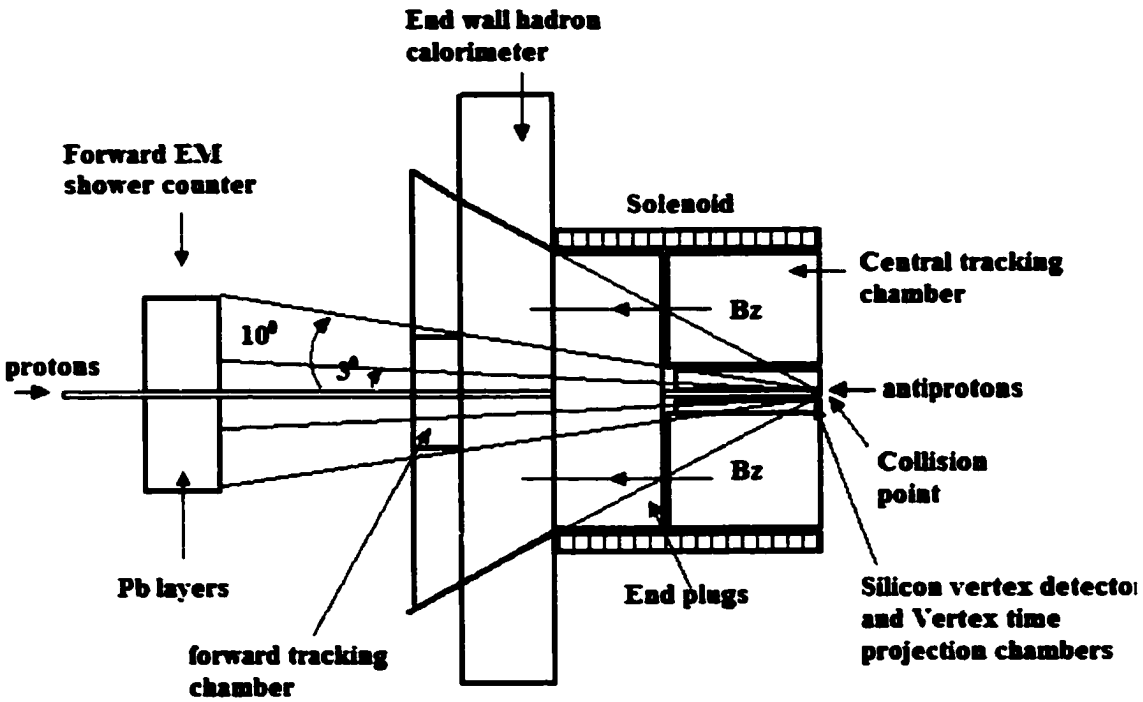


Figure 4.3 A side view of the forward (East) half of the CDF detector, the other part is in the West (on the right).

We are concerned with the detectors between the $p\bar{p}$ collision point and the forward shower counters, through which monopoles might have gone. The collisions occur in the beryllium pipe. The first detector which monopoles may go through is the silicon vertex detector (SVX) [83] that is located with its center on the nominal B0 interaction point

and consists of two cylindrical modules placed end-to-end with their axes coincident with the beam axis. Then there are eight small vertex time projection chambers (VTPC). The central tracking chamber (CTC) is a large cylindrical drift chamber surrounding the VTPC. Outside of the central detector is the forward tracking chamber (FTC). The forward shower counter is behind the FTC.

There were 30 layers of lead installed parallel and perpendicular to the beam pipe inside the forward shower counters. Between each layer, there are self-contained chambers that contain aluminum plates and fiberglass (G-10) panels [84].

The solenoid magnet coil is installed around the CTC, which produces a magnetic field of 1.4 Tesla (B_z) oriented along the incident beam direction in z-axis. We do not know exactly how the magnetic field is distributed. As an approximation (along the central axis), we use the following formula for a solenoid [85] to model this field.

$$B_z(z) = \frac{\mu_0 NI}{2L}\left[\frac{L/2-z}{\left[a^2+(L/2-z)^2\right]^{1/2}}+\frac{L/2+z}{\left[a^2+(L/2+z)^2\right]^{1/2}}\right] = B_0\left[\frac{L/2-z}{\left[a^2+(L/2-z)^2\right]^{1/2}}+\frac{L/2+z}{\left[a^2+(L/2+z)^2\right]^{1/2}}\right]/2L, \qquad (4.11)$$

where B_0 is the magnetic field from an infinitely long solenoid, z the position along central axis, a (= 2.5 m) the radius of the solenoid, and L (= 3 m) the length of the solenoid. Figure 4.4 shows the curve of $B_z(z)$, which is close to 1.4 Tesla uniformly in a wide range, with which the CDF detector was operated.

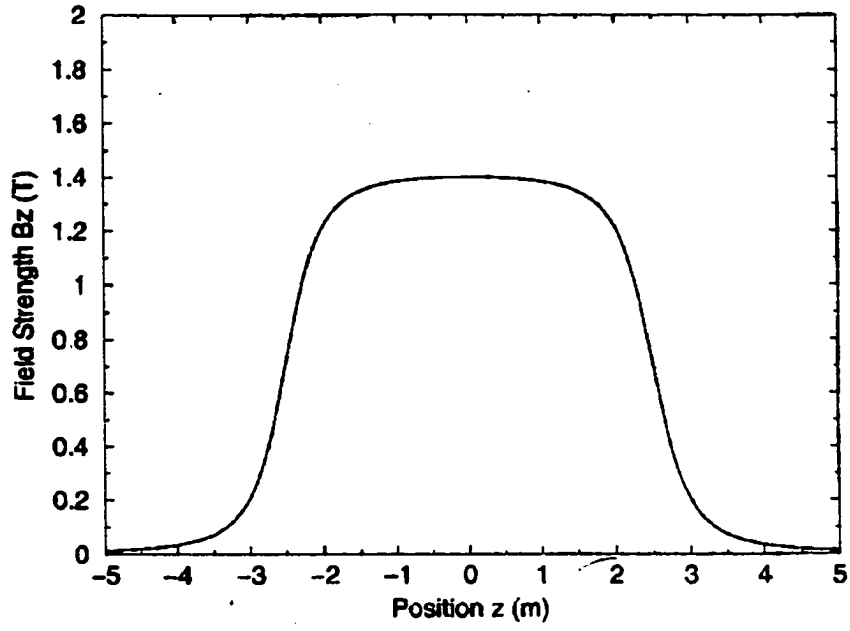


Figure 4.4 The magnetic field along the symmetry axis of the beryllium beam pipe in the CDF detector.

4.5 Energy Loss in the CDF Detector

The SVX consists of 4 radial layers of silicon strips surrounding the beam pipe. It has a number of aluminum bulkheads, a group of ladders made of Rohacell, and alumina (Al_2O_3) ears on the end of a ladder. The VTPC system is comprised of eight separate time projection chamber modules which are mounted end-to-end along the beam direction. The chambers are mainly made of a carbon fiber octagon, and they contain 3072 sense wires and 3072 pads for the measurement of track coordinates. The FTC is a radial drift chamber that contains planes of radial anode and field shaping wires which alternate with planes of cathode strips. The energy loss for those materials is shown in Figure 4.5.

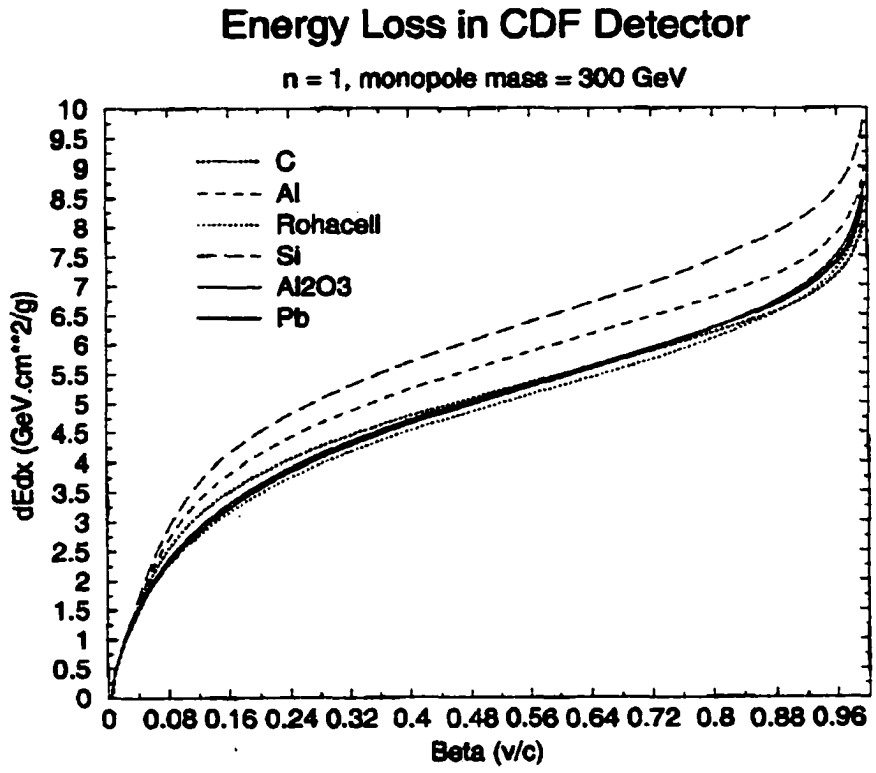


Figure 4.5 The energy loss of monopoles in the CDF detector.

The materials in the CDF detector have an angular distribution with respect to angle θ, which should be considered in the calculation of energy loss.

The range between the Pb samples and the collision at an angle (6.5°) with respect to the beam pipe in the CDF detector is about 7.5 g/cm^2. The materials in CDF detector and the corresponding ranges are listed in Table 4.3.

Table 4.3 The materials and the ranges at angle 6.5° in CDF detector

Detector	Material	Range at 6.5° (g/cm^2)
	Be pipe	0.82
SVX	C	0.94
	Al	0.6
	Si	0.01
	Al_2O_3	0.96
	Rohacell	0.0
VTPC	C	2.40
FTC	Al	1.78
Range Before Sample		7.5
Pb layer		5.71
Al-G10 between Pb		0.83

4.6 Binding Energy in Monopole Samples

People have discussed the possibility that slow magnetic monopoles interacting with matter bind to extended particles, such as nuclear and atomic systems. [86][87][88] They have found that the interaction of the monopole with the magnetic moments of these systems can be strong enough to produce bound states under certain conditions.

Consider a nucleon that has spin s and magnetic moment

$$\mu = k\mu_N s, \tag{4.12}$$

where

$$\mu_N = \frac{Ze}{2m_N}, \tag{4.13}$$

the nuclear magneton, Z is the number of proton, and k the Landé factor, or g-factor. For point-like particles with spin $s = 1/2$, $k = 2$. A magnetic monopole with magnetic charge g at the origin produces a magnetic field in Gaussian units

$$\mathbf{B} = g\frac{\mathbf{R}}{R^3}. \tag{4.14}$$

The interaction energy of a charged particle of magnetic moment $\boldsymbol{\mu}$ with a magnetic monopole ($n = 1$) of field $\mathbf{B}$ is

$$U = -\boldsymbol{\mu} \cdot \mathbf{B} = -k\frac{Z}{4mR^3}\mathbf{s} \cdot \mathbf{R}. \tag{4.15}$$

Then we have the non-relativistic Hamiltonian of a charged particle interacting with a monopole [89][86]

$$H = \frac{1}{2m}(\mathbf{P} - Ze\mathbf{A})^2 - \boldsymbol{\mu} \cdot \mathbf{B} = \frac{1}{2mR^2}\left[-\frac{\partial}{\partial R}R^2\frac{\partial}{\partial R} + (L^2 - q^2) - \frac{kZ}{2}\mathbf{s} \cdot \hat{\mathbf{R}}\right] \tag{4.16}$$

Here

$$q = \frac{1}{2}Z, \tag{4.17}$$

$$\mathbf{L} = \mathbf{R} \times (\mathbf{P} - Ze\mathbf{A}) - q\hat{\mathbf{R}} \tag{4.18}$$

Because this potential is too singular at $R = 0$, in order to allow bound states to exist, Bracci and Fiorentini assume an infinite repulsive potential (hard core) for $R \leqslant a$, the size of the particle:

$$U(R) = +\infty, R \leqslant a. \tag{4.19}$$

We then define the total angular momentum that is conserved

$$\mathbf{J} = \mathbf{L} + \mathbf{S}, \tag{4.20}$$

and apply the Schrödinger equation and bound state condition $E < 0$, thus we obtain one dimensional Schrödinger equations for the lowest angular momentum states

$$J = |q| - \frac{1}{2}, l = |q| : \tag{4.21}$$

$$\frac{1}{2m}\left(-\frac{d^2}{dR^2} + \left(|q| - \frac{Z}{4}k\right)\frac{1}{R^2}\right)\chi = E\chi \tag{4.22}$$

with corresponding boundary condition

$$\chi(a) = 0. \tag{4.23}$$

The monopole-particle interaction has been reduced to a one-dimensional problem in an effective potential:

$$V = \lambda_l(2mR^2)^{-1}, \lambda_l = |q| - \frac{Z}{4}k. \tag{4.24}$$

To obtain bound states, $\lambda_l < 0$. For $\lambda_l < -\frac{1}{4}\left(\geqslant -\frac{1}{4}\right)$, there are infinitely many (zero) bound states. Thus the condition for bound states is (for the lowest angular momentum states)

$$\frac{Zk}{2} > 2|q| + \frac{1}{2}. \tag{4.25}$$

Under those conditions, Bracci and Fiorentini [86] have estimated the binding energies for different materials. The binding energy between a monopole and a lead isotope $_{82}Pb^{207}$ with

$$S = \frac{1}{2},\ q = 41,\ k = 2.97,\ \frac{Zk}{2} = 122 > 2|q| + \frac{1}{2} = 82.5 \tag{4.26}$$

has been given:

$$E_b(\text{Pb}) = 6.9\ \text{keV}. \tag{4.27}$$

Olaussen and Sollie [87] have considered relativity and introduced the form factors of nuclei. They have derived the conditions for general spin. For the states of lowest angular momentum, $j = |q| - S$, the condition is the same as $S = 1/2$ above. Binding will occur for $j = |q| - S + 1$ if $\lambda_\pm > \frac{1}{4}$, where

$$\lambda_\pm = (S - \tfrac{1}{2})X - 2|q| - 1 \pm \sqrt{(|q|+1)^2 + (2S - 1 - |q|)X + X^2/4} \tag{4.28}$$

Here

$$X = k_m|q|, \text{ and } k_m = \frac{A}{SZ}\mu. \tag{4.29}$$

In all cases, binding occurs only if the nuclei have large anomalous magnetic moments.

For aluminum $_{13}Al^{27}$, $S = 5/2$, $|q| = 6.5$, $X = 19.7$, then $\lambda_+ = 35.6 > 1/4$, and $\lambda_- = 15.2 > 1/4$. They have given the binding energy for aluminum:

$$E_b(\mathrm{Al}) = 2.6\ \mathrm{MeV}. \tag{4.30}$$

This is a huge binding energy.

C. J. Goebbel has given a different binding energy of 0.56 MeV for aluminum using a hard core repulsion condition.[90] This shows that monopole binding energy calculations are model dependent.

But fortunately, binding energies are estimated to be in the keV range and up for many materials. It ensures that the monopole-atom complex will remain permanently bound to the material lattice based on a tunneling calculation.[88] For example, to get a 10 years life time, the binding energy would have to be only of the order of 1 eV. Even if we put $_{13}Al^{27}$ in a magnetic field of 1.5 T, the monopole-atom complex would not be extracted and can still stay in the aluminum for $\sim 10^4$ years! [88] [91] Therefore, monopoles should have been trapped in DØ and CDF aluminum and lead samples if they were produced and stopped in those materials.

Beryllium is very special. The Be pipe in the detectors is very thin but has the largest angular coverage ($\sim 4\pi$); it can stop monopoles of large charge ($n = 3,6$). According to Milton, Olaussen and Sollie, however, Be, treated as a point particle, is not expected to bind monopoles. Nevertheless, we do not think that Beryllium should be neglected. First of all, Be can trap dyons with negative electric charge. Moreover, the magnetic field of a monopole is so strong that it will disrupt the nucleus and bind to individual nucleons if not to quarks. Therefore, we strongly suspect that monopoles will bind to Be and believe that it is safe to include Be samples as well as Al and Pb in our monopole search. because $_4Be^9$ has spin-3/2 and a negative g-factor.

In order to make a better trap for trapping monopoles for current experiment, we should use a thick aluminum beam pipe (instead of Be) at the interaction point, if it is possible, to get the maximum angular acceptance with large binding energy.

Chapter 5

The Apparatus for Detection of Magnetic Monopoles

5.1 The Outline of the Monopole Detector

The principle of detecting magnetic monopoles is to convert the characteristic magnetic field generated by a magnetic monopole into an electric current or voltage which can be read out electronically. There are, however, two problems related to a monopole measurement. First, we have to find ways to distinguish between monopole signals and other magnetic signals. Second, the monopole signal is very weak, and the induced electric current may die out very quickly and may therefore not be measurable. This is because the induced current will be converted into heat by the I^2R losses of the coil. Based on Faraday's law of inductance and superconductivity, the problems can be solved by moving samples through a superconducting coil in which a magnetic monopole will produce an induced current which will persist at low temperature after the monopole has passed through the coil. This is the induction method.

In order to use the induction method, we need a superconducting coil, a cryogenic system to make it superconducting, and a device to measure the persistent induced current set up in the coil. The device we choose to measure the induced current is a SQUID (Superconducting Quantum Interference Device), which is cooled with liquid helium that is stored in a liquid helium dewar. We want to have a manageable and cost effective operating scenario for measuring samples, i.e., keep operating SQUIDs 24 hours a day so that we can complete measuring about 1000 samples in a limited time. This implies a helium loss rate $\leq$ 1 liter/hour for our helium dewar, which requires a heat

load into the liquid helium (caused by conduction and radiation) to be $\leq$ 1 Watt. This also implies a vacuum $\leq 10^{-5}$ torr, a liquid nitrogen shield absorbing heat at 50 W•hour/liter, a thin walled helium dewar, and superinsulation radiation shields. This will be discussed later.

Those required devices were built in the monopole detector that is schematically shown in Figure 5.1. Two cylindrical dewars, a liquid helium dewar and a liquid nitrogen dewar, are concentrically set in a cylindrical steel tank with a "warm bore" along the central axis. Two superconducting coils connected to two SQUIDs are immersed in the liquid helium. A monopole sample is set in a carrier attached to a nylon rope that is guided by several pulleys and connected to a stepper motor that moves the sample up and down along the warm bore through the superconducting coils surrounding the bore. The signal current from the superconducting coils is converted into a voltage in the SQUIDs and received by the data acquisition system external to the detector.

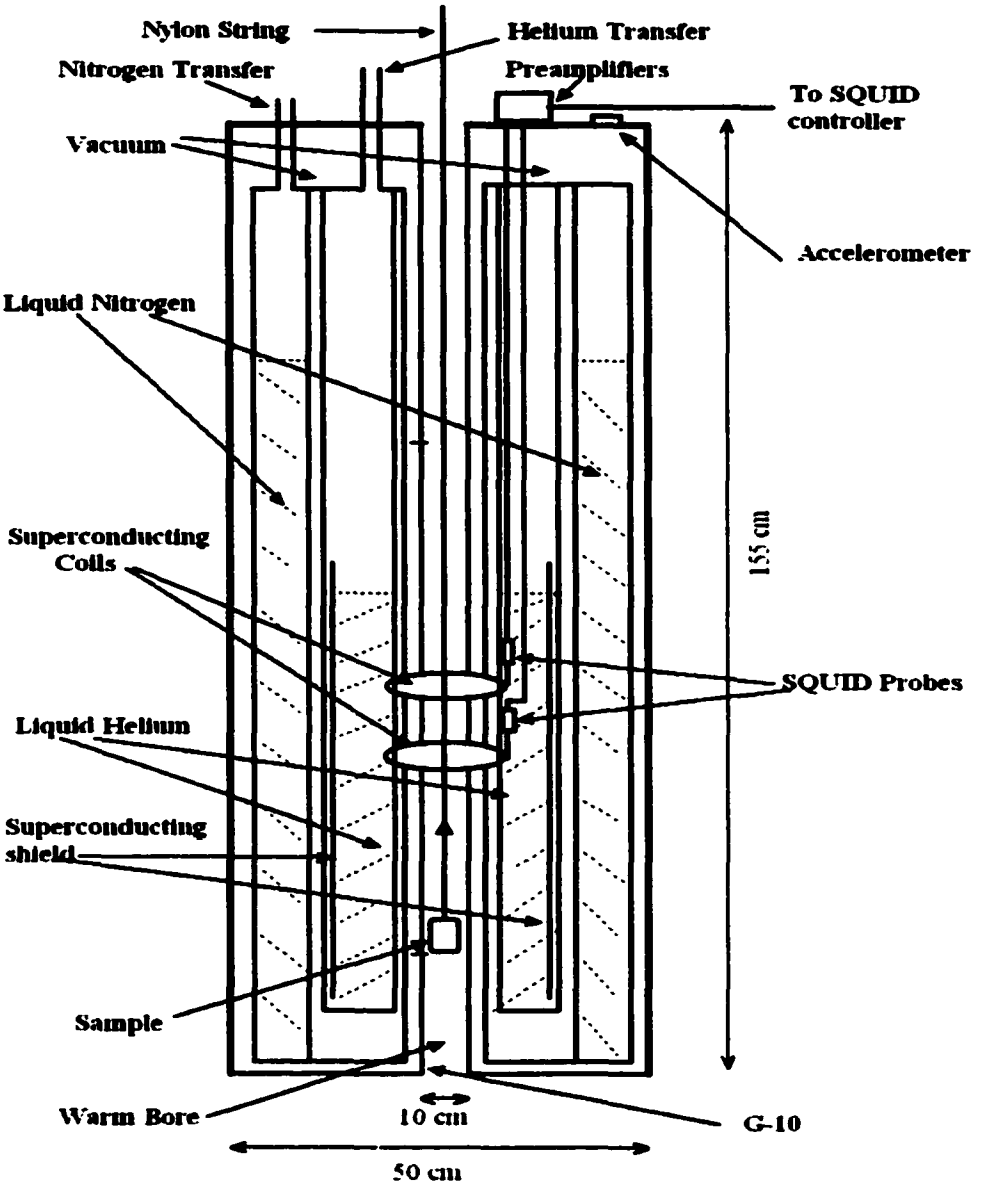


Figure 5.1 A schematic diagram of the monopole detector. The length is 155 cm for the DØ samples and 185 cm for the CDF samples.

5.2 The Monopole Signature

Suppose that a magnetic monopole passes through a ordinary conducting metal coil C bounding a surface S in the $z = 0$ plane, as shown in Figure 5.2.

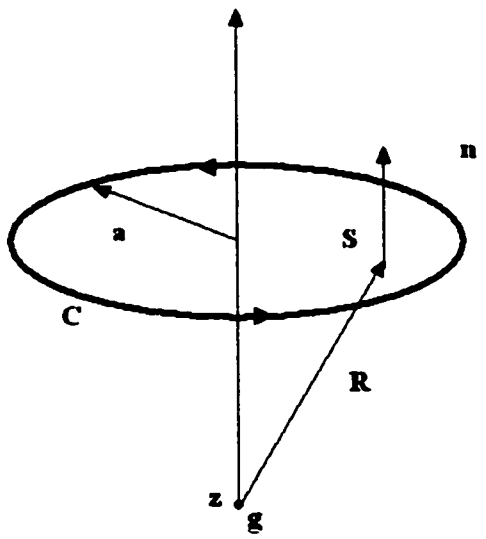


Figure 5.2 A magnetic monopole **g** passing through the conducting metal coil C along the z-axis. S is the surface bounded by C, a is the radius of the coil, and **n** the normal vector of S.

From Maxwell's equation with magnetic charge in SI units we have

$$\oint_C \mathbf{E} \cdot d\mathbf{r} = -\frac{d\Phi}{dt} - \mu_0 \int_S \mathbf{J}_m \cdot d\mathbf{S}, \tag{5.1}$$

where Φ is the magnetic flux through C, and

$$\mathbf{J}_m = g\mathbf{v}\delta^3(\mathbf{r} - \mathbf{v}t), \tag{5.2}$$

and on the plane of the loop, $r = z = 0$, thus

$$\int_S \mathbf{J}_m \cdot d\mathbf{S} = g v_z \delta(-v_z t) = g\delta(t). \tag{5.3}$$

The function $\delta(t)$ shows that the monopole intersects the plane of the coil at time $t = 0$, and so $\mathbf{J}_m$ on the plane is nonvanishing only at $t = 0$. Therefore, a current I will be induced in the coil C when the monopole is passing through the coil. The induced current I is given by

$$IR = \varepsilon = \oint_C \mathbf{E} \cdot d\mathbf{r}, \tag{5.4}$$

ε is the electromotive force that is defined as the work done for each unit of charge transferred in the coil. However, the current just induced cannot be maintained and will immediately become too weak to detect because of energy loss due to the resistance of the metal coil. The way to maintain the induced current is to replace the ordinary metal coil with a resistanceless superconducting coil. In this case, $R = 0$, i.e.,

$$\varepsilon = \oint_C \mathbf{E} \cdot d\mathbf{r} = 0, \tag{5.5}$$

and

$$-\frac{d\Phi}{dt} = \mu_0 g\delta(t), \tag{5.6}$$

Now, we let a monopole move along the symmetry axis of the superconducting coil, so the magnetic flux due to the monopole moving through the coil is

$$\Phi_g = \frac{\mu_0 g}{4\pi} \int_S \frac{\hat{\mathbf{R}} \cdot \hat{\mathbf{n}}}{R^2} dS = \frac{\mu_0 g}{2} \left[1 - 2\theta(z) + \frac{z}{(z^2 + a^2)^{1/2}} \right], \tag{5.7}$$

where **R** is a vector from the monopole to a point on the plane bounded by the coil C, z is the position on the symmetry axis, and a the radius of the coil. $\theta(z)$ is the theta function that is equal to 1 if $z \geq 0$, and, otherwise, is equal to 0.

The total flux through S is

$$\Phi = \Phi_g + \Phi_I, \tag{5.8}$$

where Φ_I is the induced flux due to the current induced in the superconducting coil and is given by

$$\Phi_I = -LI. \tag{5.9}$$

Here I is the induced current, and L is the self-inductance of the coil. Initially, there is no current flowing, so we set $\Phi = 0$ at $z = -\infty$, and obtain

$$\Phi = -\mu_0 g \theta(z). \tag{5.10}$$

Therefore, we find the induced current in the superconducting coil by combining the above equations:

$$I = \frac{\mu_0 g}{2L} \left[1 + \frac{z}{(z^2 + a^2)^{1/2}} \right], \tag{5.11}$$

which is plotted in Figure 5.3, appearing as a smoothed-out step function. The value of the step is

$$\Delta I = \frac{\mu_0 g}{L}, \text{ when } z \text{ goes from } -\infty \text{ to } \infty. \tag{5.12}$$

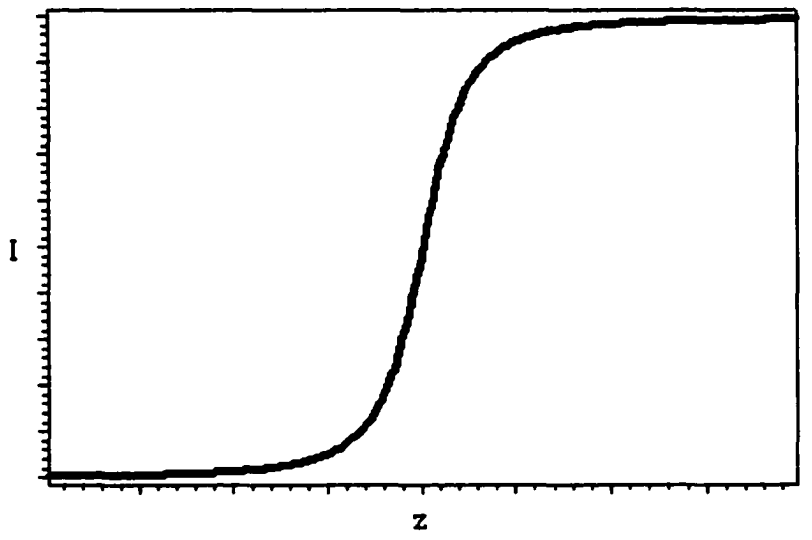


Figure 5.3 The induced current in a superconducting coil, which is the signature of magnetic monopole. The units of I and z are arbitrary in the figure.

We installed two TiNb coils in the detector, which were attached to and surrounded the inner wall of the helium dewar, and used liquid helium to cool the coil down to 4.2 K which is below the critical temperature (9.8 K) of the TiNb superconducting coil. With the liquid helium filled, the TiNb coils became superconducting and they would detect the magnetic monopole signature, the step current.

If we install a superconducting shield surrounding the coil, as is the case of our experiment, (see Figure 5.1) the shape of the step will be somewhat changed and the

magnitude of the step will be reduced approximately by a factor $\left(1 - \frac{a^2}{b^2}\right)$, where a is the radius of the coil and b that of the shield. [92]

5.3 Fundamentals of SQUIDs

Since the monopole flux linking the superconducting coils is very weak ($\sim 10^{-15}$ Wb) and therefore the induced current is weak, we need a device to convert this weak current into a measurable signal. A special device, SQUID (Superconducting Quantum Interference Device), was used for this purpose.

The SQUID is an application of the Josephson junction [93] that is an arrangement of two superconductors connected by a thin layer of insulation. In principle, the wavefunction for electrons in two superconductors have different phases. We use δ to represent the phase difference. If there is a voltage V cross the junction, the current J going through the junction is [94].

$$J = J_0 \sin\delta, \tag{5.13}$$

where J_0 is a characteristic of the junction. δ is related to V by

$$\frac{d\delta(t)}{dt} = \frac{qV}{\hbar}, \tag{5.14}$$

or

$$\delta(t) = \delta_0 + \frac{q}{\hbar}\int V(t)dt. \tag{5.15}$$

Since $\hbar$ is very small, any normal non-zero V applied will induce a rapid oscillation and

the net current is negligible. But if V is zero, we obtain a current between $-J_0$ and J_0. This is the Josephson junction.

Now we apply a high frequency ac voltage $V_a \cos\omega t$ with a dc voltage V_0, thus

$$V_0 \longrightarrow V_0 + V_a \cos\omega t. \tag{5.16}$$

Treat V_a as small and use approximation, we get

$$J = J_0\left[\sin\left(\delta_0 + \frac{q}{\hbar}V_0 t\right) + \frac{qV_a}{\hbar\omega}\sin\omega t\cos\left(\delta_0 + \frac{q}{\hbar}V_0 t\right)\right]. \tag{5.17}$$

The first term is zero on average, but the second term includes the term

$$\frac{qV_a}{\hbar\omega}\sin\omega t\sin\left(\frac{q}{\hbar}V_0 t\right), \tag{5.18}$$

which does not average to zero if

$$\omega = \frac{q}{\hbar}V_0 .(\text{the average current } \bar{J} = V_a/2V_0). \tag{5.19}$$

There should be a current if the ac voltage has just this frequency.

Since V is small, and $\varepsilon = \int \mathbf{E} \cdot d\mathbf{r} = 0$ in superconductor, we can treat the electric field $\mathbf{E}$ as small. Then we have

$$0 = \mathbf{E} = -\nabla V - \frac{\partial \mathbf{A}}{\partial t}, \tag{5.20}$$

which indicates that

$$\int V dt = -\int \mathbf{A} \cdot d\mathbf{r}. \tag{5.21}$$

Thus we can replace $\frac{q}{\hbar} V_0 t$ by $\frac{q}{\hbar}\int \mathbf{A} \cdot d\mathbf{r}$ and write the phase factor in a different way:

$$\delta = \left(\delta_0 - \frac{q}{\hbar}\int \mathbf{A} \cdot d\mathbf{r}\right). \tag{5.22}$$

Then we obtain

$$J = J_0 \sin\left(\delta_0 - \frac{q}{\hbar}\int \mathbf{A} \cdot d\mathbf{r}\right). \tag{5.23}$$

Now we put two Josephson junctions in parallel and let them form a loop as in Fig.5.4, then we apply an external magnetic field passing through the loop. There are two different currents crossing the two different junctions. The total current out of the two junctions is the sum of the two currents which have different phases for different paths. The difference between the two phases is given by

$$\delta_b - \delta_a = \frac{q}{\hbar}\oint \mathbf{A} \cdot d\mathbf{r} = \frac{q}{\hbar}\Phi, \tag{5.24}$$

where Φ is the flux going through the loop. Thus the total current is

$$J_{total} = 2J_0 \sin\overline{\delta_0}\cos\left(\frac{q}{2\hbar}\Phi\right) = J_{t0}\sin\overline{\delta_0}\cos\left(\frac{e}{\hbar}\Phi\right), \tag{5.25}$$

where $J_{t0} = 2J_0$, $\overline{\delta_0} = \frac{1}{2}(\delta_a + \delta_b)$, and $e = \frac{q}{2}$, the charge of an electron as q is the charge of an electron pair in a superconductor. Then we obtain the maximum J_{max}:

$$J_{max} = J_{f0}\left|\cos(\frac{e}{\hbar}\Phi)\right|. \tag{5.26}$$

J_{max} will itself have maxima when

$$\Phi = n\frac{\pi\hbar}{e}, \quad n = 1,2,... \tag{5.27}$$

A change in flux ($\sim \frac{h}{e} \approx 10^{-15}$ Weber) will result in a change ($\sim J_{f0}$) in the current. This forms the basis of the operation of SQUIDs.

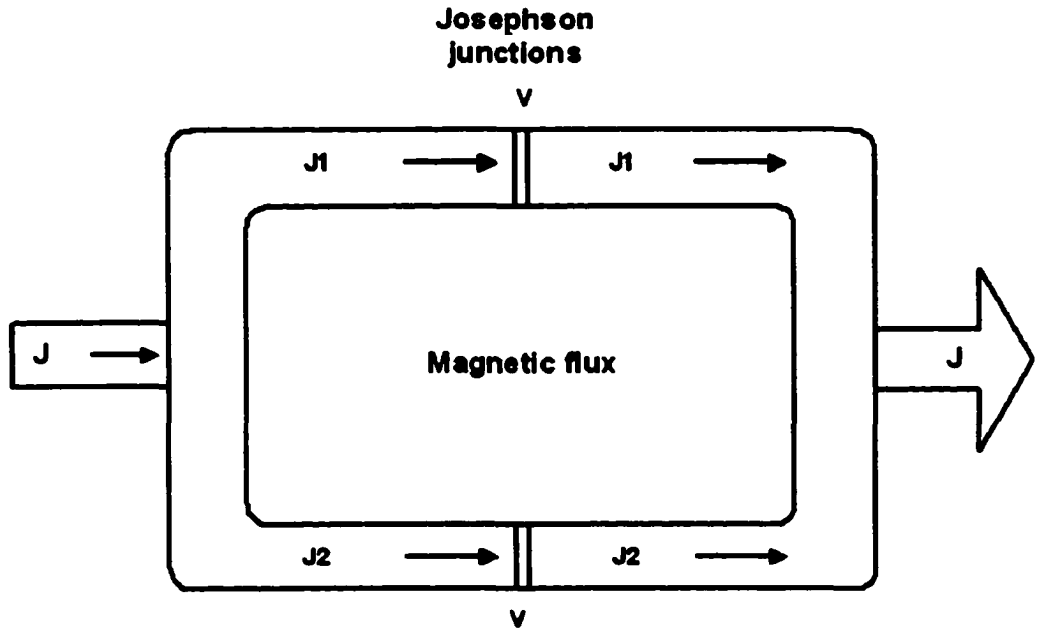


Figure 5.4 A Josephson junction pair forming a loop. The current J is affected by the flux linking the loop

A SQUID is made of a superconducting coil with the Josephson junctions in it. It gives rise to an output voltage signal that is a periodic function of the flux threading the coil as described above. The minimum flux variation it can measure is of the order of

fractions ($\sim 10^{-5}$) of the flux quantum $\Phi_0 (= h/2e = 2.07 \times 10^{-15}$ Wb). There are two different types of SQUID: one is a dc SQUID that contains two Josephson junctions as described above and depends on the dc interference; the other is an rf SQUID that contains only one junction. [95] In our experiment, we used two dc SQUIDs that were made by Quantum Design. The SQUID probes were attached to the liquid helium dewar inner wall, each inductively connected to a TiNb coil at one end, and to a preamplifier on the top of the detector at the other end. The signals from the preamplifiers were sent to two SQUID controllers external to the detector and to the DAQ (Data Acquisition System). The SQUID electronics is shown in Figure 5.5.

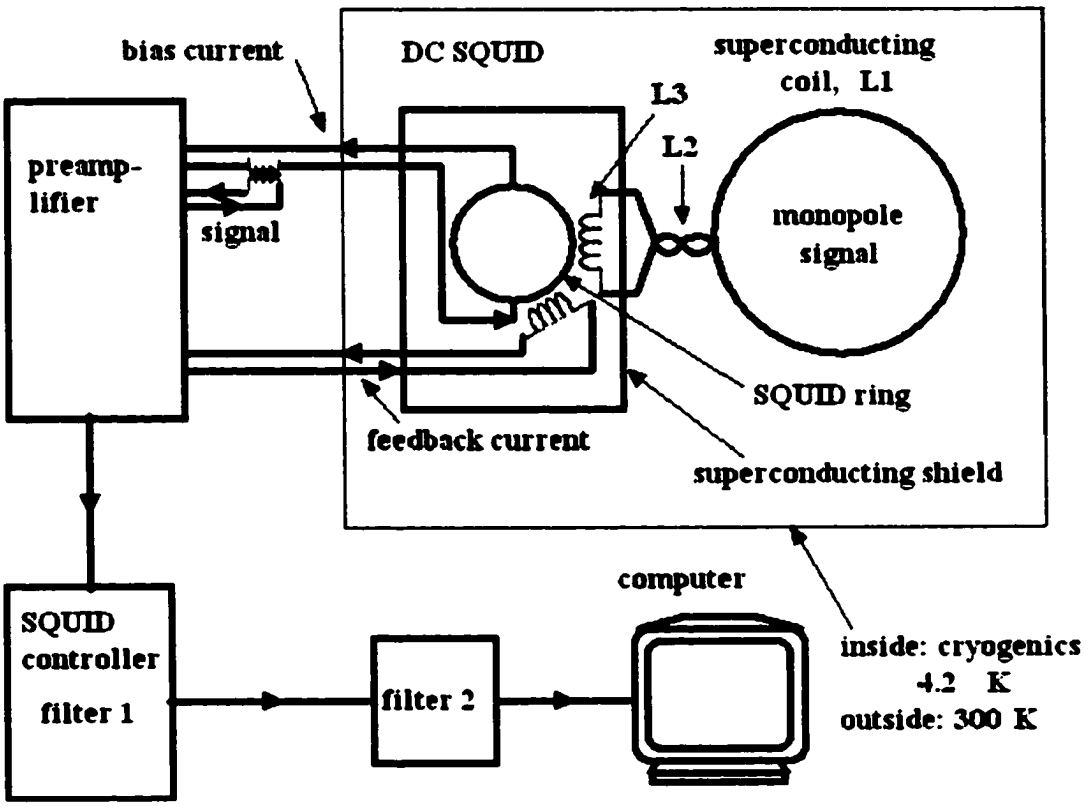


Figure 5.5 The flux passed through the superconducting coil is converted into a current change that induces a flux change in the DC SQUID ring, which induces a feedback current and is converted into an amplified voltage as an output signal to the DAQ.

5.4 Cryogenics

In order to create superconductivity, we need to produce low temperature. The temperature (~ 9 K) required for the SQUIDs and the superconducting coils we choose can be produced by liquid helium (4.2 K). But the liquid helium is boiling off all the time. Thus, in order to keep the superconductivity long enough for us to efficiently measure monopole samples, we need to maintain a low helium boil off rate. The helium boil off or loss rate is related to the thermal conductivity of the helium dewar and the residual gas as well as infrared radiation. We use vacuum pumping and other means to reduce conduction and radiation to keep the helium boil off rate as low as possible.

As we have noted, the nitrogen dewar and helium dewar were installed in a large cylindrical tank of steel in which a vacuum was prepared between the dewars and the walls of the tank. The tank had an inner wall and an outer wall. It was 152 cm long and had a radius of 23 cm for the outer wall. The inner warm bore wall was a G-10 tube of 10.5 cm in radius. G-10 is an electrically non-conductive fiber glass reinforced plastic, and it was used to reduce thermal noise. We used liquid nitrogen to pre-cool the detector (~ 77 K) and provide a radiation shield for the helium. The nitrogen dewar was made of aluminum and also concentrically placed between the helium dewar and the outer wall of the tank See Figure 5.1.

We used an oil diffusion pump backed by a mechanical pump to pump down the vacuum space in the detector from its bottom. An ionization pressure gauge was installed at the top of the detector to read the vacuum pressure. We could attain a vacuum ~ 10^{-5} torr with liquid helium in the internal dewar, which is good enough for the experiment.

Radiation and gas conduction in the vacuum space contribute to the liquid helium boil off rate. They were reduced by the installation of superinsulation material in the vacuum space. The superinsulation material is a thin (~ 0.02 mm) mylar film aluminized

on both sides, and has a high reflectivity in the infrared region. We wrapped the helium dewar with ~ 20 layers of superinsulation and the nitrogen dewar with ~ 30 layers for both inner and outer shields. Also we wrapped the G-10 tube with ~ 2 layers of superinsulation. To avoid electrical contact between layers, we spaced superinsulation with nylon material (Remay) between each layer. The heat loss with the superinsulation installed can be estimated based on the empirical curve in Figure 5.6. By multiplying the area (~ 1.5 m^2) of the superinsulation layers and using the conversion between the helium level or volume and the helium percentage in the dewar:

$$30 \text{ inches} = 100\%, 3\% = 1 \text{liter}, \tag{5.28}$$

and the liquid helium heat-volume conversion:

$$1 \text{Watt} = 1 \text{liter/hour}, \tag{5.29}$$

the heat loss rate can be converted into helium boil off rate in terms of the loss of percentage of the liquid helium in the dewar per hour with respect to the vacuum pressure: (see Figure 5.7)

$$\dot{P}_l = 0.3\%/\text{hour} + 9\%/\text{hour}\left(\frac{p}{5 \times 10^{-4}\text{Torr}}\right), \tag{5.30}$$

where p is the vacuum pressure in the helium dewar. The first term corresponds to radiation and the second term corresponds to conduction.

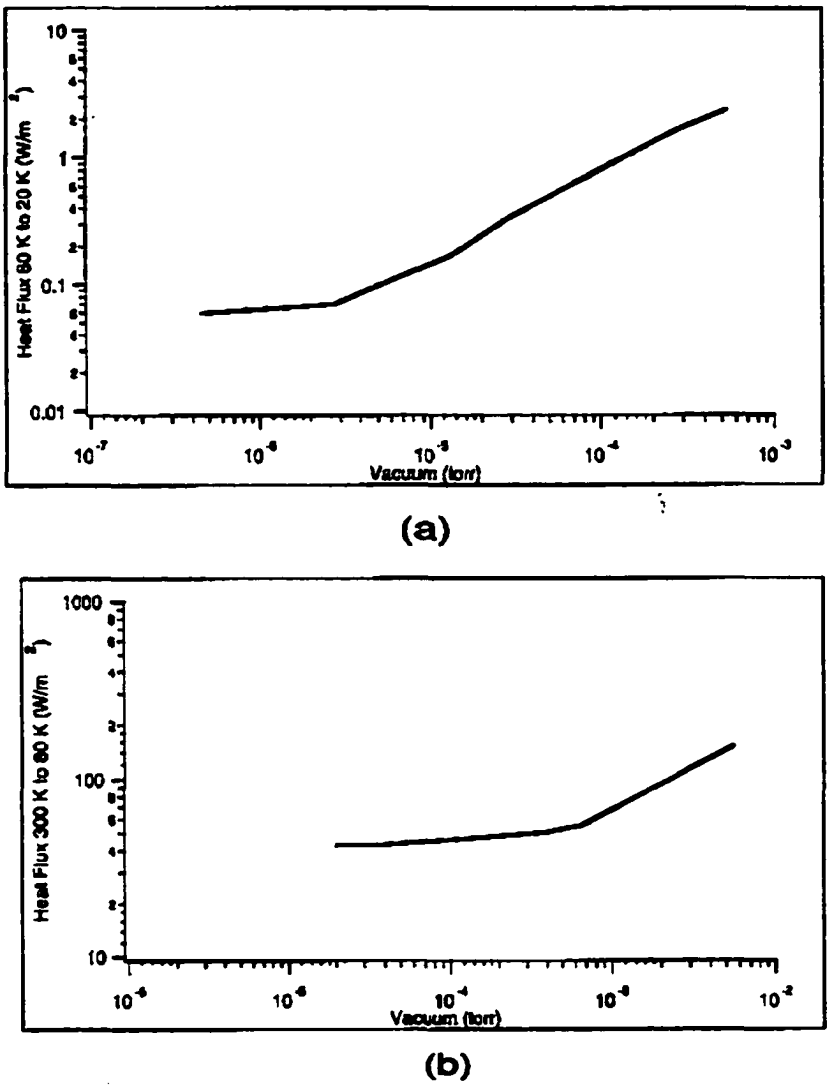


Figure 5.6 Heat flux vs vacuum: (a) from 80 K to 20 K (to LHe dewar); [96] (b) from 300 K to 80 K (to LN_2 dewar) [97] for ~ 10 layers of superinsulation.

In addition, the conduction down the liquid helium dewar contributed to the helium boil off rate. Suppose that the helium dewar has a cross-sectional area A, which is in the horizontal plane, and a change in temperature ΔT when one makes a change in vertical position Δz. The heat loss $\dot{Q}\left(\frac{dQ}{dt}\right)$ is a function of A and temperature gradient

$$\dot{Q} = \frac{\alpha \Delta T A}{\Delta z}, \tag{5.31}$$

where α is the heat loss coefficient, which is a function of temperature; for stainless steel, α has values of 0.3 W/K•m at 4 K, 0.7 W/K•m at 10 K, 5 W/K•m at 40 K, and 8 W/K•m at 80 K, and can be approximated as $\alpha \approx 0.1T$. Then,

$$\dot{Q} = \frac{\alpha \Delta T A}{\Delta z} \approx 0.1T \frac{dT}{dz} A = \frac{1}{20} \frac{dT^2}{dz} A. \tag{5.32}$$

The region above the liquid helium level ($z \geq 0$, 77 K$\geq T \geq$ 4.2 K) was mainly responsible for the heat conduction. Integrating from 0 to $z = L$, and T_0 (4.2K) to T (77 K), we get

$$\dot{Q} \approx \frac{1}{20} \frac{T^2}{L} A = \frac{AT^2}{20L}, \tag{5.33}$$

where $A = 8 \times 10^{-4}$ m^2, L is the distance between the liquid helium surface and the top of the helium dewar. $L = 7.5 + d$ in inches, where d is the distance between the helium level and the highest helium level where helium could be filled (117%), and 7.5 in is the distance between the highest helium level and the top of the helium dewar. Using the conversions above, we convert heat loss to $77K$ into helium loss or boil off rate as a function of the helium percentage (LHe refers to the % fill as defined above)

$$\dot{P}_2 = \frac{36}{7.5 + 0.30(117 - \text{LHe})} (\%/\text{hour}). \tag{5.34}$$

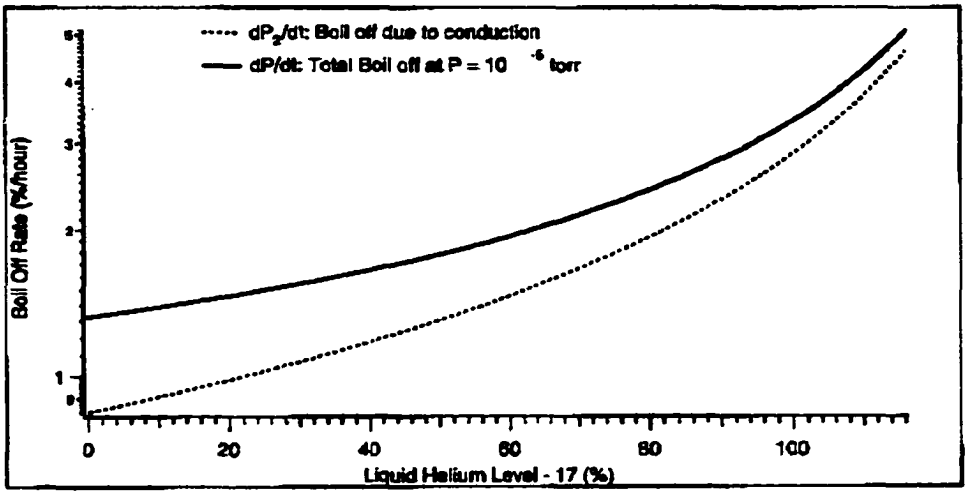
This is the loss due to conduction.

Resistance heating (up to 75 mW) in the "normal" part of the liquid helium monitor (a 60-inch long conductor folded in half) immersed in helium, when it was turned on,

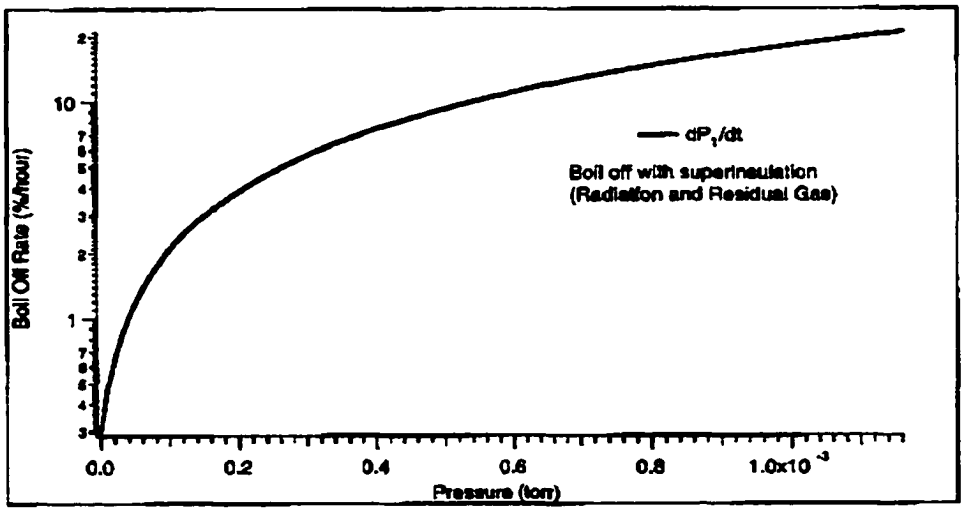
also caused a significant boil off rate; we turned it off when measuring samples. Thus, the total helium boil off rate at $p = 1.0 \times 10^{-5}$ torr, the pressure we used for the measurement, will be

$$\dot{P}_T = P_1(\sim 0.5) + \dot{P}_2 \ . \tag{5.35}$$

$\dot{P}_T$, $\dot{P}_1$, and $\dot{P}_2$ are plotted in Figure 5.7. We observed ~ 1.7%/hour under steady continuous operation with a 20% fill, which agrees with the $\dot{P}_T$ curve.



(a)



(b)

Figure 5.7 (a) The liquid helium boil off rate dP_2/dt caused by the conduction in the dewar wall and the total liquid helium boil off rate dP/dt vs helium level; (b) the liquid helium boil off rate dP_1/dt caused by the radiation and conduction of the residual gas in the vacuum space vs vacuum pressure.

There are three steps to cool down the system. First, we establish a vacuum by running the mechanical and diffusion pumps to pump down to ~ 10^{-4} torr. Secondly, we transfer liquid nitrogen to cool the detector down to ~ 77°. This will take about one week. Before we transferred liquid nitrogen into the nitrogen dewar, however, we had to fill the liquid helium dewar with helium gas to keep out air and water from the helium dewar and the He transfer line. If we did not do this, the moisture might ice up and block the transfer line. We needed to perform a helium transfer once daily to operate continuously for an extended time. The nitrogen transfer (about once daily) was controlled automatically by sensors and a controller. A computer was used to monitor nitrogen filling. The time interval between nitrogen fills was about 20 hours without liquid helium inside the helium dewar, and about 25 hours with liquid helium inside the helium dewar.

The last step is to transfer liquid helium to prepare for the operation of the SQUIDs and the superconducting coils. The liquid helium transferring with the SQUIDs off was done manually. To conserve expensive liquid helium, the helium transfer rate is important. If the rate is too high, helium is evaporated inefficiently by not cooling the detector and this valuable commodity is wasted. We adjusted the rate by keeping ~ 2 lb of overpressure in the LHe supply dewar. It took about 40 minutes to complete liquid helium transfer. Eight carbon resistors were installed in the helium dewar at different heights to measure the temperatures at the corresponding positions. We transferred about 35 – 40 liters of liquid helium (the helium controller read about 24 – 30% of the helium dewar, 3% ≈ 1 liter) each time, and waited for about two hours for stabilizaction of the SQUID outputs until the helium level then dropped close to where the superconducting coils (~ 16%) were located. Also, the helium boil off rate dropped to about 2% per hour, which was close to the calculated rate. That amount of helium could last, at that a boil off rate, for about 18 hours during which we could measure about 22 samples plus 8 runs on the one chosen background sample. With liquid nitrogen filling into the nitrogen

dewar, the vacuum would be improved because of cryo-pumping (absorption of gas by the cold porous surface [26]). And with liquid helium filling the helium dewar, the vacuum could reach $\leq 10^{-5}$ for the same reason, at a temperature of 4.2 K. The detector now is ready to operate the superconducting coils and the SQUIDs.

5.5 Noise

Noise is always a problem in detecting monopoles. We had to deal with three different types of noise: thermal noise, mechanical noise, and electronic noise.

Thermal Noise

Thermal noise is generated by Brownian motion of electrons in a resistor or other electric circuit. It exists wherever the temperature is greater than 0 K. The intrinsic noise due to a SQUID has been estimated to be of the order of $10^{-4}\Phi_0/\sqrt{\text{Hz}}$ ($\sim 10^{-11}$ G•cm$^2/\sqrt{\text{Hz}}$) and can be ignored. [98] But the liquid helium dewar was made of stainless steel and its inner wall was inside the coils. We know that stainless steel is electrically conductive and, thus, a source of thermal noise. Another steel wall at liquid nitrogen temperature to enclose the inner wall of the helium dewar was also placed concentrically inside the detection coils. So we should study the thermal noise in the stainless dewar and this steel wall and see how much the thermal noise influenced our measurement.

In general, in any resistor, the random Brownian motion causes a small fluctuating voltage across the resistor. The average voltage is zero, but the mean square voltage is not zero. The mean square voltage developed by a resistor in any frequency interval df is given by [99]

$$d\langle V^2\rangle = 4kTRdf, \tag{5.36}$$

where k is the Boltzmann constant, T the temperature, R the resistance. Then

$$d\langle I^2\rangle = \frac{4kTdf}{R}. \tag{5.37}$$

This fluctuating current gives rise to a fluctuating magnetic field set up in a circuit of inductance of L. Since $\Phi = BS = LI$, we get

$$d\langle B^2\rangle = \frac{4kTL^2df}{S^2R}. \tag{5.38}$$

Here S is the area of the horizontal cross section of the dewar, and L is the inductance of the dewar. If we consider the dewar as a one turn solenoid, we have

$$L = \frac{\mu_0 NS}{l},\ S = \pi r^2,\ N = 1, \text{ and } R = \rho\frac{c}{S_c} = \frac{2\pi r\rho}{lt} \tag{5.39}$$

where l is the length of the dewar, r the radius of the dewar, ρ the resistivity, t the thickness, c the perimeter, and S_c the area of the vertical section of the metal portion of the dewar. Thus,

$$d\langle B^2\rangle = \frac{32\pi \times 10^{-14}kTt}{\rho rl}df \text{ in Tesla}^2 \bullet \text{Hz}. \tag{5.40}$$

We set $df = 1$ Hz, $T \approx 10$ K (an approximation, higher than the He temperature but lower than the N_2 temperature), and $\rho = 5.0 \times 10^{-7}/\Omega \bullet m$. For the helium dewar, $l = 1.397$ m, $t = 0.0006$ m, $r = 0.0855$ m. Thus we obtain the field fluctuation caused by the helium dewar

$$d\langle B^2\rangle = \frac{32\pi \times 10^{-14} \times 1.38 \times 10^{-23} \times 10 \times 0.0006}{5 \times 10^{-7} \times 0.0855 \times 1.397} = 1.4 \times 10^{-30} Tesla^2 \bullet Hz. \tag{5.41}$$

and the flux fluctuation or thermal noise

$$\Delta\Phi_1 = (d\langle B^2\rangle S^2)^{1/2} = \left(1.4\times10^{-30}\times(\pi\times0.0855^2)^2\right)^{1/2}$$
$$= 2.7\times10^{-17} Tesla\bullet m^2\bullet\sqrt{\text{Hz}} = 2.7\times10^{-9} Gauss\bullet cm^2\bullet\sqrt{\text{Hz}} \tag{5.42}$$

For the steel wall between the G-10 and the helium dewar at the liquid nitrogen temperature (77 K), l = 1.22 m, t = 0.0006 m, r = 0.0635 m. Thus the field fluctuation caused by the steel wall is

$$d\langle B^2\rangle = \frac{32\pi\times10^{-14}kTt}{\rho rl}df = \frac{32\pi\times10^{-14}\times1.38\times10^{-23}\times77\times0.0006}{5\times10^{-7}\times0.0635\times1.22}$$
$$= 16.55\times10^{-30}\ \text{Tesla}^2\bullet\text{Hz}\,, \tag{5.43}$$

and the flux fluctuation or thermal noise is

$$\Delta\Phi_2 = (d\langle B^2\rangle S^2)^{1/2} = \left(16.55\times10^{-30}\times(\pi\times0.0635^2)^2\right)^{1/2}$$
$$= 5.15\times10^{-17}\ \text{Tesla}\bullet\text{m}^2\bullet\sqrt{\text{Hz}} = 5.2\times10^{-9}\ \text{Gauss}\bullet\text{cm}^2\bullet\sqrt{\text{Hz}}\,, \tag{5.44}$$

So the total flux fluctuation per Hz is

$$\Delta\Phi_T = \sqrt{\Delta\Phi_1^2+\Delta\Phi_2^2} = 5.8\times10^{-9}\ \text{Gauss}\bullet\text{cm}^2. \tag{5.45}$$

Compared with the flux of one monopole, $\Phi_g = 4.14\times10^{-7}$Gauss•cm^2, the thermal noise $\Delta\Phi_T$ should be quite negligible.

Mechanical Noise

There were two sources of mechanical noise that affected signals: internal liquid helium boiling and external vibration caused by the environment. When the helium dewar is

filled with liquid helium, the helium is boiling and the helium bubbles hit the coils and make the coils move slightly. This causes a change of flux, or noise. Therefore, the liquid helium level inside the dewar is related to this type of noise which affected the SQUID signals. In the beginning, we tried to fill as much helium as we could, e.g., 80% of the dewar (32 liters), to keep low temperature for a long time. However, the more helium transferred, the longer the helium boiling noise lasted. This type of noise caused a large fluctuation of signals that made data taking impossible. We finally found that when the helium level fell below the detection coils, the SQUIDs abruptly became very stable. (Jeon also observed this phenomena. [26]) Presumably, this was because the helium bubbles did not interact directly with the coils at that position. We took data when the liquid helium fell below that level.

Our apparatus was set up in a building with a high ceiling (~ 15 m), which is near an airport. To reduce the vibrations caused by the environment including the ground and airplanes, the detector was suspended from a large aluminum frame by 12 aluminum rods each bolted to the frame via a vibration damper. (see Figure 5.8) The aluminum frame was anchored on one wall of the building. The vibration of the wall would propagate to the frame. Also the vibration coming from the ground, which was partly caused by airplanes landing and taking off, would cause vibration of the frame. Four of the supports could be adjusted along the vertical direction, while the other eight supports could be adjusted along horizontal directions. There were also 12 dampers filled with air at a chosen pressure (vertical pressure is 38 lb, horizontal pressure is 33 lb) to further reduce vibration. We used an accelerometer to measure the vibration of the detector and recorded it with the Labview program (by National Instruments). The typical vibration (as a velocity) was around 10 – 15 mV (peak-to-peak, ~ 10^{-3} cm/second) as measured by the accelerometer, which turns out to be good enough for data collection. Therefore, the mechanical noise in our experiment is sufficiently under control.

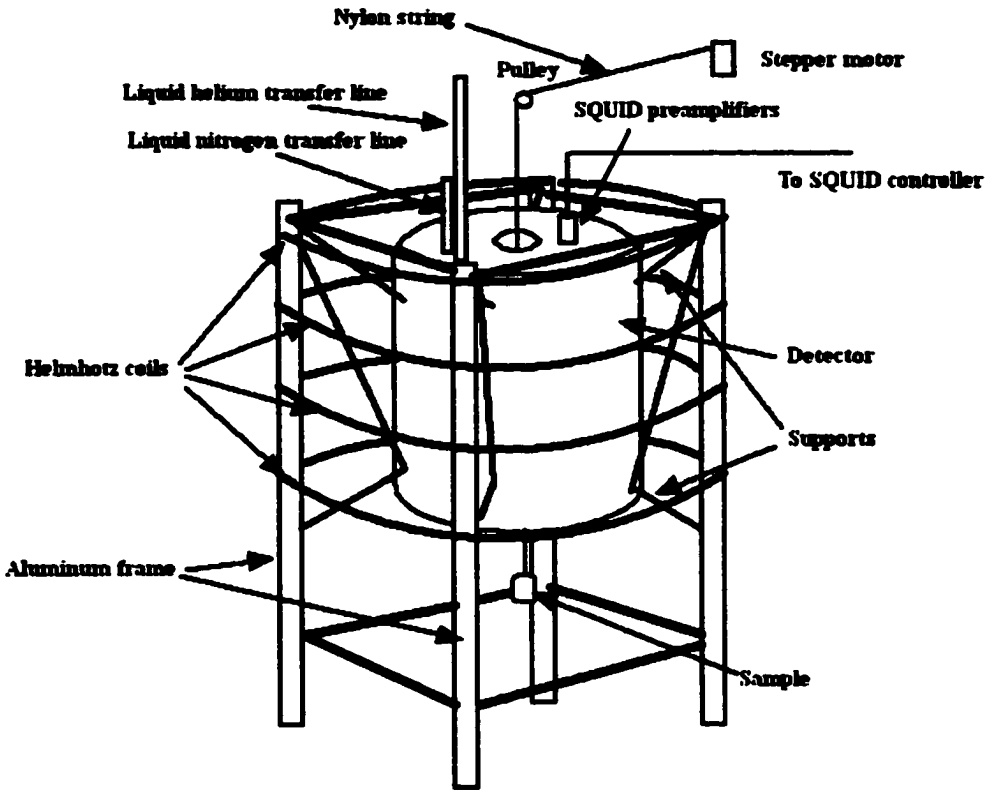


Figure 5.8 The monopole detector suspended on the aluminum frame. The stepper motor is anchored on the wall of the building.

Electronic Noise

We have observed that the SQUIDs were very sensitive to electronic noise that caused the output signals to jump drastically on the computer screen. Since we had to run 20 up-and-down cycles for each sample to obtain statistically satisfactory results and we had over 1000 samples (about 222 aluminum samples and 800 lead samples) to measure continuously over a period of time (e.g., one month), we must reduce the electronic noise effectively to keep the SQUIDs stable for a sufficient length of time.

However, controlling the electronic noise was very difficult as it was hard to identify

the sources. In principle, any electronic devices and elements cause electronic noise. We tested all the devices we used, i.e., vacuum pump station, printer, computers, various electronic meters, resistors inside the dewars, refrigerator, fans, etc.. Also we checked environmental factors such as weather and airplanes, as well as some devices other people used nearby, such as lasers, welding equipment, and public clocks. We have observed that SQUIDs did not operate well during thunderstorms and welding. The liquid helium level detector, liquid nitrogen filling controller, and the resistors inside the helium dewar, also caused the SQUIDs' signal to "jump" (i.e., reset the SQUID controllers at random times). It was reasonably easy to find that a periodic (1 minute) noise of 20 mV magnitude for 4 seconds which bothered us was caused by an IBM clock outside of the laboratory. We modified the Labview DAQ program and only took data when this was not present. Also, it took some time to find that the ground current loops and associated noise from electronic connection between the devices. The counter weights used to balance the sample (when the sample was moved up and down) had an interaction with the SQUID preamplifiers on the top of the tank and induced electronic noise.

In dealing with those electronic noises, we cut off ground current loops, set an electronic shield between the weights and the SQUID preamplifiers, and turned off the devices that affected the SQUIDs when we took data. Also, we avoided operating the apparatus during thunderstorms and welding operation. As a result, the electronic noise has been significantly reduced and operation became possible.

5.6 Stabilizing, Reducing, and Homogenizing the Ambient Magnetic Field

The ambient magnetic field in the detector comes mainly from the earth's field and also comes from the electronic devices and the environment. The earth has a magnetic field of about –470 mG, which at our location points down at an angle of ~ 75° with respect to the vertical direction. The vacuum tank was made of mild steel and can reduce

the earth's field inside the tank. A Mu metal shield attached to the inside of the tank also helped reduce the earth's field. However, the distribution of the ambient field inside the detector was not uniform. The variation of the field caused by inhomogeneous ferromagnetic materials and noises could affect the monopole signature. The Mu shield actually helped homogenize the field distribution. Also we installed two degaussing coils, each consisting of 280 turns of copper wire on the extension of the vacuum tank, to reduce and homogenize its inhomogeneous magnetization with an AC current ($I \sim 2.3$ A, 60 Hz). But there was still a significant gradient in the magnetic field strength. Especially, after liquid helium was filled and the lead shield became superconducting, magnetic flux was trapped in the warm bore and changed somewhat the gradient of the field distribution. Since it is impossible to completely cancel the ambient field, the best thing we could do was to make the ambient field as small and flat as possible in the region close to the detection coils. In a homogenous ambient field the monopole signature would not be affected.

We used a modified Helmholtz coil arrangement in addition to the Mu shield and the degaussing coils to reduce and homogenize the ambient field. The Helmholtz coils consist of two pairs of two coils. Each coil consists 40 turns of copper wire. The radius of the coils is 1.0 meter. The four coils were installed from at the bottom of the tank to the top at equal distance, surrounding the tank along the center axis. We input different currents for each pair. For the bottom pair, we used large current I_b (0.70A) to reduce the opposing earth's field; a smaller current I_t (–0.3 A) was used for the top pair to balance the bottom coils. Figure 5.9 shows the Helmholtz coils set-up. We did not obtain a perfectly uniform field along the warm bore, but the field distribution we used in Figure 5.10 was sufficiently good for us to take data.

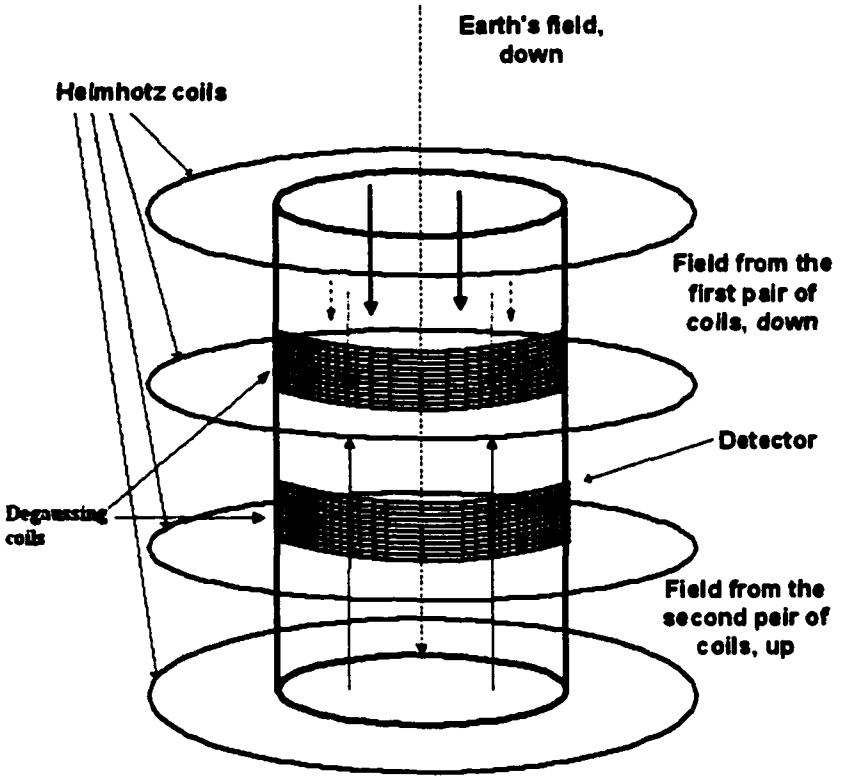


Figure 5.9 The "Helmholtz" coils and degauss coils. The bottom Helmholtz coil pair produces a field to reduce the earth's field while the top one produces a field to balance the bottom's field. Each coil has different current, which is different from the original Helmholtz coil setting with two currents of equal magnitude but opposite directions.[100]

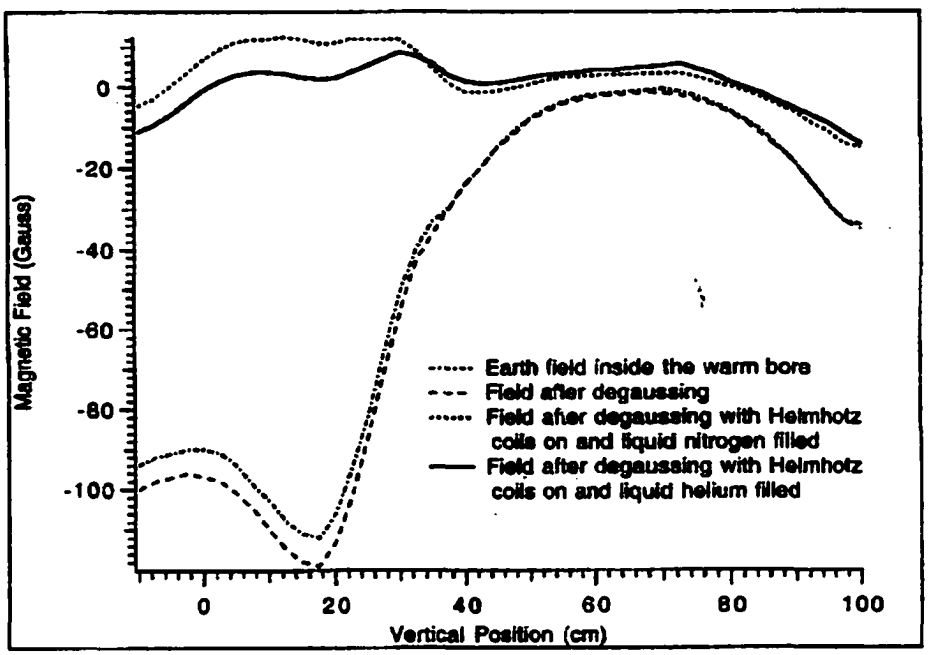


Figure 5.10 Magnetic field distributions, as indicated.

The ambient magnetic field may fluctuate due to the changes in the environment. A superconducting shield was installed in the liquid helium dewar to reduce such fluctuation. The superconducting shield we used is a lead sheet. The thickness of the sheet is 0.2 mm and the superconducting transition temperature is 7.32 K. In most cases, significant fluctuations were not observed during the operation of SQUIDs. We only observed that welding, airplane taking off and landing, and thunderstorms had interference with the SQUIDs and maybe the field also, so we avoided operation in those cases.

5.7 Calibration of the Detector and Monopole Signal

The monopole signal is read by the SQUIDs in terms of a voltage that is converted from the current induced by the flux linking the superconducting loop. The flux linking the

superconducting loop is converted into the flux going through the paired Josephson junction loop, which induces a readable voltage change as the output from the SQUID. [see Figure 5.5] The relationship between the input flux and the output voltage is determined by the transfer function. The transfer function is defined by

$$TF = \frac{\Delta V}{\Delta \Phi}(\mathrm{mV}/\Phi_0) = \left(\frac{\Delta V}{\Delta \Phi_s}\right)\left(\frac{\Delta \Phi_s}{\Delta I}\right)\left(\frac{\Delta I}{\Delta \Phi}\right), \tag{5.56}$$

where $\Phi_0 = \frac{4\pi g_D}{2} = 2.07 \times 10^{-7}\mathrm{G{\cdot}cm^2}$ (1 superconducting fluxoid unit), $\Delta\Phi_s$ the flux change in the SQUID, $\Delta\Phi$ the flux change in the detection coil, ΔI the induced current change in the SQUID, and $\left(\frac{\Delta V}{\Delta \Phi_s}\right), \left(\frac{\Delta \Phi_s}{\Delta I}\right), \left(\frac{\Delta I}{\Delta \Phi}\right)$ are the conversion factors that depend on the features of the SQUID and the setting of the apparatus. For the SQUIDs we used, $\left(\frac{\Delta \Phi_s}{\Delta I}\right) = 4.60\ \Phi_0/\mu\mathrm{A}$, (calibration of SQUID sensor as supplied by Quantum Design), and $\left(\frac{\Delta V}{\Delta \Phi_s}\right)$ was measured (by a test pulse injection procedure) to be 0.60 V/Φ_0. We proceed to calculate $\left(\frac{\Delta I}{\Delta \Phi}\right)$.

In our apparatus, the superconducting coil of radius a was surrounded by a superconducting cylinder of radius b. According to K. Milton [92], if the wall of the cylinder is far away from the coil, or $\left(\frac{a}{b}\right)^2 \ll 1$, we have the flux for a single monopole passing through the coil (in Gaussian units)

$$\Phi = \frac{4\pi g}{c} = 2\Phi_0. \tag{5.57}$$

Correcting for $\left(\frac{a}{b}\right)^2$, we have

$$\Phi = \left(1 - \frac{a^2}{b^2}\right)\frac{4\pi g}{c}. \tag{5.58}$$

In our case, a = 3.88 in, b = 5.8 in, which give the factor $\left(1 - \frac{a^2}{b^2}\right)$ = 0.55, thus

$$\Phi \rightarrow 0.55\Phi. \tag{5.59}$$

Since the flux in a superconducting coil is conserved as a result of the Meisner effect, we have

$$\Phi + I(L_1 + L_2 + L_3) = \text{constant} = n\Phi_0. \tag{5.60}$$

where Φ is the total flux arising from the monopoles passing through the coil, I the induced current in the coil, L_1, L_2, and L_3 the self inductances of the detection coil, the interconnecting lead, and the input coil coupled to the SQUID ring, respectively (see Figure 5.5). For a one turn coil, the inductance L_1 can be obtained by [101]

$$L_1 = 0.004\pi a\left(\ln\frac{8a}{\rho} - 1.75\right). \tag{5.61}$$

Here a is the radius of the coil, ρ the wire radius, both in cm; L_1 is in μH. In our case, a = 3.88 in = 9.855 cm, and ρ = 0.008 in = 0.020 cm, which give L_1 = 0.807 μH. Considering that the interconnecting lead is a short twisted pair, we ignore L_2. The SQUID specification sheet gives L_3 = 1.66 μH. From above formula, we have

$$\Delta I = \frac{\Delta\Phi}{L_1 + L_2 + L_3}. \tag{5.62}$$

Considering the cylinder shield, it becomes

$$\Delta I = \frac{0.55 \times \Delta\Phi}{L_1 + L_2 + L_3} = \frac{0.55 \times \Delta\Phi}{0.81 + 0 + 1.66}. \tag{5.63}$$

Therefore, if $\Delta\Phi = 1\Phi_0$, $\Delta I = 0.224\ \Phi_0/\mu\text{H} = 0.46 \times 10^{-9}$ A, or

$$\frac{\Delta I}{\Delta \Phi} = 0.46 \times 10^{-9}\ \mathrm{A}/\Phi_0. \tag{5.64}$$

Thus, we obtain the transfer function for the SQUID

$$\begin{aligned} TF = \frac{\Delta V}{\Delta \Phi}(mV/F_0) &= \left(\frac{\Delta V}{\Delta \Phi_s}\right)\left(\frac{\Delta \Phi_s}{\Delta I}\right)\left(\frac{\Delta I}{\Delta \Phi}\right) \\ &= 0.60(V/\Phi_0) \times 4.6(\Phi_0/\mu A) \times 0.46 \times 10^{-9}(A/\Phi_0) \\ &= 1.27 mV/\Phi_0 = 2.5 mV/\Phi_s. \end{aligned} \tag{5.65}$$

This is just the "a priori"expected response.

To determine the actual response, we used a pseudopole to calibrate our detector. The pseudopole was a solenoid as shown in Figure 5.11.

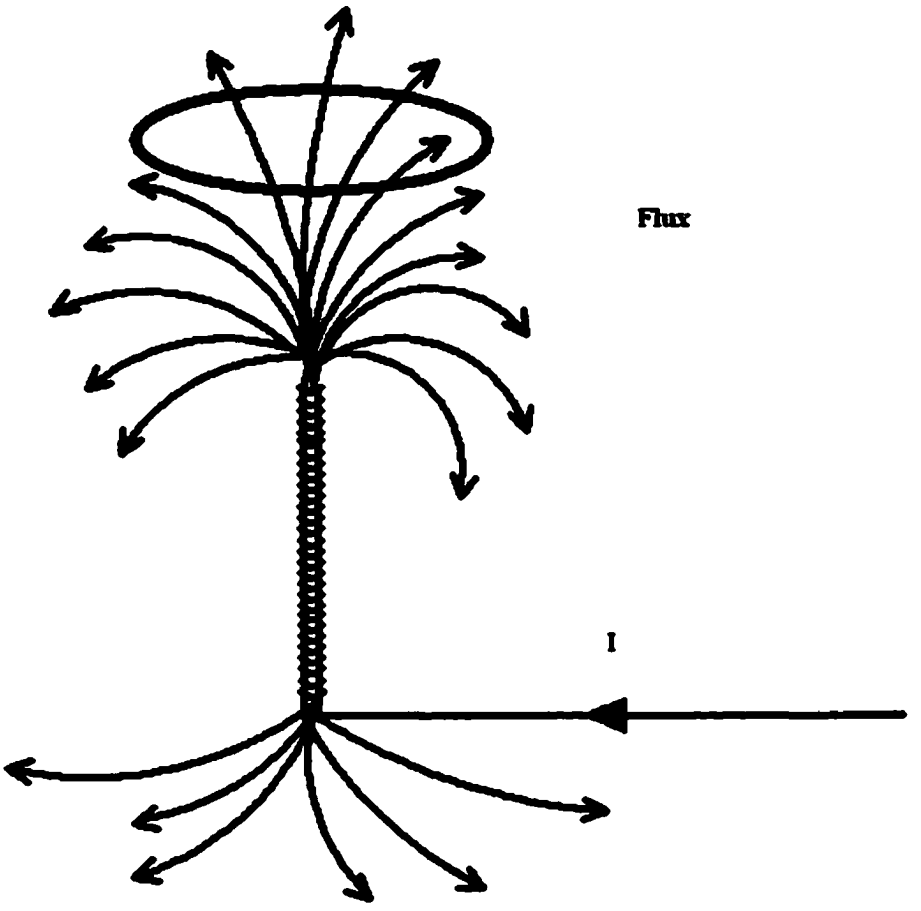


Figure 5.11 One end of the pseudopole mimics a monopole of a magnitude corresponding to the current *I*.

The calibration included two steps. First, we put one end of the pseudopole in the superconducting coil and turned on and off the current in the pseudopole, which simulated the presence of monopoles. We tried several different values of the current in the pseudopole, which corresponded to different values of monopole charge or different number of of monopoles . The relation between the current and the effective magnetic charge was linear, which is shown in Figure 5.12.

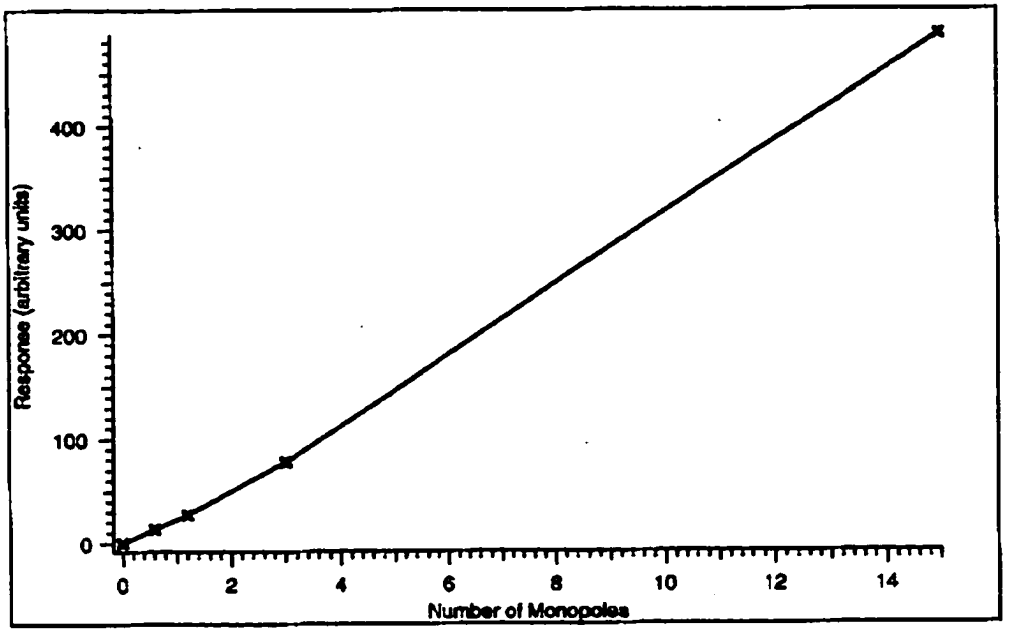


Figure 5.12 Relative calibration via Fourier transforms using on/off switching of pseudopole. The response (proportional to the output voltage) is proportional to the number of monopoles.

Then, we read the output values of voltage by the Labview program and divided the outputs by the corresponding number of monopoles, thus obtained the actual measured transfer function: 2.4 mV/Φ_g. The estimated value above is very close to the actual value. Also we moved the pseudopole up and down to simulate a monopole tranversing the coil, then we obtained a step curve. Figure 5.13 shows a pseudopole-simulated

monopole curve (~ 60 monopoles) and a dipole curve.

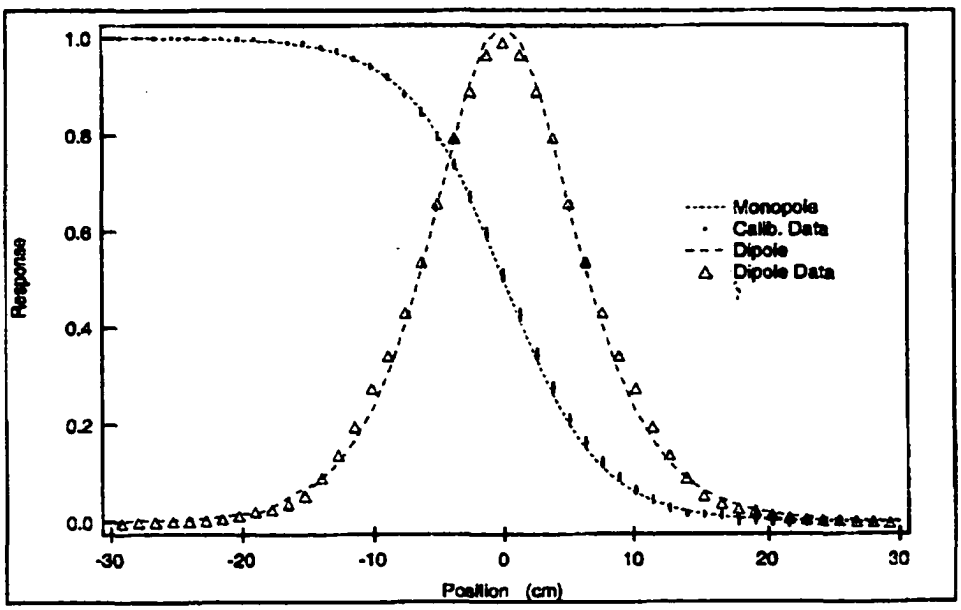


Figure 5.13 A monopole curve and a dipole curve obtained from the pseudopole. The values from calculation agree with the measurement.

Second, we bound the end of pseudopole to an Al sample, and set a current to give a flux corresponding to a given number of monopoles. Then we let it transverse up and down through the superconducting coils. The signal simulated monopoles in the sample. In this way we see what a monopole signal really would look like. The signal of the pseudopole (~ 2.3 poles) in a sample containing dipoles is shown in Figure 5.14, and, again, gives

$$5.5 \text{ mV}/2.3 \text{ poles} = 2.4 \text{ mV/pole}. \qquad (5.66)$$

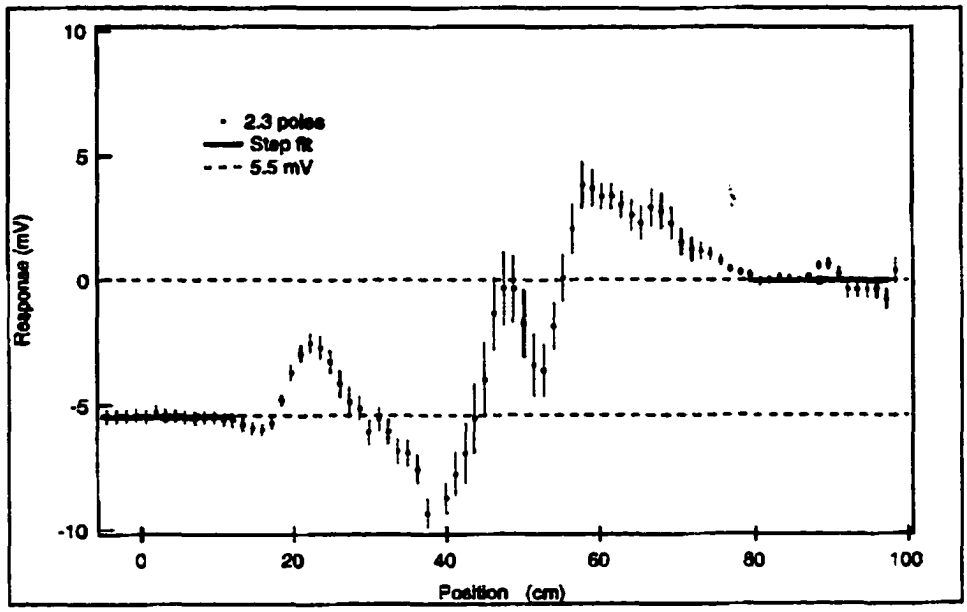


Figure 5.14 Calibrated monopole signal gives (5.66)

Chapter 6

Analysis and Results

6.1 The Strategy of Analysis

As stated in the introduction, the search for monopoles has one main objective: to set new limits on the production cross section and mass of monopoles. Finding monopoles means seeing the "step" signals that match the monopole signatures (e.g., 2.4 mV step signal from the SQUID for an $n = 1$ monopole). We shall find a limit on the number of possible events based on a statistical analysis of the steps. This number N can be used to set a limit on the cross section σ and accepted cross section σ_A by

$$\sigma \leq \frac{N}{\epsilon AL} \text{ and } \sigma_A \leq \frac{N}{\epsilon L}, \sigma_A = \sigma A \tag{6.1}$$

where ϵ is the efficiency of using samples, A the acceptance for detection of monopoles in samples, and L the luminosity of proton-antiproton colliding beams in the Tevatron. Then, we use the Drell-Yan cross section curve, as a function of the monopole mass, to set the limit on monopole masses.

The probability for the production of monopoles is modelled by the monopole Drell-Yan cross section as discussed in Chapter 3. However, the probability for those monopoles to be detected has been significantly reduced by the energy loss and the angular cuts. Thus, only those that have high enough energies and move within the small solid angles exposed by the sample materials can be measured, which correspond to the cross section accepted, σ_A. The ratio σ_A/σ is defined as acceptance A.

We have written a Monte Carlo program (see Appendix) to calculate the Drell-Yan cross section σ and cross section accepted σ_A, using the energy loss of monopoles in the CDF and DØ detectors, to get the acceptance A. We also use this program to select CDF samples as it tells which part of the materials has a significant acceptance for monopoles and which does not, due to the 1.4 T solenoidal magnetic field. It turns out that not all the CDF Pb samples have a significant acceptance. The ratio of the number of samples used to all (used plus unused) is the efficiency ϵ.

The total luminosity L delivered by the Tevatron over the years of operation covered was determined by the CDF and DØcollaborations to be about $180 \pm 5\%$ pb^{-1}. [102]

6.2 Data Acquisition and Analysis

Monopole sample materials including Al cylinders, Be pipe, and Pb layers were cut into small pieces, each Al sample having a size less than 7.5 cm in diameter by 7.5 cm in length. A beryllium sample has a length of 7.6 cm, a diameter of 5.0 cm and a wall thickness of 0.5 cm. We put a sample in a carrier made of copper wires that was proven to be sufficiently unmagnetized and held by a nylon string connected to a stepper motor. The sample was moved up and down by the stepper motor through the superconducting loops for a meter long distance as one cycle. Each cycle took about one minute. We took 20 cycles for one sample. Also we measured the background (an empty carrier or a specified ordinary sample such as an Al sample) after every two or three samples.

The magnetic signals from the SQUIDs were the amplified analog voltages. They went into the SQUID controllers, passed through a low pass filter, and were displayed on a oscilloscope. Meanwhile, the signals coming out of the controllers were digitized by an Analog/Digital converter on a board in a Mac computer. The digitized signals (voltages) were simultaneously recorded and plotted out by the Labview program on the computer. The Labview (by National Instruments) data acquisition (DAQ) program had a data

taking rate of 1000 Hz. The 1000 numbers for one second were grouped by 100 and then averaged in each group. Thus, the program recorded 10 numbers from averaging for the signal per second. However, because the Labview program did not take exact 1000 numbers per second and less than 60 seconds were used for each minute, only about 9,000 numbers for one sample per channel were recorded.

The Labview DAQ had six channels receiving data for two SQUIDs (DC1 and DC2), vertical position of the sample read by an optical encoder, vibration noise read by an accelerometer, the time, and the number of increments taken by the step motor. These were displayed in four graphical windows on the computer screen so that we could monitor the data taking. The four windows are shown in Figure 6.1.

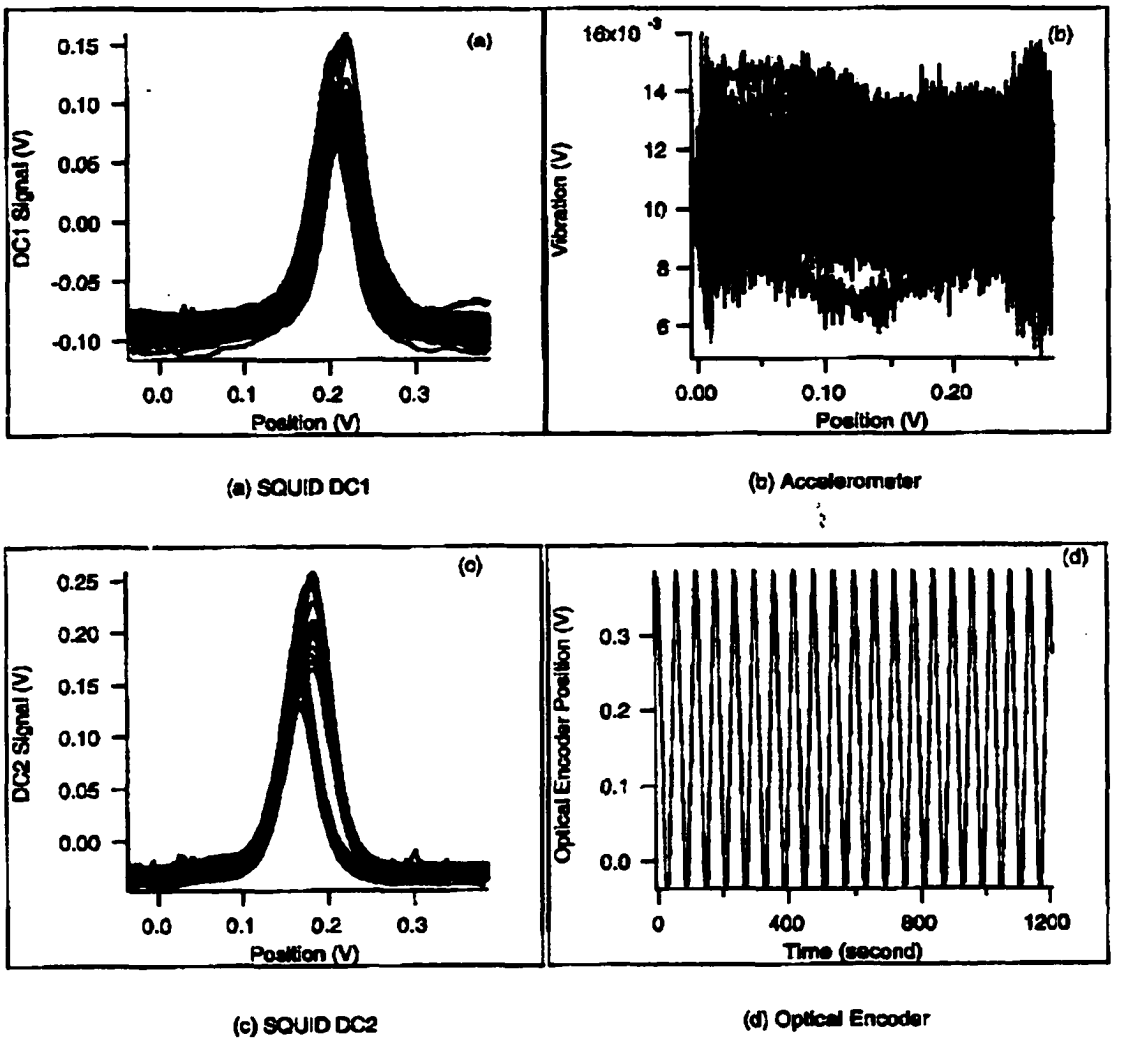
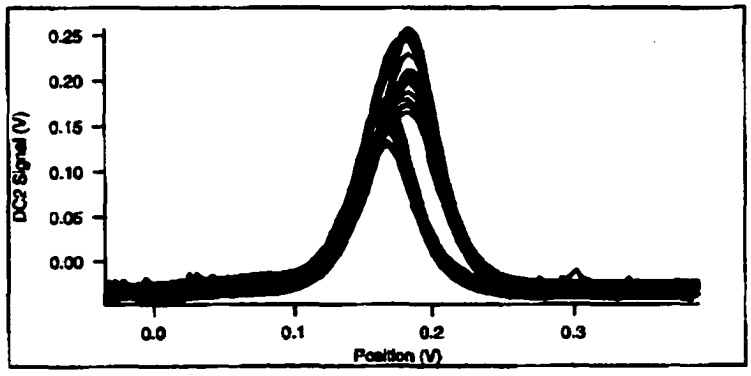


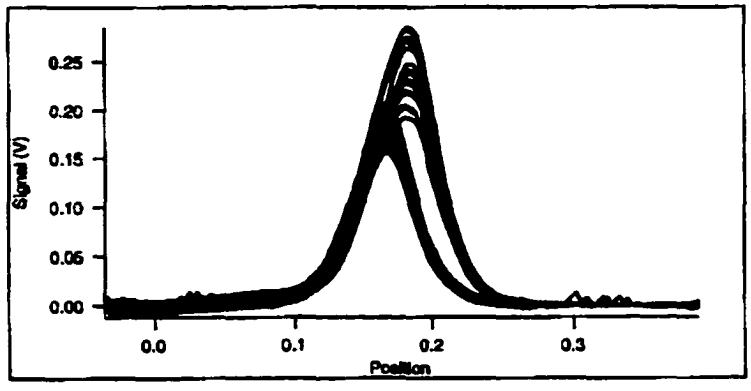
Figure 6.1 The Labview windows show the outputs: SQUIDs signal, position of a sample, and vibration noise.

The data analysis includes several steps. Since we had 20 cycles of traces for one sample and these traces were not at the same level because of the SQUID drift, the traces formed a band of width about 5 to 50 mV wide. The drift caused a larger error, but being linear caused no significant bias. Thus, we can compress the band by subtracting a value (that at one given position in one of the "flat end regions") from all traces. Then, the

errors from the random drift are canceled out. This is the first step. Second, we edit the compressed curves by throwing away those spurious numbers that were created by misbehaviors of the SQUIDs. Third, we group the 8,000 numbers into 92 position bins and take average of each group. Thus, we obtain 92 numbers for each sample, which forms the SQUID response vs vertical position curve. We perform the same procedure to process the data from both DC1 and DC2. Then, we take average between the DC1 and DC2 curves for each sample and subtract the background curve from the sample curve. Now we have obtained the processed signal curve for a sample. At last, we take average over ten numbers on the flat (not exactly flat in many cases) parts corresponding to the ends of two tails of the processed curve. There are 60 points between the two ten-points, which usually include useless signals such as magnetic dipoles in the sample and are excluded from the analysis. The first and the last few points (about 6 points) are also excluded as they are affected by the starting and stopping vibrations of the nylon string. Then we do a subtraction between the two endpoint values obtained from averaging. The value obtained from the subtraction is just the step that describes the magnetic signal in the sample. The procedure is shown in Figure 6.2.

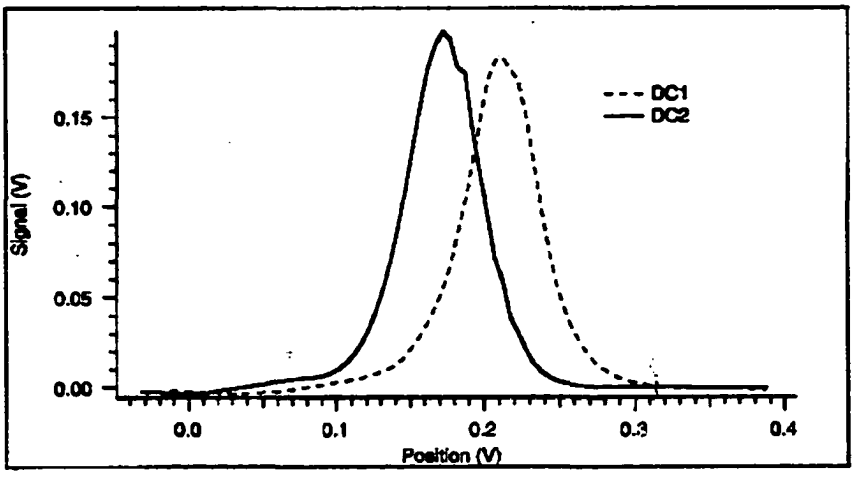


(a) Before compression

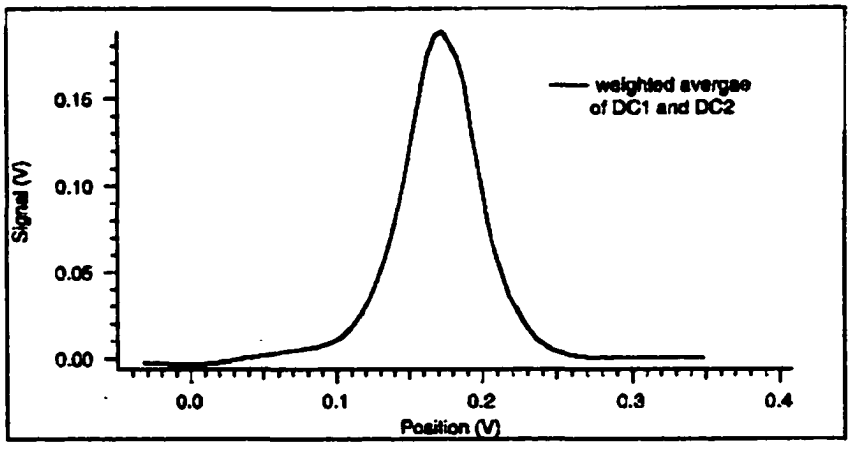


(b) After compression

(a) This sample has a big permanent dipole and a drift of typical ~ 25 mV. (b) Compress 20 traces to cancel linear drift.

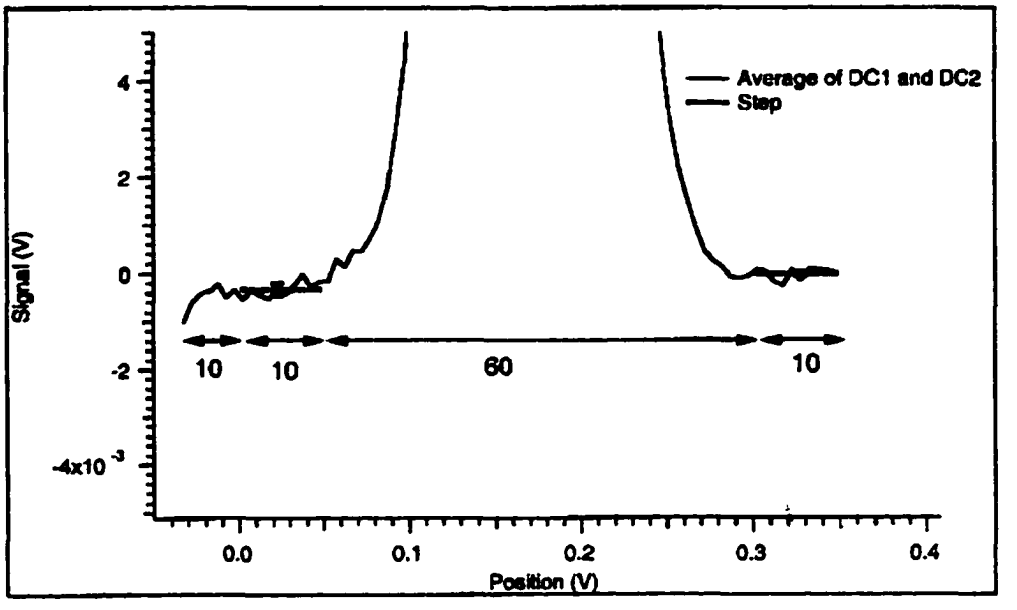


(c) Average of traces



(d) Average of DC1 and DC2 curves

(c) Average 20 traces obtained by each SQUID. (d) Average the two curves from DC1 and DC2.



(e) Take step and get results.

(e) Start from the 10th point in the left tail and take average over the following 10 points, then skip 60 points from some useless signals such as dipoles, and take average over the following 10 points in the right tail. The difference between the two values from averaging is the "step" for this sample.

Figure 6.2 The steps of data analysis.

The errors are also obtained from the analysis. There are two types of error: statistical error dS and systematic error sS. The statistical error is caused by signal drifting and all kinds of noise. The systematic error is caused by big dipoles in the sample, and the background change due to the changes in temperature and time. The systematic error usually changes the shape of the curve and make it difficult to determine

the true size of the steps. Now we will calculate those errors.

We know that compressing the 20 traces of data and averaging will produce errors at each point x, which can be described by the standard deviation. $\sigma_s^1(x)$ and $\sigma_s^2(x)$ are the standard deviations corresponding to DC1 and DC2. Then we do weighted average over the two curves to get an averaged signal curve $S^{12}(x)$ and error $\sigma_s^{12}(x)$ for the averaged curve. [103] We define a quantity d by

$$d(x) = \frac{1}{(\sigma_s^1(x))^2} + \frac{1}{(\sigma_s^2(x))^2}, \tag{6.2}$$

and the weighted average is

$$S^{12}(x) = \frac{\frac{S_1(x)}{(\sigma_s^1(x))^2} + \frac{S_2(x)}{(\sigma_s^2(x))^2}}{d(x)}, \tag{6.3}$$

and the weighted averaged error is

$$\sigma_s^{12}(x) = 1/\sqrt{d(x)}\,. \tag{6.4}$$

The value of the step is the difference between the two tails. We take 10 points close to each end, and take average over the 10 points, then we obtain the averaged values for two tails:

$$S_{T1} = \frac{\sum_{i=1}^{N} S^{12}(i)}{N}, S_{T2} = \frac{\sum_{i=K}^{N+K} S^{12}(i)}{N}, \tag{6.5}$$

where $N = 10$, and $K(= 60)$ is the distance between two tails. Thus the step is

$$S = S_{T2} - S_{T1}. \tag{6.6}$$

Also we get errors for two tails:

$$\sigma_{s1}^{12} = \frac{\sqrt{\sum_{i=1}^{N} \sigma_s^{12}(i)}}{N}, \sigma_{s2}^{12} = \frac{\sqrt{\sum_{i=K}^{N+K} \sigma_s^{12}(i)}}{N} \tag{6.7}$$

The statistical error for the step is given by

$$dS = \sqrt{(\sigma_{s1}^{12})^2 + (\sigma_{s2}^{12})^2}. \tag{6.8}$$

Similarly, we have

$$sS_1 = \sqrt{\frac{\sum_{i=1}^{N} (S^{12}(i))^2}{N} - S_{T1}^2}, \tag{6.9}$$

and

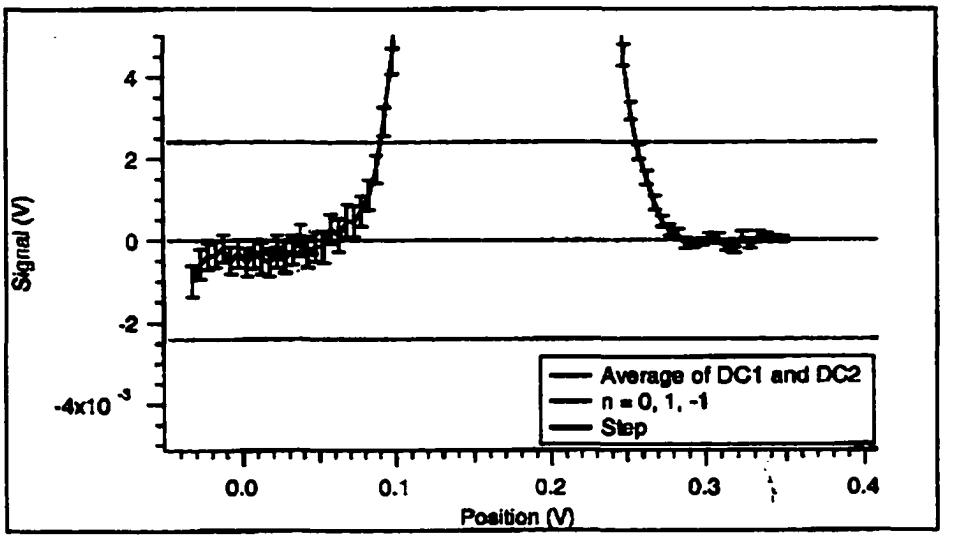
$$sS_2 = \sqrt{\frac{\sum_{i=K}^{N+K} (S^{12}(i))^2}{N} - S_{T2}^2}. \tag{6.10}$$

Thus the systematic error is defined by

$$sS = \sqrt{\frac{(sS_1)^2 + (sS_2)^2}{N}}, \tag{6.11}$$

which gives a measure of the "flatness" of the steps.

The data analysis was conducted with the WaveMetrics's Igor program, and the processed signal is shown in Figure 6.3.



Point	ThisStep	dThisStep	sThisStep
0	0.312211	0.119622	0.0625854
1	10	60	10

Figure 6.3 The results are listed in the appended table. The step (ThisStep) is 0.31 mV. The statistical error dS is calculated based on the error bars in the curve, which is small (0.12 mV) compared with the monopole signal, 2.4 mV. The systematical error sS is obtained based on the standard deviation of two pieces of the averaged ten-point line in either tails, which is also small (0.06 mV) as the tails are quite flat.

6.3 The DØ Samples and Results

We had some 222 aluminum samples and 6 Be samples. The efficiency ϵ is 0.94. The

distribution of the steps for Al samples is plotted out as a histogram in Figure 6.4.

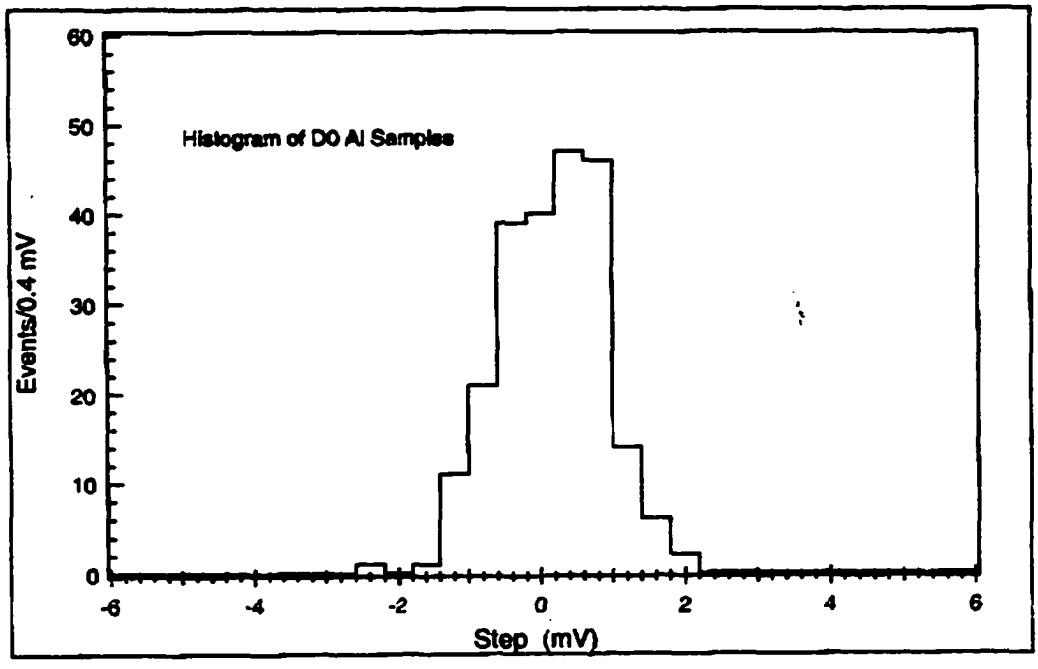


Figure 6.4 The histogram of DØ Al samples. The rms is 0.73 mV

The histogram is well described by a Gaussian curve whose standard deviation σ_s is the root-mean-squared deviation obtained from the data

$$\sigma_s = 0.73 \text{ mV},$$

and the mean

$$\bar{S} = 0.16 \text{ mV}.$$

We know the monopole signals should be at

$$\bar{S}_m = \begin{pmatrix} \pm 2.4 \text{ mV for } n = \pm 1 \\ \pm 4.8 \text{ mV for } n = \pm 2 \\ \pm 7.2 \text{ mV for } n = \pm 3 \\ \pm 14.4 \text{ mV for } n = \pm 6 \end{pmatrix}, \tag{6.12}$$

which are labeled in a subsequent graph.

The histogram shows 8 events are located within the 90% confidence interval of the $n = \pm 1$ Gauss distribution. We have remeasured all the eight samples and they all fell within ± 1.47 mV of $n = \pm 0$, which implies that they are very unlikely monopole events Therefore, the next thing we need to do is to set a limit for the number of possible events based on the histogram (ignoring remeasurements) so that we can set a limit on the cross section for monopole production. If there were monopole events occurring, we assume they would have had a Gaussian distribution centered on the monopole signal, ± 2.4 mV, with the same standard deviation as that of the samples. The distributions of possible monopoles and samples are shown in Figure 6.5. Then, we take a one-sided 90% confidence limit for monopole charge of $n = -1$ by cutting the Gaussian curve of events on the right side at the position that is 1.28 σ_s away from $n = -1$, which is -1.47 mV. Similarly, a one-sided 90% confidence limit for $n = 1$ can be obtained by cutting the Gauss curve for $n = 1$ at 1.47 mV. We find eight samples in total in the two 90% confidence intervals, where 10.4 are expected from the Gaussian distribution of samples. According to Feldman and Cousins [104], the 90% confidence upper limit for eight events observed when ten are expected is 4.2 signal events. Therefore,

$$N \leq 4.2 \text{ for } n = \pm 1. \tag{6.13}$$

No samples were found within 1.28 σ_s of $|n| \geq 2$ positions, and the closest being

$3.08\sigma_s$ away from $n = -2$. The 90% confidence limit for zero events observed and zero expected is 2.4 signal events . Therefore,

$$N \leq 2.4 \text{ for } |n| \geq 2. \tag{6.14}$$

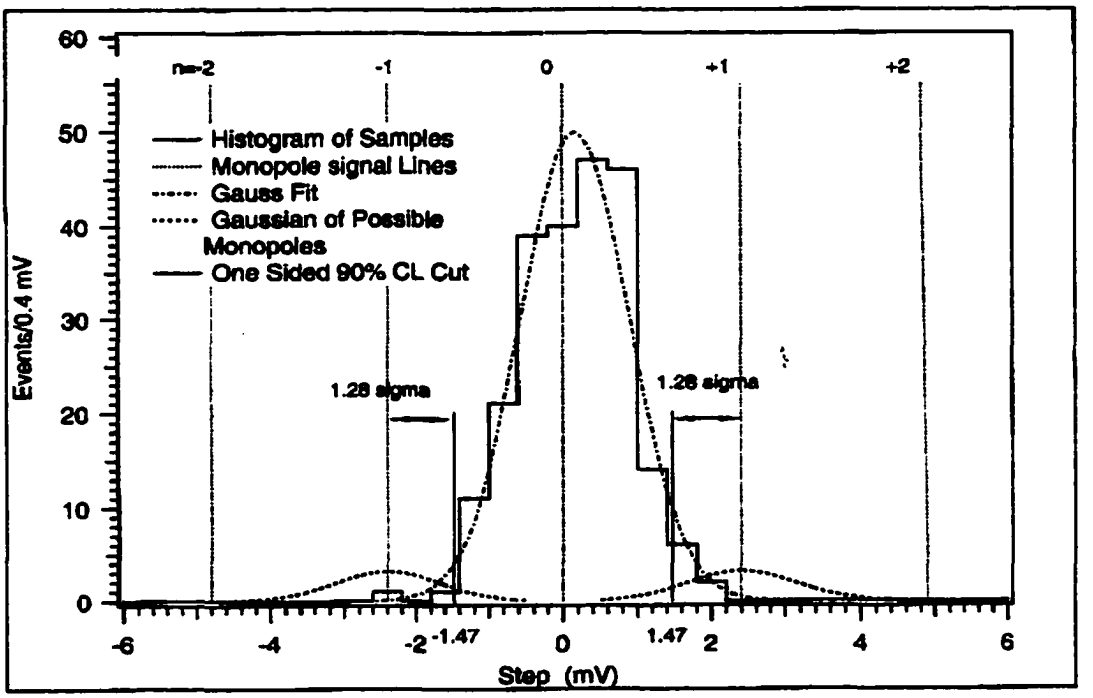


Figure 6.5 The histogram of steps for Al samples is described by a Gaussian curve whose standard deviation is the rms of the steps. The limit on the number of events is based on the cuts at ± 1.47 for $n = \pm 1$ on the two Gaussian curves of events with the same standard deviation of samples.

There are two approaches to calculate acceptance. The first one is an approximation assuming factorization into an angular acceptance A_Ω and a mass acceptance A_m, in which the total acceptance A is calculated by the product of A_Ω and A_m, and gives a

qualitative insight to the process. This method was used in our paper published in Physical Review Letters [31, later we call this paper PRL paper]. A_Ω can be obtained from the geometric configuration of the aluminum extension cylinder of the DØ detector, which gives about 0.12. In this case, the angular distribution is assumed to be isotropic. The mass acceptance is a function of ranging out of monopoles due to the energy loss in the detector and the distribution $\frac{d\sigma}{dM}$ in energy of the produced monopoles based on the Drell-Yan model. We estimated the lowest energy E_L and highest energy E_H, with which monopoles were accepted in the samples based on the energy loss calculation. Then we cut the $\frac{d\sigma}{dM}$ curve at E_L and E_H. The ratio of the cut area to that of the total area under the $\frac{d\sigma}{dM}$ curve gives the mass acceptance. This is shown in Figure 6.6. In this way we get

$$A_m = \begin{pmatrix} 0.29 \text{ for } |n| = 1 \\ 0.015 \text{ for } |n| = 2 \end{pmatrix}. \tag{6.15}$$

Thus, we can calculate the cross section limits using the formula in 6.1. Furthermore, we can find the mass limit using the Drell-Yan cross section as a function of monopole mass $\sigma(m)$.

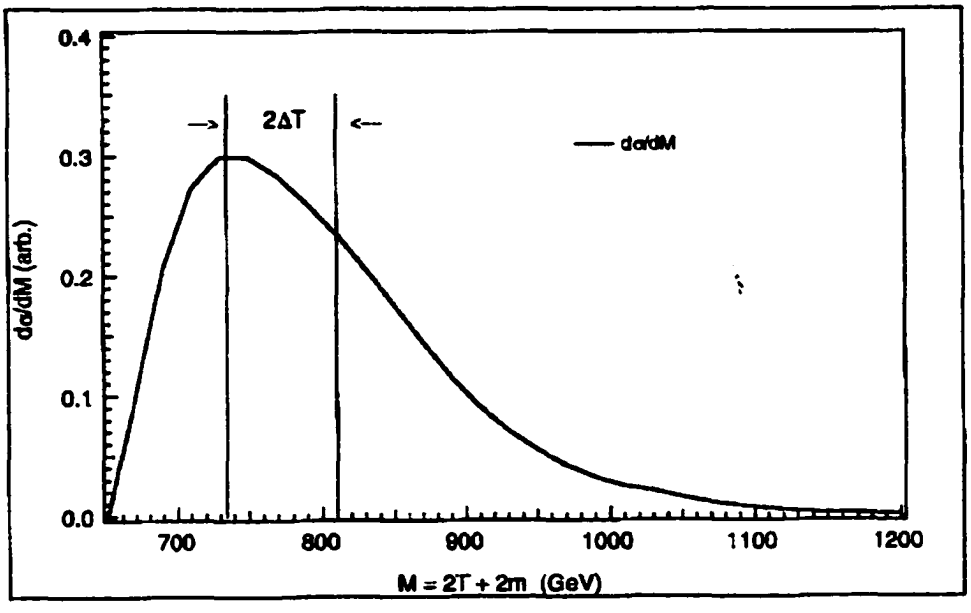


Figure 6.6 Cut $\frac{d\sigma}{dM}$ at E_L and E_H to get mass acceptance. T is the kinetic energy of monopoles and the mass m = 325 GeV.

For $|n| \geq 3$, the acceptance of the Al sample is very small, but somewhat better for Be. We have six Be samples taken from the beryllium beam pipe. The solid angle acceptance is about 0.95, and the mass acceptance is 0.0065 for $|n| = 3$, and 0.13 for $|n| = 6$. As the Drell-Yan cross section becomes very large with increasing n, we need to think about whether this cross section for large n, say, $n = 3,6$, is consistent with the unitarity limit on the corresponding cross section. Based on Milton and Gamberg's estimation, [105] the required unitarity of a partial wavefunction [106] would be violated for $n \geq 3$ and angular momentum $J \sim 1$. Therefore, we use the unitarity limit to the cross section for $n = 3,6$, which is equivalent to the Drell-Yan cross section for $n = 3$, and find mass limits based on the unitarity curve. The results obtained in this approach are listed in Table 6.1.[31]

Table 6.1 PRL limits on cross sections and masses of monopoles from DØ samples at 90% CL (ϵ is included in A_Ω with isotropic angular distribution)

n	$\|n\| = 1$	$\|n\| = 2$	$\|n\| = 3$	$\|n\| = 6$
Sample	Al	Al	Be	Be
A_Ω	0.12	0.12	0.95	0.95
A_m	0.29	0.015	0.0065	0.13
N	≤ 4.2	≤ 2.4	≤ 2.4	≤ 2.4
σ(pb)	≤ 0.70	≤ 7.8	≤ 2.3	≤ 0.11
M(GeV)	≥ 295	≥ 260	≥ 325	≥ 420

However, the acceptance obtained this way is not really correct since different monopoles have different $\frac{dE}{dx}$ in different materials. In addition, the Lorentz transformation from $q\bar{q}$ center-of-mass frame to the laboratory frame mixes the energies and angles of monopoles (the "factorizing" into $A_\Omega$and A_m is an approximation). A better approach is to Monte Carlo simulate and track every produced monopole and determine which are accepted and which are not. In this approach, we do not separate A into A_Ω and A_m. We even do not need to know A. Instead, we just calculate cross section accepted $\sigma_A(m)$ as a function of monopole mass. Then we take the value of σ_A, which is equal to $\frac{N}{\epsilon L}$, and use the $\sigma_A(m)$ curve to find the monopole mass m corresponding to σ_A. m obtained this way is just the lower mass limit of monopole. Furthermore, we find the upper limit on the cross section, which corresponds to m on the Drell-Yan total cross section curve $\sigma(m)$. The corresponding acceptance can be obtained by simply dividing $\sigma(m)$ by $\sigma_A(m)$. This procedure is shown in Figure 6.7.

Now we calculate σ_A corresponding to the data:

$$\sigma_A \leq \frac{N}{\epsilon L} = \frac{4.2}{0.94 \times 172} = 0.026 \text{ pb, for } n = 1, \tag{6.16}$$

$$\sigma_A \leq \frac{2.4}{0.94 \times 172} = 0.0148 \text{ pb, for } n = 2, \tag{6.17}$$

$$\sigma_A \leq \frac{2.4}{1.0 \times 172} = 0.014 \text{ pb, for } n = 3,6. \tag{6.18}$$

In the $\sigma_A(m)$ curve, $\sigma_A \leq 0.026$ pb corresponds to $2m \geq 516$ GeV, and thus $\sigma \leq 0.95$ pb from the $\sigma(m)$ curve, for $n = 1$. Similarly, we obtain the new limits for cross section and mass for $n = 2,3,6$, which are listed in Table 6.2 and also shown in Figure 6.7.

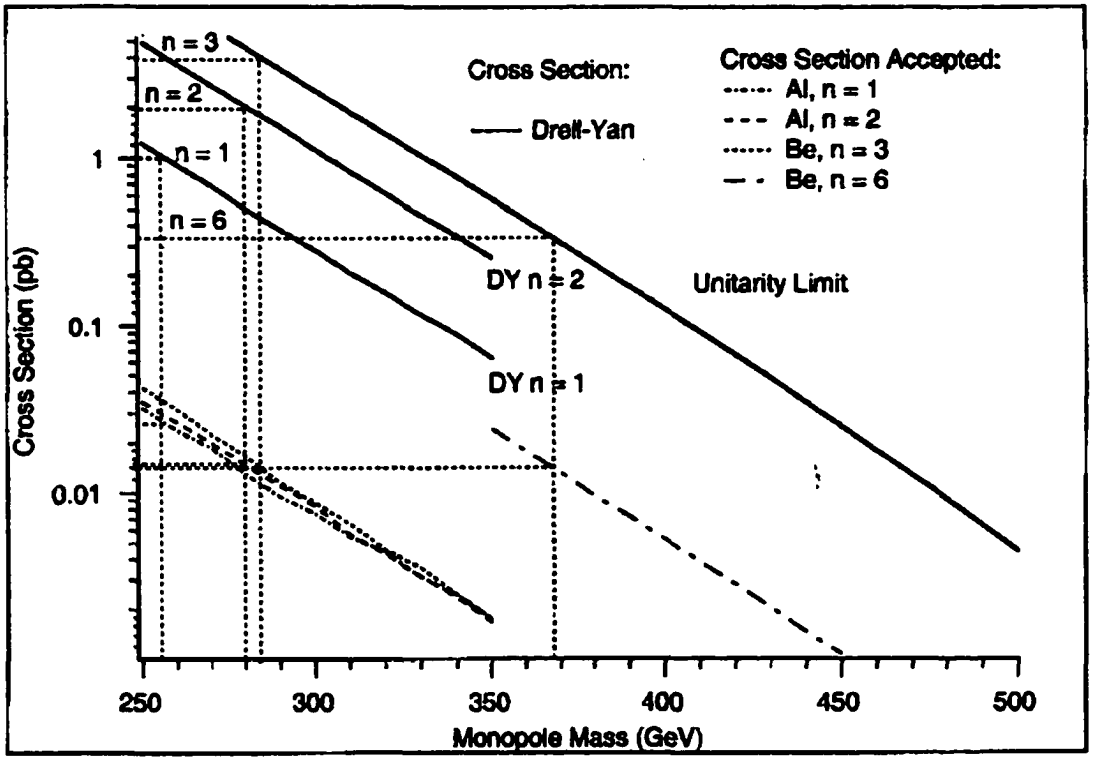


Figure 6.7 Find the limit for m from $\sigma_A(m)$, then find the limit for σ from $\sigma(m)$.

Table 6.2 Revised limits on cross sections and masses of monopoles from DØ samples at 90% CL with Monte Carlo Calculation

n	$\|n\| = 1$	$\|n\| = 2$	$\|n\| = 3$	$\|n\| = 6$
Sample	Al	Al	Be	Be
ϵ	0.94	0.94	1.0	1.0
A	0.025	0.007	0.0035	0.042
N	≤ 4.2	≤ 2.4	≤ 2.4	≤ 2.4
σ(pb)	≤ 1.02	≤ 2.0	≤ 3.95	≤ 0.33
M(GeV)	≥ 256	≥ 280	≥ 284	≥ 368

6.4 CDF Samples and Results

We took 12 square (2×2 meter^2) layers of lead closest to the IR (interaction range) point from the CDF detector, of which six were located on the East side and the other six on the West side. Each layer had an octagonal hole at the center, where the Be beam pipe passed through. Each layer was cut into about 68 small rectangular pieces, and each piece was rolled into a cylinder of about 7.5 cm in height and 7.5 cm in diameter. We had about 816 Pb sample cylinders in total.

Out of the 816 samples, only 664 samples have been successfully measured . The rest of them were immeasurable due to huge dipoles caused by the (ferromagnetic) red paint on these samples (first layer). The histogram of the step signals obtained from measurements are shown in Figure 6.8. The long tails of the distribution indicate that some of the measurements must have big systematic errors so they should be excluded. The error distributions are plotted in Figure 6.9. In order to reduce the rms of the samples, we made cuts on errors

$$sS < 0.3, \text{and } dS < 0.45, \tag{6.19}$$

we have obtained a new histogram with a reduced rms, which is shown in Figure 6.10.

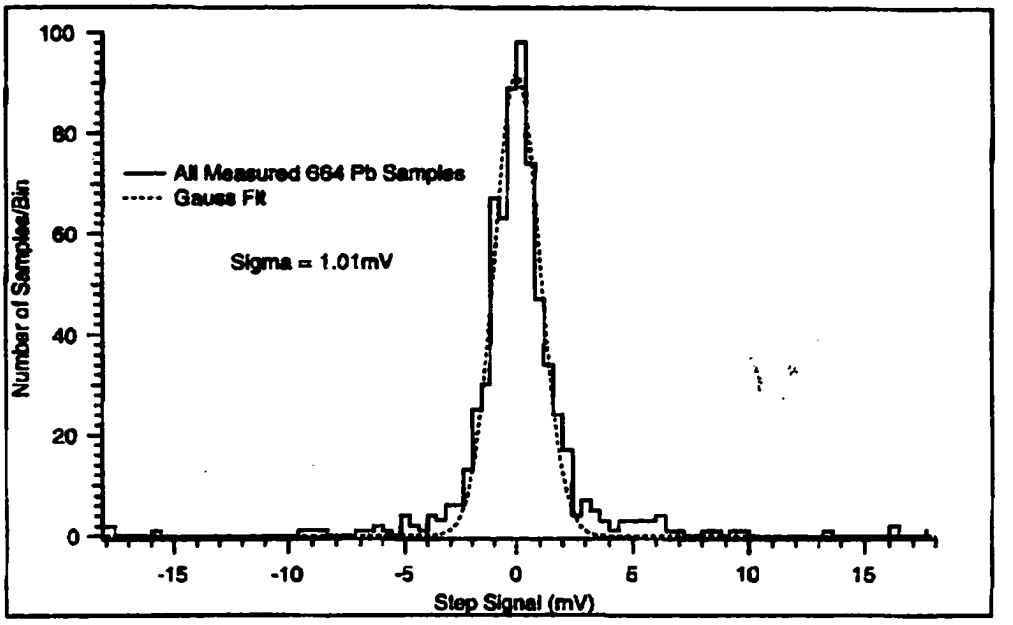
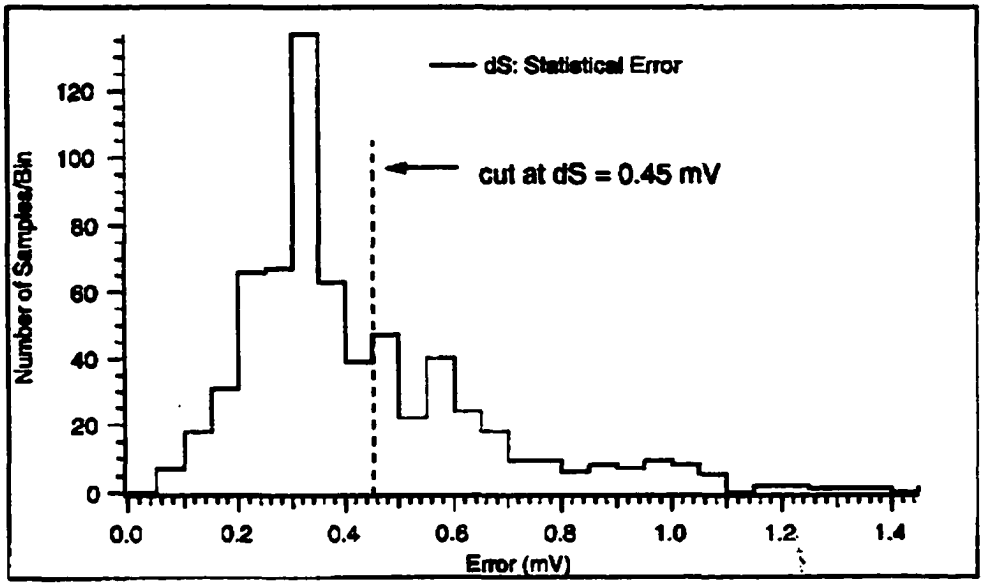
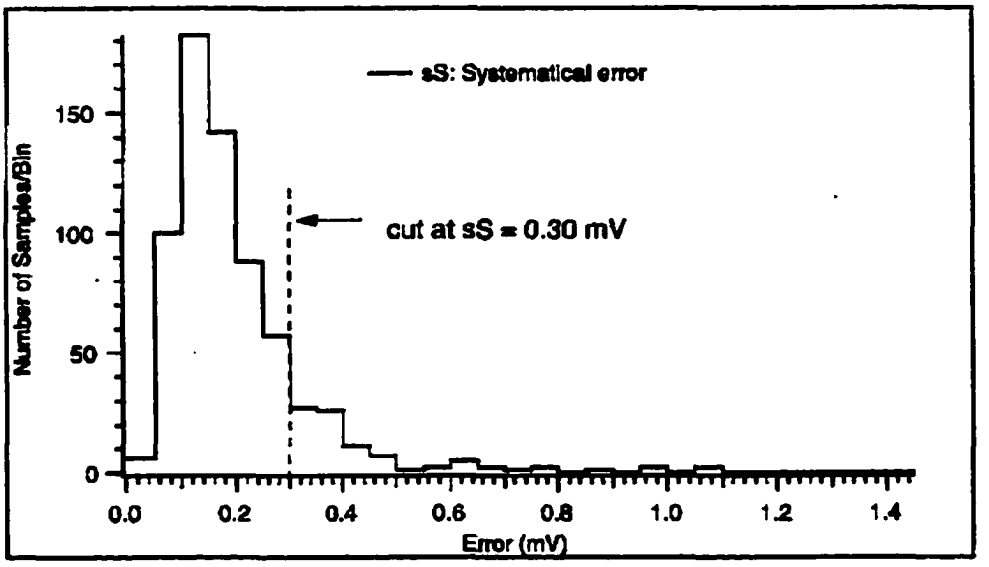


Figure 6.8 The histogram of all measured lead samples. The rms is 1.01 mV.



(a) Statistical error distribution



(b) Systematical error distribution

Figure 6.9 (a) The statistical error distribution. (b) The systematic error distribution.

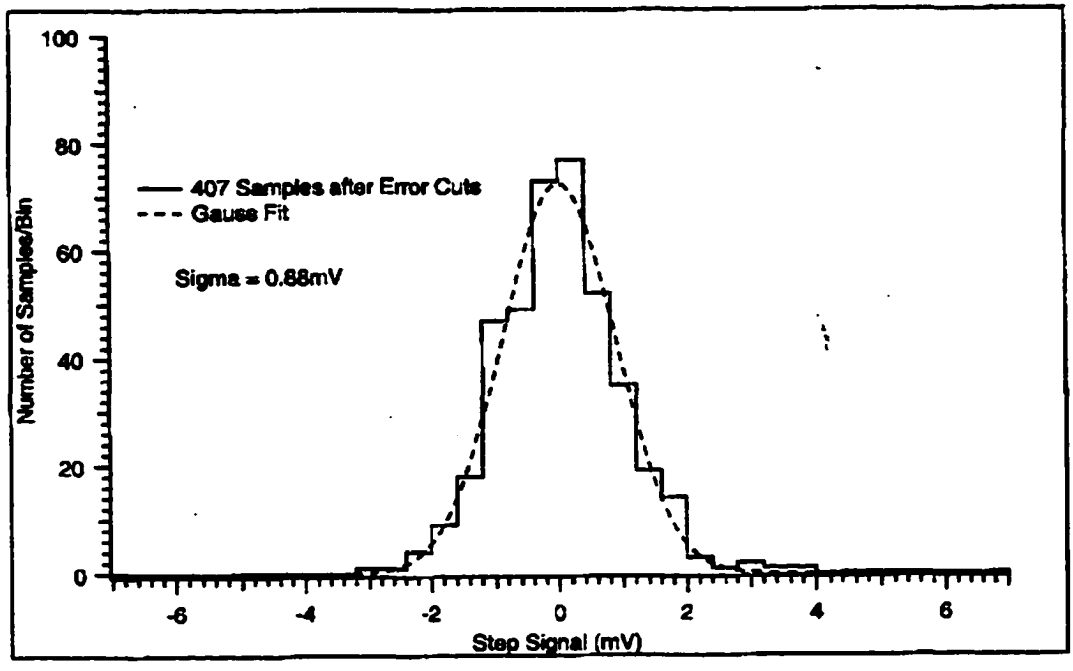


Figure 6.10 The rms of the histogram is reduced from 1.01 mV to 0.88 mV after error cuts.

The Monte Carlo calculation has shown that the magnetic field produced by the solenoid magnet has had a significant effect on monopole tracking and energy loss. The effect should be considered when we select samples and calculate acceptance. In the absence of the field, monopoles would move along straight trajectories and be accepted in the entire area of a lead sample layer covered by the angle θ ($3° \leq \theta \leq 10°$). Thus, all samples of the layer should be selected. In the presence of the field, however, the longitudinal momentum of monopoles will be changed by the field (acceleration along /against the field direction). As a result, the direction of motion and the energy will be changed during the motion. Thus, the monopoles with positive magnetic charge moving along the direction of the field will track along a curve bent towards the center of the layer while those moving against the field will move away from the center.

Symmetrically, the monopoles with negative magnetic charge moving against the direction of the field will track along a curve bent towards the center of the layer while those moving along the field will move away from the center. Therefore, the monopoles reaching the lead layers were not uniformly distributed, only a small ring around the center ($3° \leq \theta \leq 7.5°$) accepted monopoles, where 52 samples were expected in that region. In this case, we need at most 52 samples out of 68 for each layer. This is shown in Figure 6.12.

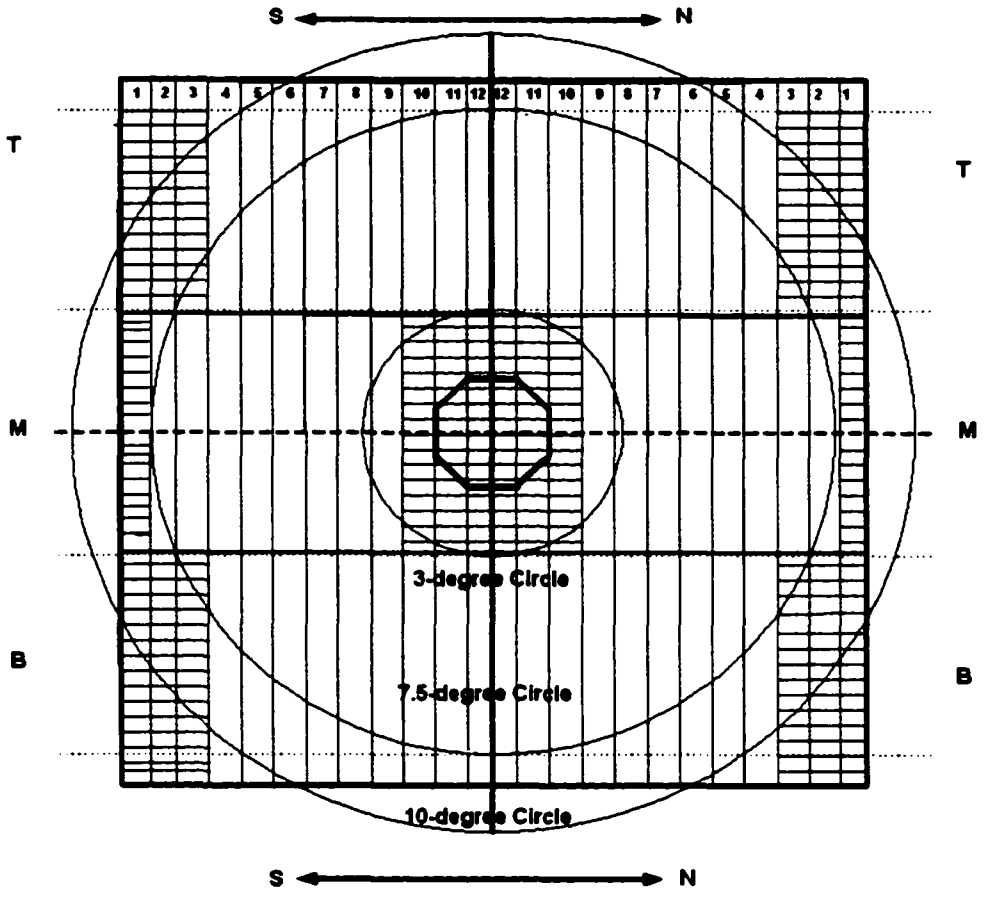


Figure 6.11 A lead sample layer is cut into 68 samples. The Monte Carlo simulation shows that only the samples (52 in one layer) subtending an angle $3° \leq \theta \leq 7.5°$ have significant acceptance and should be considered. The cross hatched samples and others with large dS and sS errors are excluded from the analysis.

The magnetic field also has affected the acceptance for different layers. In the absence of the magnetic field, the monopoles have a somewhat uniform energy distribution, so all six layers accept monopoles for $n = \pm 1$, as is shown in Figure 6.12.

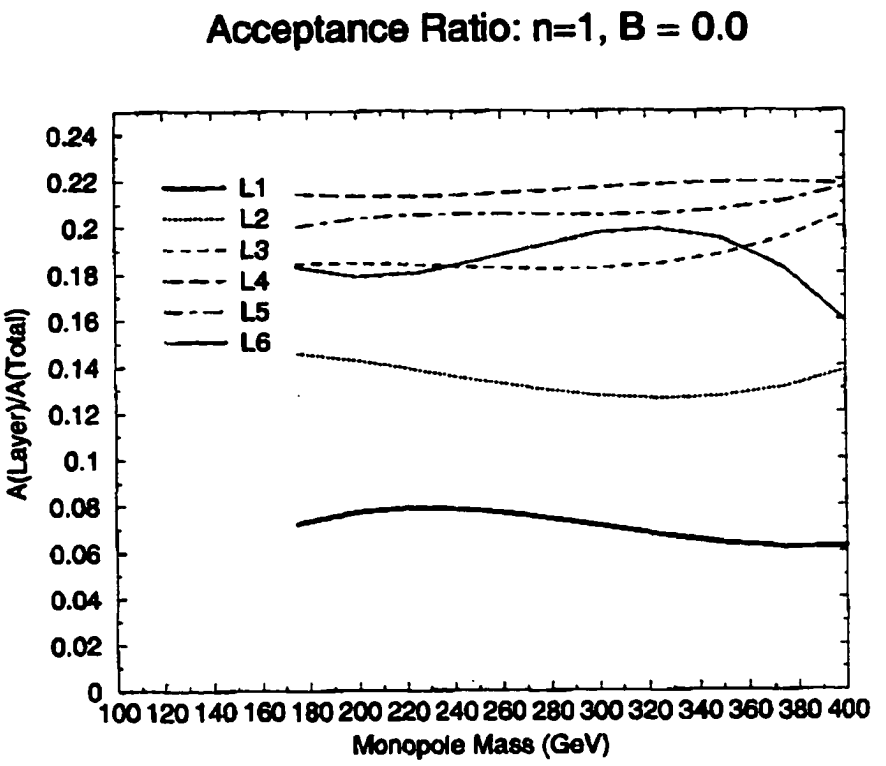


Figure 6.12 The ratio of the acceptance for one layer (L1 through L6, equally separated in the Forward Shower Calorimeter with L1 being the closest to the IR point) to that for the total six layers for $n = 1$ without magnetic field.

But the magnetic field will change the energy of monopoles. The monopoles of charge $n(> 0)$ will gain an energy of about $70n$ GeV if they are moving along the direction of the field, and will lose $70n$ GeV if they are moving against the direction of the field. Symmetrically, the monopoles of charge $n(< 0)$ will gain an energy of about

$70n$ GeV if they are moving against the direction of the field, and will lose $70n$ GeV if they are moving along the direction of the field. Thus, the monopoles moving out of the field do not have a uniform energy distribution and are not accepted by each layer. The Monte Carlo simulation has shown that the first three layers have almost no acceptance in the presence of the field. We can only use the samples from layers 4,5,6 for $n = \pm 1$. For $n = \pm 2$, layer 2 has about 90% of total acceptance while layer 3 shares about 10%. We just use the layer 2 samples for our analysis for $n = \pm 2$ case. For $n = \pm 3$, only layer 2 has acceptance. The energy loss (~ 900 GeV lost in the materials before the lead layers) is too large for monopoles with charge of $6g$ ($n = 6$) to reach the sample layers. Thus, the $n = \pm 6$ case has been excluded from the CDF analysis. Figure 6.13 shows the acceptance for $n = \pm 1, \pm 2, \pm 3$.

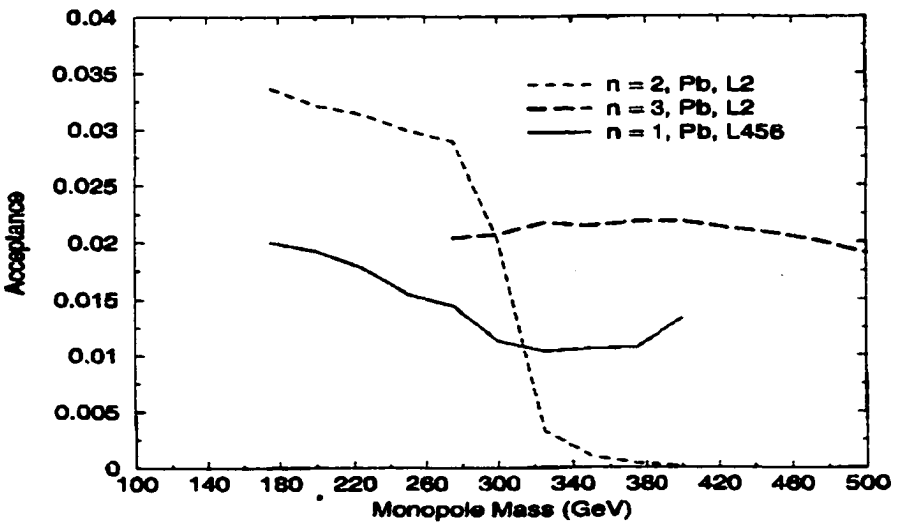


Figure 6.13 Acceptance for $n = \pm 1, \pm 2, \pm 3$.

There should be 312 samples in total taken from layers 4,5,6, which were expected

to be used for the $n = 1$ analysis. However, only 187 measured samples have been actually used due to dS and sS error cuts. The efficiency of the samples, ϵ, can be obtained by taking the ratio between the sum of the areas cut by $\theta(3° \leq \theta \leq 10°)$ of all used samples and the area of the region covered by $\theta(3° \leq \theta \leq 10°)$ for each layer and averaging over the ratios. In this way, $\epsilon(n = \pm 1)$ of the samples is estimated to be 0.53. The steps of those samples form a histogram shown in Figure 6.14.

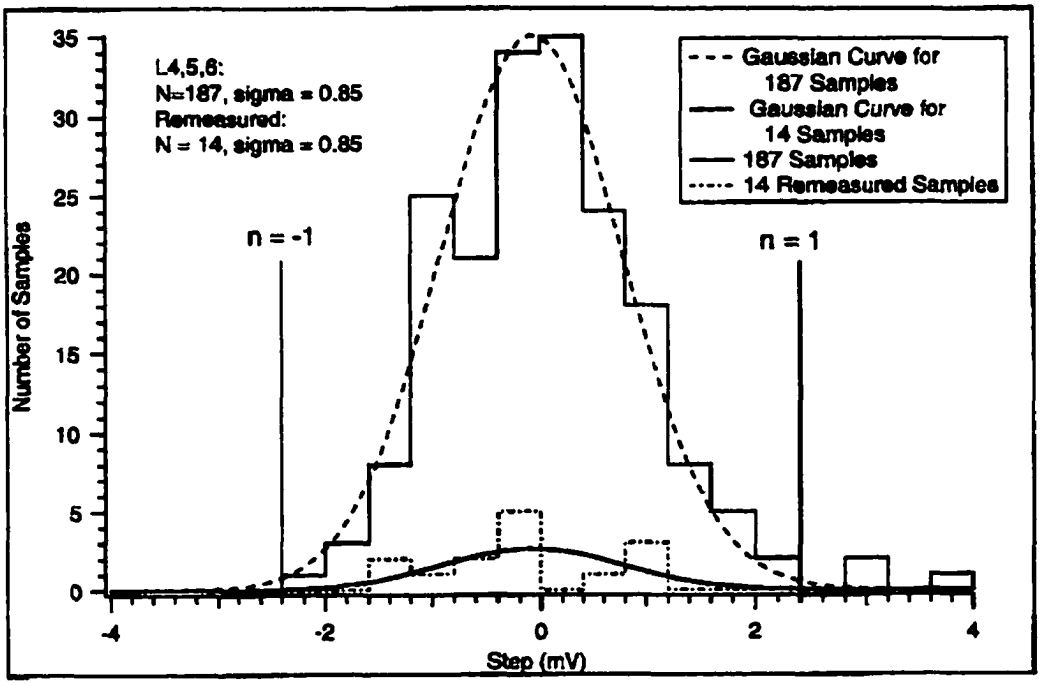


Figure 6.14 The histogram of steps of 187 layers 4, 5, 6 (L4,5,6) samples for $n = \pm 1$ after error cuts: $dS < 0.45$ mV and $sS < 0.30$ mV. The "rms" deviation (σ_s) of the 187 samples and the 14 remeasured samples are 0.85 mV.

Again, we use a Gaussian distribution, which has the same standard deviation as that of the histogram and is centered on zero, to describe the histogram. Then, we take

another Gaussian distribution centered at ±2.4 mV for $n = \pm 1$, which still has the same standard deviation as that of the histogram. Now, if we make a 90% confidence level cuts at ±1.31 mV, we would have too many events in the tail to get a "good" limit. We restrict the "monopole region" to a one-sided 80% confidence interval which cuts at ±1.6 mV. Now only 14 samples out of that region need to be remeasured. After those 14 samples were remeasured, they all have fallen within ±1.6 mV of $n = 0$. For the Gaussian distribution centered at $n = 0$, ±1.6 mV is equal to $\pm 1.88\sigma_s$, at which two tails are cut and only 6% of the area under the Gaussian curve is out in the tails. Thus, the expected number of samples in the tails should be $6\% \times 187 = 11$. Using Feldman and Cousin's table, we find the upper limit number for 14 observed while 11 expected is 10.5 for 90% confidence level and 7.32 for 68% confidence level. Averaging 7.32 and 10.5, we take $N = 8.9$ as an approximate upper limit number of events for 80% confidence level. Thus, the upper limit on the accepted cross section is

$$\sigma_A \leq \frac{N}{\epsilon L} = \frac{8.9}{0.53 \times 180} = 0.093 \text{ pb}, \tag{6.20}$$

which corresponds to the lower mass limit from the $\sigma_A(m)$ curve in Figure 6.15:

$$m \geq 204 \text{ GeV}. \tag{6.21}$$

From the Drell-Yan $\sigma(m)$ curve, we obtain the upper limit for cross section

$$\sigma(m \geq 204) \leq 4.8 \text{ pb}. \tag{6.22}$$

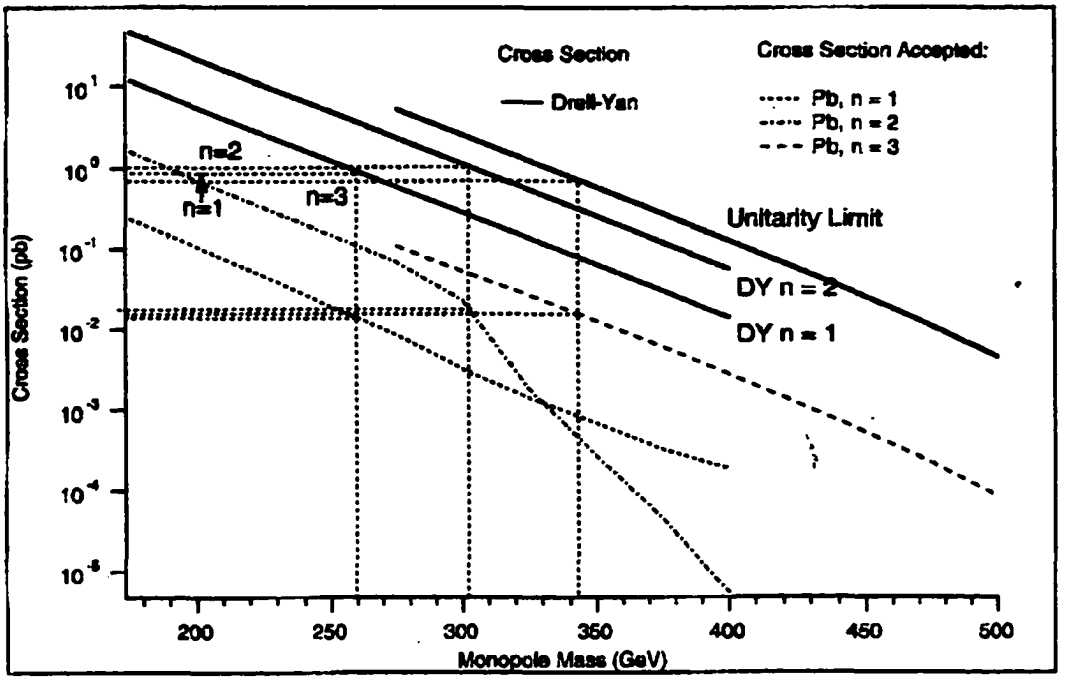


Figure 6.15 The accepted cross section and corresponding Drell-Yan cross section as a function of monopole mass for CDF samples. The results are derived from the cross section curves.

We can improve the cross section limit using the data from the remeasurement. The remeasured 14 samples form a small Gaussian distribution with the same standard deviation centered at the origin. But nothing appears beyond ±1.6 mV while 6% × 14 = 0.84 events are expected. Feldman and Cousin's table gives 1.07 as the 80% confidence level upper limit for events. Since possible monopoles in the 14 samples occur with only 80% probability, the expected limit N should be corrected as 1.07/80% = 1.34. Thus the accepted cross section is

$$\sigma_A \leq \frac{N}{\epsilon L} = \frac{1.34}{0.53 \times 180} = 0.014 \text{ pb} \tag{6.23}$$

which corresponds to

$$m \geq 260 \text{ GeV}. \tag{6.24}$$

Therefore, we obtain an improved limit for cross section from the Drell-Yan curve

$$\sigma(m \geq 260 \text{ GeV}) \leq 0.9 \text{ pb}. \tag{6.25}$$

We can also take the average of the original step values and remeasured values for the remeasured 14 samples. Then we find three of them fall out of ±1.6 mV: 2.29 mV, 2.11 mV, and −1.77 mV. Based on Feldman and Cousin's table, we obtain 5.36 as the upper limit on the events for 1 expected and 3 observed. But we still need to divide it by 80% and get

$$N \leq 5.36/80\% = 6.7. \tag{6.26}$$

Thus,

$$\sigma_A \leq \frac{N}{\epsilon L} = \frac{6.7}{0.53 \times 180} = 0.07 \text{ pb}, \tag{6.27}$$

which implies, from the Drell-Yan curve in Figure 6.15, that

$$m \geq 213 \text{ GeV and } \sigma \leq 3.6 \text{ pb}. \tag{6.28}$$

This result is better than that from the original data but worse than that from just the remeasurement data.

We have used 90 measured samples ($dS < 0.6$, $sS < 0.4$) from layer 2 for $n = \pm 2$ and 95 ($dS < 0.8$, $sS < 0.6$) for $n = \pm 3$. The efficiencies for those samples are: $\epsilon(n = \pm 2) = 0.83$, $\epsilon(n = \pm 3) = 0.87$. The histograms and the Gaussian distributions for $n = \pm 2$ and $n = \pm 3$ in Figures 6.16 and 6.17 also have the standard deviation of 0.85 mV and are centered on zero.

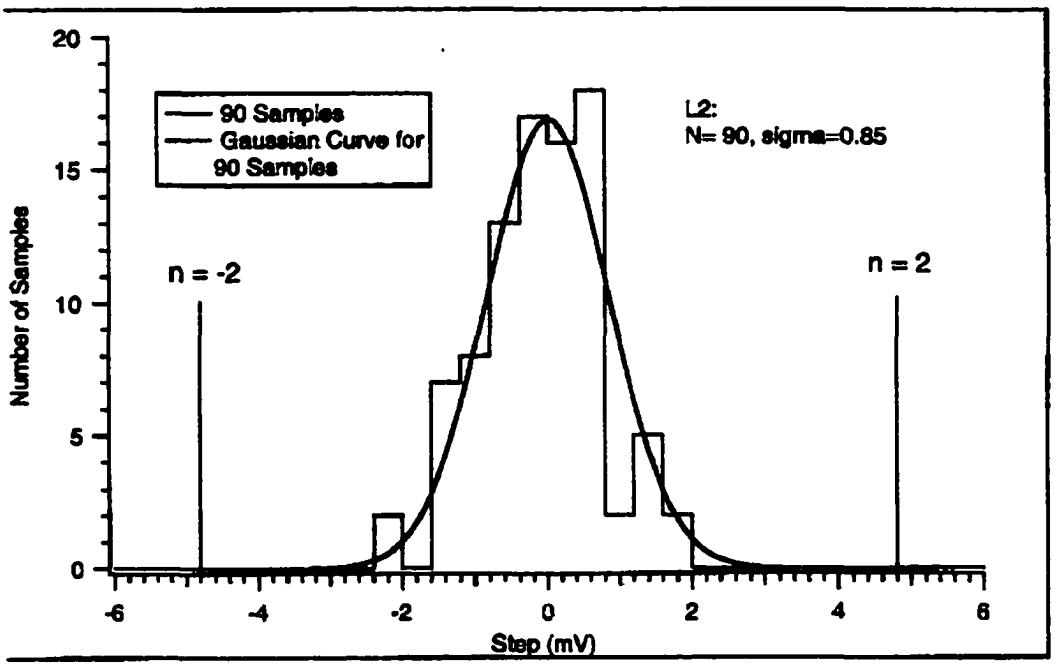


Figure 6.16 The histogram of steps of 90 layer 2 (L2) samples for $n = \pm 2$ after error cuts: $dS < 0.60$ mV and $sS < 0.4$ mV. The "rms" deviation (σ_s) of the 90 is 0.85 mV.

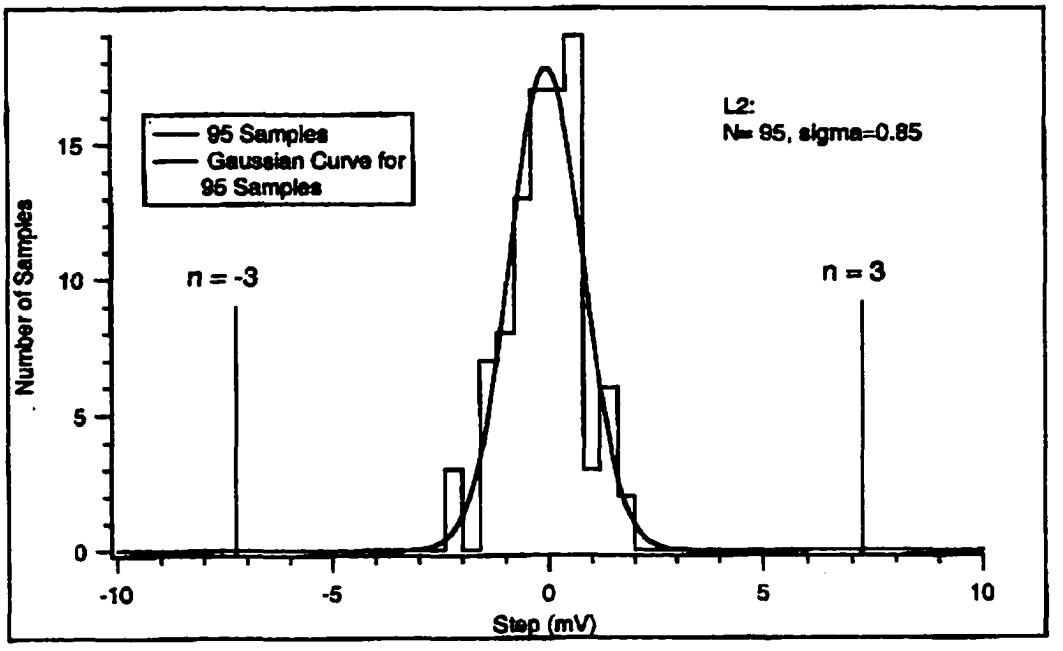


Figure 6.17 The histogram of steps of 95 layer 2 (L2) samples for $n = \pm 3$ after error cuts: $dS < 0.60$ mV and $sS < 0.40$ mV. The "rms" deviation (σ_s) of the 95 is 0.85 mV.

The one-sided 90% confidence cuts for $n = \pm 2$ is ±3.57 mV, and ±5.9 mV for $n = \pm 3$. But no events have been found and none expected beyond ±3.57 mV of $n = 0$. Thus, the upper limit on the number of events at 90% confidence level is $N = 2.44$ for $n = \pm 2, \pm 3$ from Feldman and Cousin's table. The accepted cross section for $n = \pm 2$ is

$$\sigma_A \leq \frac{N}{\epsilon L} = \frac{2.44}{0.83 \times 180} = 0.0163 \text{ pb}, \tag{6.29}$$

and the accepted cross section for $n = \pm 3$ is

$$\sigma_A \leq \frac{N}{\epsilon L} = \frac{2.44}{0.87 \times 180} = 0.0156 \text{ pb}. \tag{6.30}$$

From the accepted cross section curve in Figure 6.16, we find lower mass limit is

$$m = 303 \text{ GeV, for } n = \pm 2, \tag{6.31}$$

and obtain from the Drell-Yan curve the upper limit for cross section

$$\sigma(m = 303 \text{ GeV}) = 1.03 \text{ pb for } n = \pm 2. \tag{6.32}$$

Similarly, we obtain mass limit from Figure 6.16

$$m = 343 \text{ GeV, for } n = \pm 3 \tag{6.33}$$

and cross section limit

$$\sigma(m = 343 \text{ GeV}) = 0.72 \text{ pb for } n = \pm 3. \tag{6.34}$$

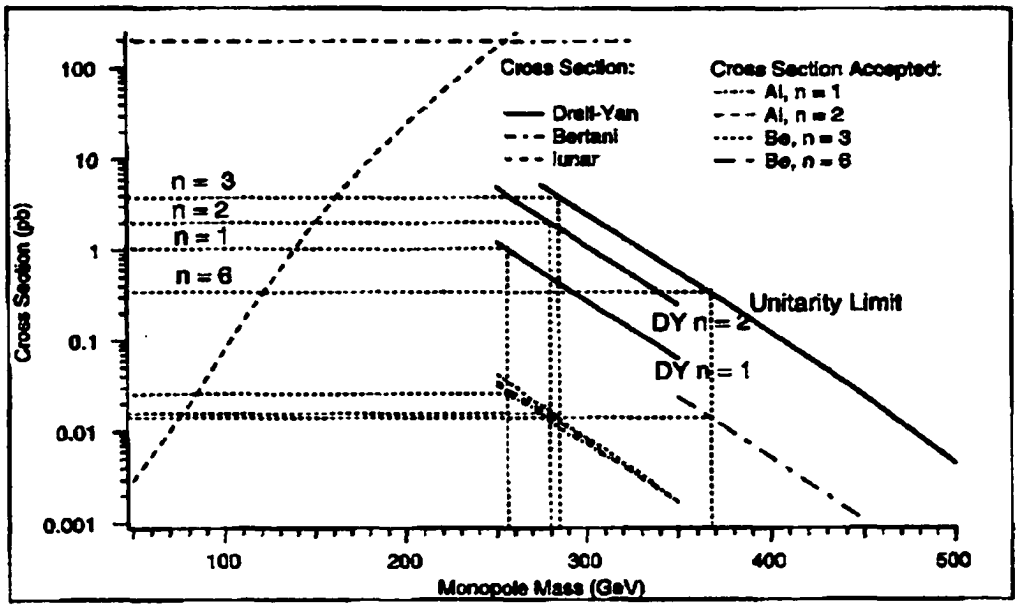
which are obtained from the unitarity curve in Figure 6.16. These results are better than those obtained from DØ samples. They are listed in Table 6.3.

Table 6.3 New limits on cross sections and masses of monopoles from CDF Pb samples at 80% CL ($n = \pm 1$) and 90% CL ($n = \pm 2, \pm 3$) with Monte Carlo Calculation.

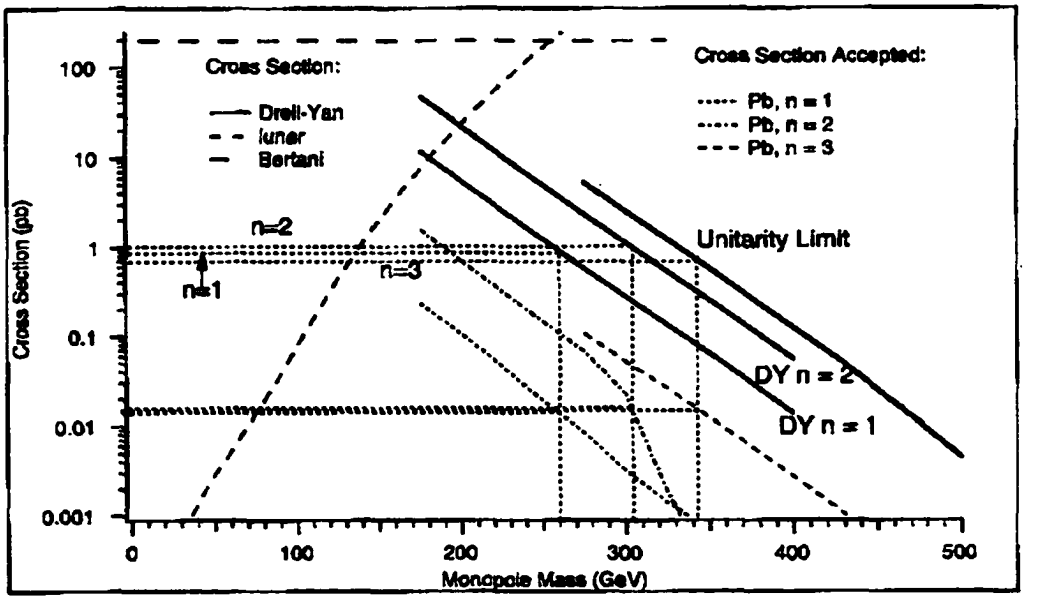
n	$\|n\| = 1$	$\|n\| = 2$	$\|n\| = 3$
ϵ	0.53	0.83	0.87
N	$\leq$ 1.34	$\leq$ 2.44	$\leq$ 2.44
A	0.015	0.018	0.022
σ(pb)	$\leq$ 0.89	$\leq$ 1.03	$\leq$ 0.72
M(GeV)	$\geq$ 260	$\geq$ 303	$\geq$ 343

6.5 Discussions and Conclusions

The results we have obtained from both DØ and CDF samples are better than those of Bertani, the best results of the previous accelerator based monopole searches. The cross sections have been improved by a factor of 200, and the mass limit raised by a factor of $\geq$ 2. Also, we are above lunar mass limit. The comparison is shown in Figure 6.18.



(a)



(b)

Figure 6.18 A comparison with previous searches: (a) DØ results; (b) CDF results.

Although our results are very good compared to others, they can be improved by selecting better samples and using better apparatus. For example, if we use a thick aluminum beam pipe (instead of Be) at the interaction point, we can get the maximum angular acceptance with large binding energy. Also, if we build a new detector which is not magnetized and allows a flatter magnetic field in the warm bore, we can reduce the errors of measurement and increase the efficiency of the samples. The limits on cross section can be further reduced while the limits on mass can be further increased.

On the other hand, our results like the previous ones are model dependent. We can have different results for different models. In absence of a complete quantum theory of magnetic monopoles, we have chosen the Drell-Yan process for leptons as the model for monopole production. First, the Drell-Yan model describes a simple way for monopoles to be produced, e.g., by a single photon process. Second, the inclusion of a factor of β^3 in the cross section has reduced the effect of the large monopole coupling constant, which is a problem in a perturbative quantum field theory of monopoles. Third, the results from this model are conservative in that other corrections or models give larger cross section. Therefore, the Drell-Yan model with β^3 correction appears practical and reasonable.

Nevertheless, we do not want close the door to other models or theories about monopoles. Even for the Drell-Yan model, it is clear that we need to consider some other cases such as different angular distributions since we know very little about monopoles, and the features of monopoles such as spin imply different, as yet undetermined, angular distributions. So far we have used the angular distribution in the Monte Carlo calculation of

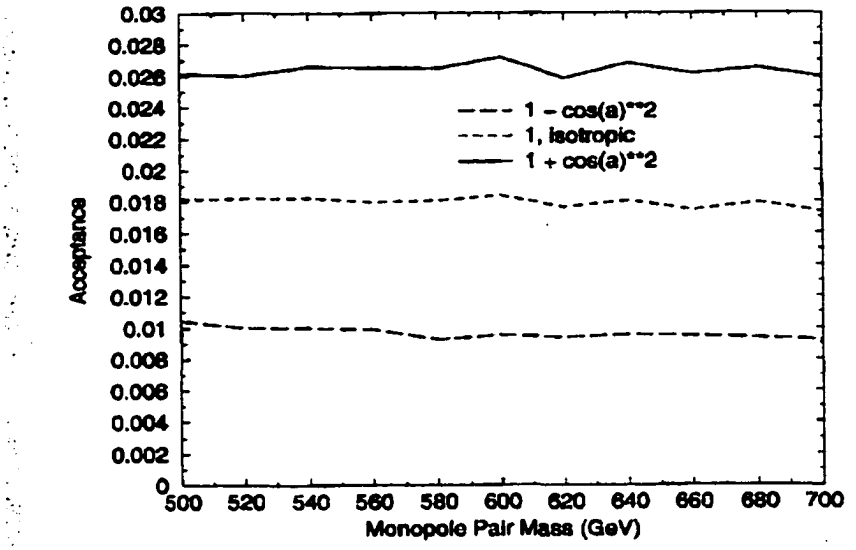
$$1 + (\cos\theta)^2, \tag{6.35}$$

which corresponds to the coupling spin 1/2 leptons to photons. All Monte Carlo results given above are obtained using the $(1 + (\cos\theta)^2)$ distribution. Now let us consider

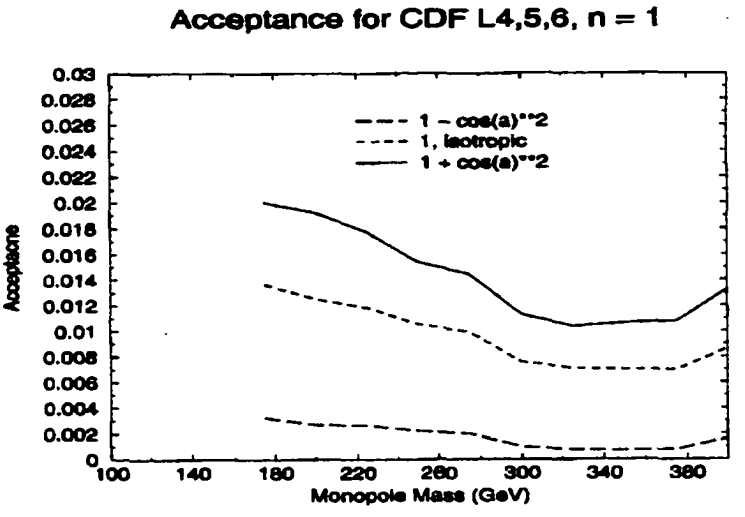
angular distributions given by

$$1, \text{ and } 1 - (\cos\theta)^2. \text{ (i.e., isotropic and } (\sin\theta)^2 \text{ respectively)} \qquad (6.36)$$

This leads to different acceptances which are shown in Figure 6.19.



(a)



(b)

Figure 6.19 Acceptance for different angular distributions of monopoles production: (a) DØ case; (b) CDF case.

A comparison of results with different angular distributions is given in Table 6.4.

Table 6.4(a) Results for DØ samples with different angular distributions.

(n = 1)

Angular Distribution	$1 + (\cos\theta)^2$	1	$1 - (\cos\theta)^2$
ϵ	0.94	0.94	0.94
N	$\leq$ 4.2	$\leq$ 4.2	$\leq$ 4.2
A	0.025	0.018	0.011
σ(pb)	$\leq$ 1.02	$\leq$ 1.4	$\leq$ 2.2
M(GeV)	$\geq$ 256	$\geq$ 246	$\geq$ 230

Table 6.4(b) Results for CDF samples with different angular distributions.

(n = 1)

Angular Distribution	$1 + (\cos\theta)^2$	1	$1 - (\cos\theta)^2$
ϵ	0.53	0.53	0.53
N	$\leq$ 1.34	$\leq$ 1.34	$\leq$ 1.34
A	0.015	0.01	0.003
σ(pb)	$\leq$ 0.89	$\leq$ 1.3	$\leq$ 4.7
M(GeV)	$\geq$ 260	$\geq$ 250	$\geq$ 204

No magnetic monopoles have been found in our experiment, but this experiment is very efficient in setting limits on cross sections and masses of monopole. With higher energy accelerators becoming available, e.g., the LHC (Large Hadron Collider, the center mass energy will be 14 TeV), the cross section and mass limits can be further improved with this type of experiment. Figure 6.20 shows possible cross section and mass limits that will be reached at the LHC. For example, the mass limit can be improved from about 500 GeV (Tevatron) to 1300 GeV (LHC) obtained, given the same cross section of 0.1 pb. Therefore, future searches for magnetic monopoles should be continued not just because it is important to confirm the existence or nonexistence of monopoles but

because it is doable.

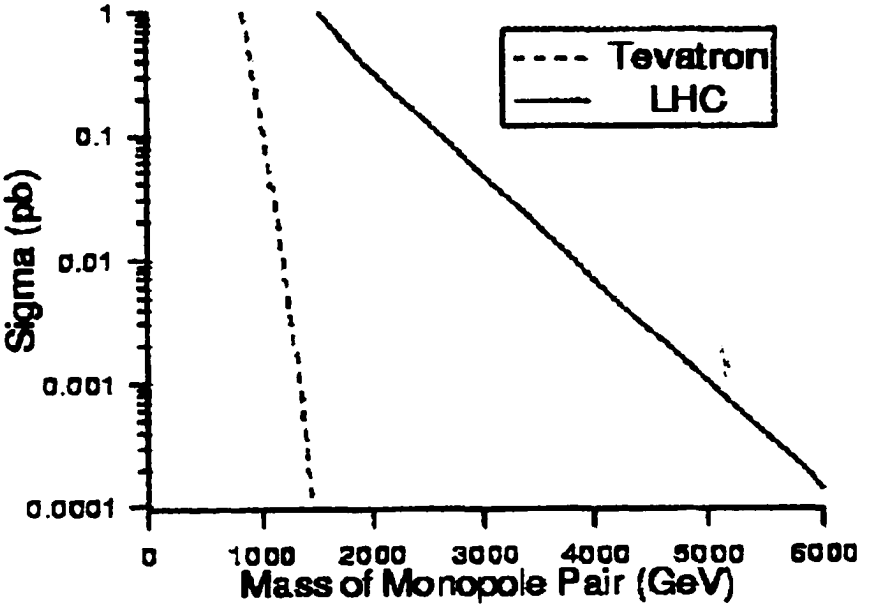


Figure 6.20 The Drell-Yan cross section for Tevatron and LHC. For the same cross section limit, the mass limit will be significantly raised.

Bibliography

[1] William Gilbert, De Magnete, English translation by P. F. Mottelay, New York, Dover Publications, 1958.

[2] F. Cajori, A History of Physics—In Its Elementary Branches including the Evolution of Physical Laboratories, The MacMillan Company, 1929, p.231.

[3] F. Cajori, A History of Physics—In Its Elementary Branches including the Evolution of Physical Laboratories, The MacMillan Company, 1929, p.234.

[4] J. C. Maxwell, Treatise on Electricity and Magnetism, 3rd edition (1891), 2 vols., reprints, Dover, New York (1954).

[5] H. Poincaré, Compt. Rendus **123**, 530 (1896).

[6] J. J. Thomson, Electricity and Matter, Schribners, New York, 1904, p.26.

[7] P. A. M. Dirac, Proc. Roy. Soc. London **A 133**, 60 (1931).

[8] P. A. M. Dirac, Phys. Rev. **74**, 3845 (1948).

[9] G. t 'Hooft, Nucl. Phys. **B 79**, 276 (1974), A. Polyakov, Sov. Phys.–**JETP 20**, 194 (1974).

[10] H. Bradner et al., Phys. Rev. **114**, 603 (1959).

[11] P. B. Price et al., Phys. Rev. Lett. **59**, 2523 (1987).

[12] P. B. Price et al., Phys. Rev. Lett. **65**, 149 (1990).

[13] M. Bertani et al., Eur. Phys. Lett. **12**, 613 (1990).

[14] J. L. Pinfold et al., Phys. Lett. **B 316**, 407 (1993).

[15] B. Abbott et al., Phys. Rev. Lett. **81**, 524 (1998).

[16] L. Gamberg, G. R. Kalbfleisch, K. A. Milton, Found. Phys. **30**, 543 (2000).

[17] W. V. R. Malkus, Phys. Rev. **83**, 899 (1951).

[18] P. B. Price et al., Phys. Rev. Lett.**35**, 487 (1975).

[19] L. W. Alverez, Proceedings of the 1975 International Symposium on Lepton and Photon Interactions at High Energies, Stanford University, August 21-27, 967, 1975.

[20] B. Cabrera, Phys. Rev. Lett.**48**, 1378 (1982).

[21] P. H. Eberhard et al., Phys. Rev. **D 4**, 3260 (1971); L. W. Alvarez, LRL Physics Note-470, 1963 (unpublished).

[22] A. D. Caplin et al., Nature **321**, 402 (1986).

[23] S. Orito et al., Phys. Rev. Lett. **66**, 1951 (1991).

[24] M. Ambrosio et al., Phys. Lett.**B 406**, 249 (1997).

[25] E. Goto et al., Phys. Rev. **132**, 387 (1963).

[26] H. Jeon and M. J. Longo, Phys. Rev. Lett. **75**, 1443 (1995).

[27] E. N. Parker, Astrophys. J. **160**, 383 (1970).

[28] F. C. Adams et al., Phys. Rev. Lett. **70**, 2511 (1993).

[29] K. Freese and E. Krasteva, Phys. Rev. **D 59**, 063007 (1999).

[30] V. A. Rubakov, Pis'ma Zh. Eksp. Teor. Fiz. **33** 658 (1981) [JETP Lett. **33**, 744 (1981)]; C. G. Callan, Jr., Phs. Rev. **D 26**, 2058 (1982).

[31] G. R. Kalbfleisch, K. A. Milton, M. Strauss, L. Gambetg, E. H. Smith, W. Luo, Phys. Rev. Lett. **85**, 5292 (2000).

[32] S. Drell, T. Yan, Phys. Rev. Lett. **25** 316 (1970).

[33] H. A. Bethe, J. Schwinger, J. F. Carlson, and L. J. Chu, Transmission of Irises in Waveguides, 1942, in Bethe Papers, pp. 294-5.

[34] Y. Aharonov and D. Bohm, Phys. **Rev. 115**, 485 (1959).

[35] M. Blagojevic, Phys. Rep. **4 & 5**, 233-346 (1988).

[36] Ta-Pei Cheng and Ling-Fong Li, Gauge theory of elementary particle physics, Clarendon Press, 1984, p.459.

[37] L. Gamberg and K. A. Milton, Phys. Rev. **D 61**, 075013 (2000).

[38] K. A. Milton and L. L. DeRaad, J. Math. Phys. **19**, 375 (1978).

[39] J. Schwinger, Phys. Rev. **144**,1087 (1966).

[40] J. Schwinger, Phys. Rev. **173**, 1536 (1968).

[41] J. Schwinger, Phys. Rev. **D12**, 3105 (1975).

[42] D. Zwanziger, Phys. Rev. **D 3**, 880 (1971).

[43] Ta-Pei Cheng and Ling-Fong Li, Gauge theory of elementary particle physics, Clarendon Press, 1984, Chap.5.

[44] R. Rajaraman, Solitons and Instantons—An introduction to Solitons and Instantons in Quantum Field Theory, North Holland Publishing Company, 1982, p.69.

[45] J. Preskill, Ann. Rev. Nucl. Sci. **34**, 461 (1984).

[46] T. W. Kirkman and C. K. Zachos, Phys. Rev. **D 24**, 999 (1981).

[47] S. Coleman, The Magnetic Monopole Fifty Years Later, in The Unity of the Fundamental Interactions, edited by A. Zichichi, Plenum Press, 1983.

[48] T. M. Cho and D. Mason, Phys. Lett. **B 391**, 360 (1997).

[49] J. Schwinger, Particles, Sources, and Fields, Addison-Wesley Publishing Company, 1970, 3-8, and 3-9.

[50] R. Feynman, Phys. Rev. Lett. **23**, 1415(1969).

[51] J. D. Bjorken, Phys. Rev. **179**, 1547(1969).

[52] C. G. Callan and D. Gross, Phys. Rev. Lett. **22**, 156 (1969).

[53] H. D. Politzer, Phys. Rev. Lett. **30**, 1346 (1973), D. J. Gross and F. Wilczek, Phys. Rev. Lett. **30**, 1343 (1973).

[54] G. Sterman, *et el.*, Review of Modern Physics **67** No.1 Jan. 1995.

[55] A. D. Martin, et al., Eur. Phys. J. **C4**, 463 (1998).

[56] E. Reya, Phys. Rep. **69**, No.3 (1981) 195-333.

[57] I. Aitchison and A. Hey, Gauge Theories in Particle Physics, Adam Hilger, 1989, p.327.

[58] M. Gluck, E. Hoffmann, and E. Reya, 1982, Z.Phys. **C13**, 119.

[59] A. D. Martin et al., Phys. Rev. **D 47**, 867 (1988).

[60] H. L. Lai, et al., Phys. Rev. **D 51**, 4763(1995).

[61] M. Gluck, E. Reya, A. Vogt, Z. Phys. **C 67**, 433-447 (1995).

[62] H. L. Lai, et al., Phys. Rev. **D 55**, 1280 (1997).

[63] DØ Collaboration: B. Abbott et al., FERMILAB-PUB-98-207-E, e-Print Archive: hep-ex/9807018, F. Bedeschi, talk at 1999 Hadron Collider Physics Conference, Bombay, January, 1999.

[64] WA70 collaboration: M. Bonesini et al., Z. Phys. **C 38** (1988) 371, E706 collaboration: L. Apanasevichi et al., hep-ex/9711017.

[65] V. D. Barger and R. J. N. Phillips, Collider Physics, Addison-Wesley Publishing Comapany, Inc., 1997, p.158,

[66] J. C. Collins, E. E. Soper, and G. Sterman, in Perturbative Quantum Chromodynamics, ed. A. H. Mueller, World Scientific, 1989, p.9.

[67] J. Schwinger, L. L. DeRaad, Jr., K. A. Milton, and Wu-yang Tsai, Classical Electrodynamics, Advanced Book Program, Perseus Books, 1998, p.553.

[68] J. Schwinger, K. Milton, Wu-yang Tsai, L. L. DeRaad, Jr., and D. C. Clark, Ann. Phys., Vol.101, 451 (1976).

[69] Steven P. Ahlen, Rev. Mod. Phys. **52**, No.1, January 1980.

[70] N. Bohr, Philos. Mag. **25**, 10 (1913); Philos. Mag. **30**, 581 (1915).

[71] H. Bethe, Ann. Physik **5**, 325 (1930), Z. Phys. **76**, 293 (1932).

[72] F. Bloch, Ann. Phys. (Leipzig) **16**, 285 (1933); Z. Phys. **81**, 363 (1933).

[73] U. Fano, Ann. Rev. Nucl. Sci. **13**, 1 (1963).

[74] R. M. Sternheimer, Phys. Rev. **88**, 851 (1952); R. M. Sternheimer, M. J. Berger, and S. M. Seltzer, Atomic. Data and Nuclear Data Tables. **30**, 261-271 (1984).

[75] R. M. Sternheimer and R. F. Peierls, Phys. Rev. **B 3**, 3681 (1971).

[76] W. R. Leo, Techniques for Nuclear and Particle Physics Experiments, Springer-Verlag, 1987, p.21.

[77] Y. Kasama, C. N. Yang, and A. S. Goldhaber Phys. Rev. **D15**, 2287 (1977).

[78] S. P. Ahlen, Phys. Rev. **D 17**, 229 (1978).

[79] G. Carrier, M. Krooks, and C. Pearson, Functions of A Complex Variable, Mcgraw-Hill Book Company, 1966, p. 189.

[80] S. P. Ahlen and K.Kinoshita, Phys. Rev. **D 26**, 2347 (1982).

[81] DØ Collaboration, S. Abachi et al., Nucl. Inst. and Meth. in Phys. Res. **A 338**(1994) 185-253.

[82] CDF Collaboration, F. Abe et al., Nucl. Inst. & Meth. in Phys. Res. **A 271** (1988) 387-403.

[83] W. C. Carithers, et al., Nucl. Inst. & Meth. in Phys. Res. **A 289** (1990) 388-399.

[84] G. Brandenberg, et al., Nucl. Inst. & Meth. in Phys. Res. **A 267** (1988) 257-271.

[85] V. D. Barger, M. G. Olsson, Classical Electricity and Magnetisom, Allyn and Bacon, Inc., 1987, p.203.

[86] L. Bracci, G. Fiorentini, Nucl. Phys. **B 232** (1984) 236-262.

[87] K. Olaussen, R. Sollie, Nucl. Phys. **B 255** (1985) 465-479.

[88] L. Gamberg, G. Kalbfleisch, and K. Milton, Found. of Phys. **30**, No. 4, 543-565 (2002); K. Milton, "Remarks on Binding", "Summary of Monopole Binding to Magnetic Moments", unpublished.

[89] T.T.Wu and C. N.Yang, Nucl. Phys. **B 107** (1976) 365-380.

[90] C. J. Goebel, "Binding Nuclei to Monopoles", in Monopole '83, ed. J. L. Stone, Plenum, 1984, p.333.

[91] K. Milton, G. Kalbfleisch, W. Luo, L. Gamberg, Int. J. Mod. Phys. **A 17**, 732-750 (2002).

[92] K. Milton, Electromagnetism II Examination, 1997, unpublished.

[93] B. D. Josephson, Phys. Lett. **1**, 251(1962).

[94] R. Feynman, Feynman Lectures on Physics, Vol.3, Addison-Wesley Publishing Co., 1965, Chap.21; A. Barone and G. Paterno, Physics and Applications of the Josephson Effect, John Wiley & Sons, 1982, Chap.9; J. B. Ketterson and S. N. Song, Superconductivity, Cambridge University Press, 1999, Part I.

[95] T. Van Duzer and C. W. Turner, Principles of Superconductive Devices and Circuits, Elsevier North Holland, 1981, Chap.5.

[96] W. N. Boroski, T. H. Nicol, and C. J. Schoo, Fermilab TS/Engineering, unpublished.

[97] W. N. Boroski, T. H. Nicol, and C. J. Schoo, Design of the Multilayer Insulation System for the Superconducting Supercollider 50 mm Dipole Cryostat, in Supercollider 3, Plenum Press, ed. J. Nonte, 1991, p. 849.

[98] A. Barone and G. Paterno, Physics and Applications of the Josephson Effect, John Wiley & Sons, 1982, pp.409-412.

[99] C. Delaney, Electronics for the Physicist, Ellis Horwood Limited, 1980, chap.11.

[100] V. D. Barger, M. G. Olsson, pp.199-202.

[101] J. Schwinger, L. L. DeRaad, Jr., K. A. Milton, and Wu-yang Tsai, Classical Electrodynamics, p.324; H. J. Frisch, Summary of Induction Detectors and Techniques, in Monopole 83', p.516.

[102] Fermi News, March 8, 1996, p.6.

[103] S. L. Meyer, Data Analysis for Scientists and Engineers, John Wiley & Sons, Inc., 1975, p.146.

[104] G. J. Feldman and R. D. Cousins, Phys. Rev. **D 57**, 3873 (1998).

[105] K. A. Milton and L. Gamberg's notes, unpublished.

[106] I. Aitchison and A. Hey, Gauge Theories in Particle Physics, p.377.

Appendix

Monte Carlo Program for Pb Samples

There are three kinds of programs used in the monopole project:

1. The Labview programs used for data acquisition;

2. The Igor programs used for data analysis; and

3. The Monte Carlo programs used for energy loss and cross section calculations.

I wrote the Monte Carlo programs for different samples. The following porgram is for the lead samples in the CDF detector.

ccccccccccccccccccccccccccccccccccccccccccccccccccccccccccccccccccccccc

Some subroutines and functions used in this program are listed as follows. M is the energy of monopole pair and m the mass of monopole.

dSdM: main program, gives $\frac{d\sigma}{dM}(M,m)$ and $\frac{d\sigma_A}{dM}(M,m)$ 142

ds_dm(): compute $\frac{d\sigma}{dM}(M)$ and $\frac{d\sigma_A}{dM}(M)$ given m 143

Eloss() comppute energy loss in the detectors 160

lossBe() energy loss in Be pipe 162

lossSVX() energy loss in silicon vertex detector 191

lossVTPC() energy loss in vertex time projection chamber 196

lossFTC() energy loss in forward tracking chamber 198

rangePb() energy loss and range in Pb layers 183

lossAlG10() energy loss in the materials between Pb layers 164

solid() energy loss in the given material 166

Bfield()	magnetic field in the materials	172
Spb()	energy loss at low speed	183
g1()	interpolation function	184
coef()	apply coeficients (obtained from Igor program) for curve fitting	200
g()	interpolation function	190
solidPb()	energy loss in the Pb layer	184
Bfield1()	homogenous magnetic field inside the solenoid	174
Bfield2()	inhomogenous magnetic field	178
layers()	get weight function (for Monte Carlo calculation) for each layer	157
dS()	get $\frac{d\sigma_A}{dM}$ for given mass m and given energy M	158
DYw()	get $\frac{d\sigma}{dM}$ for given mass m and given energy M	157
prot()	get quark distribution functions using CTEQ parametrizaiton	211


```
ccccccccccccccccccccccccccccccccccccccccccccccccccccccccccccccccccccccc
c This Monte Carlo program in Fortran is used to calculate the Drell-Yan cross
c section dσ/dM and the accepted cross section dσA/dM as the functions of mass M
c for magnetic monopoles in the CDF detector. The total cross section σ and
c σA can be obtained by integrating dσA/dM and dσA/dM over mass M.
ccccccccccccccccccccccccccccccccccccccccccccccccccccccccccccccccccccccc
program dSdM
implicit double precision(a-h,o-z)
double precision mm,m0
parameter (n=9)
dimension j(n)
data j/200,225,250,275,300,325,350,375,400/
z = 1.0
m0 = 10.0
```

```
do 1 i=1,n
mm = j(i)*1.0
call ds_dm(i,z,mm)
1 continue
stop
end


ccccccccccccccccccccccccccccccccccccccccccccccccccccccccc
c This program is used to compute the cross section with CTEG5 data
c by using Monte Carlo method
c This program has considered the angular distribution and use the
c angular distribution in the lab frame to restrict the angular
c distribution in the CM frame based on the Lorentz transformation.
subroutine ds_dm(ii,z,mm)
Implicit Double Precision (A-H, O-Z)
double precision mm,Ie,Mnu,mmj,m
c Drell-Yan pair production cross section
parameter (n=1000,kk=1300)
dimension w1(n),w2(n),w3(n),w4(n),w5(n),w6(n),wd(n),x(n)
dimension w11(n),w22(n),w33(n),w44(n),w55(n)
ccccccccccccccccccccccccccccccccccccccccccccccccccccccccc
print*,'ds_dm'
print*,'n:',n
alpha = 1.0/137.0
pie = 4.0*atan(1.0)
rts = 1800.0
wIe = 3.8935E+8
```

```
arfa1 = 3.0/180.0*pie
arfa2 = 10.0/180.0*pie
ct1 = Cos(arfa1)
ct2 = Cos(arfa2)
ct3 = -ct2
ct4 = -ct1
Emax = 900.00
Rmax = 150.00
ccccccccccccccccccccccccccccccc
print*,'ct1,ct2:',ct1,ct2
Xmin = 1.0000E-05
mmj = 2.0*mm
ss1 = 660.0*tan(arfa1) !cm
ss2 = 660.0*tan(arfa2) !cm
Ie = 3.8935E+8
dm = (rts - 2.0*mm)/(1.0*(n-1))
print*,'dM=',dm
mmj = 2.0*mm + 0.0001
kkk = 0
print*,'before 20'
L1 = 1
L2 = 2
L3 = 3
L4 = 4
L5 = 5
L6 = 6
L11 = 11
```

```
L22 = 22
L33 = 33
L44 = 44
L55 = 55
Ld = 0
Rgd = 0.0
ccccccccccccccccccccccccccc
do 20 j = 1,n-1
do 3 i=1,n
x(i) = 0.0
w1(i)=0.0
w2(i)=0.0
w3(i)=0.0
w4(i)=0.0
w5(i)=0.0
w6(i)=0.0
wd(i)=0.0
w33(i)=0.0
w44(i)=0.0
w22(i)=0.0
w11(i)=0.0
w55(i)=0.0
3 continue
m = mmj + (j-1)*dm
am = m
ave_m1 = 0.0
ave_m2 = 0.0
```

```
ave_m3 = 0.0
ave_m4 = 0.0
ave_m5 = 0.0
ave_m6 = 0.0
ave_m11 = 0.0
ave_m22 = 0.0
ave_m33 = 0.0
ave_m44 = 0.0
ave_m55 = 0.0
ave_md = 0.0
i_rand = 0
ccccccccccccc
n1 = 0
n2 = 0
n3 = 0
n4 = 0
n5 = 0
n6 = 0
n11 = 0
n22 = 0
n33 = 0
n44 = 0
n55 = 0
nd = 0
Sm1 = 0.0
Sm2 = 0.0
Sm3 = 0.0
```

```
Sm4 = 0.0
Sm5 = 0.0
Sm6 = 0.0
Sm11 = 0.0
Sm22 = 0.0
Sm33 = 0.0
Sm44 = 0.0
Sm55 = 0.0
Smd = 0.0
print*,'before 4,j=',j
pm = 0.0
pmL = 0.0
Emc = 0.0
do 4 i =1,n-1
am1 = am + rand(0)*dm
q = am1**2
x1 =Xmin + rand(0)
x2 = q/(x1*rts**2)+ Xmin
costCM = 1-2.0*rand(0)
i_rand = i_rand + 1
do while((x1 .gt. 1.0).or.(x2 .gt. 1.0))
am1 = am + rand(0)*dm
q = am1**2
x1 = rand(0)+Xmin
x2 = q/(x1*rts**2)+ Xmin
costCM = 1-2.0*rand(0)
i_rand = i_rand + 1
```

```
end do
x(i) = x1
bet = sqrt(abs(1.0 - (2.0*mm)**2/am1**2))
c do angular limitation and Lorentz transformation
ccccccccccccccccccccccccccccccccccccccccccccccccccccc
etaCM =abs(x2-x1)/(2.0*sqrt(x1*x2))
gamCM=sqrt(etaCM**2+1.0)
estar = am1/2.0
estar = am1/2.0
if(costCM .lt. 0.0) then
pstar = -sqrt(abs(estar**2-mm**2))
else
pstar=sqrt(abs(estar**2-mm**2))
endif
eLb = etaCM*pstar*costCM+gamCM*estar
if(costCM .lt. 0.0) then
pLb = -sqrt(abs(eLb**2-mm**2))
else
pLb = sqrt(abs(eLb**2-mm**2))
endif
costLb=(gamCM*pstar*costCM+etaCM*estar)/pLb
ccccccccccccccccccccccccc
c Drell-Yan
ccccccccccccccccccccccccccc
ave_md = ave_md + am1
nd = nd + 1
c print*,'before DYw, q=',q,i
```

```
call DYw(z,bet,x1,x2,q,wd(i))
c print*,'after DYw, q=',q,i
if(Smd .lt. wd(i)) then
Smd = wd(i)
endif
ccccccccccccccccccccccccccccccccccc
c do energy loss
ccccccccccccccccccccccccccccccccccc
st = 0.99999999
if(abs(costLb) .gt. st) then
goto 4
endif
call Eloss(R0,cs0,h0,y0,Eout,z,mm,eLb,costLb)
if(Eout .le. mm) then
goto 4
endif
if(abs(cs0) .gt. st) then
goto 4
endif
d1 = 140.0 !cm, constant field region
d2 = 400.0 !cm, not constant field region
if(abs(h0) .lt. d1) then
call Bfield1(z,Eout,cs0,mm,Eout1,cs1,h0,h1,y0,y1)
call Bfield2(z,Eout1,cs1,mm,Eout2,cs,h1,h,y1,y,L)
else
call Bfield2(z,Eout,cs0,mm,Eout2,cs,h0,h,y0,y,L)
endif
```

```
c First cut by the iron
if(L .eq. 0) then
goto 4
endif
c Count particles in the opposite direction
if(cs .eq. 0.0) then
goto 4
endif
tann = sqrt(abs(1.0-cs**2))/abs(cs)
dd = 660.0 - abs(h)
yy = y + tann*dd
ccccccccccccccccccc
c angl cuts
ccccccccccccccccccc
if((yy .lt. ss1) .or. (yy .gt. ss2)) then
goto 4
endif
Ein3 = Eout2
ccccccccccccccccccccccccc
c First Layer
ccccccccccccccccccccccccc
call rangePb(Rg1,z,Ein3,mm,cs,Eout3)
Rg1 = Rg1 + R0
if(Eout3 .le. mm) then
ave_m1 = ave_m1 + am1
n1 = n1 + 1
call layers(z,costCM,bet,x1,x2,q,w1(i))
```

```
if(Sm1 .lt. w1(i)) then
Sm1 = w1(i)
endif
goto 4
else
call lossAlG10(Rg11,E11,z,Eout3,mm,cs)
Rg11 = Rg11 + Rg1
if(E11 .le. mm) then
ave_m11 = ave_m11 + am1
n11 = n11 + 1
call layers(z,costCM,bet,x1,x2,q,w11(i))
if(Sm11 .lt. w11(i)) then
Sm11 = w11(i)
endif
goto 4
endif
endif
c Second Layer
Ein4 = E11
call rangePb(Rg2,z,Ein4,mm,cs,Eout4)
Rg2 = Rg2 + Rg11
if(Eout4 .le. mm) then
ave_m2 = ave_m2 + am1
n2 = n2 + 1
call layers(z,costCM,bet,x1,x2,q,w2(i))
if(Sm2 .lt. w2(i)) then
Sm2 = w2(i)
```

```
endif
goto 4
else
call lossAlG10(Rg22,E22,z,Eout4,mm,cs)
Rg22 = Rg22 + Rg2
if(E22 .le. mm) then
ave_m22 = ave_m22 + am1
n22 = n22 + 1
call layers(z,costCM,bet,x1,x2,q,w22(i))
if(Sm22 .lt. w22(i)) then
Sm22 = w22(i)
endif
goto 4
endif
endif
c Third Layer
Ein5 = E22
call rangePb(Rg3,z,Ein5,mm,cs,Eout5)
Rg3 = Rg3 + Rg22
if(Eout5 .le. mm) then
ave_m3 = ave_m3 + am1
n3 = n3 + 1
call layers(z,costCM,bet,x1,x2,q,w3(i))
if(Sm3 .lt. w3(i)) then
Sm3 = w3(i)
endif
goto 4
```

```
else
call lossAlG10(Rg33,E33,z,Eout5,mm,cs)
Rg33 = Rg33 + Rg3
if(E33 .le. mm) then
ave_m33 = ave_m33 + am1
n33 = n33 + 1
call layers(z,costCM,bet,x1,x2,q,w33(i))
if(Sm33 .lt. w33(i)) then
Sm33 = w33(i)
endif
goto 4
endif
endif
c Fourth Layer
Ein6 = E33
call rangePb(Rg4,z,Ein6,mm,cs,Eout6)
Rg4 = Rg4 + Rg33
if(Eout6 .le. mm) then
ave_m4 = ave_m4 + am1
n4 = n4 + 1
call layers(z,costCM,bet,x1,x2,q,w4(i))
if(Sm4 .lt. w4(i)) then
Sm4 = w4(i)
endif
goto 4
else
call lossAlG10(Rg44,E44,z,Eout6,mm,cs)
```

```
c print*,'4,after AlG,Eout:',E44
Rg44 = Rg44 + Rg4
if(E44 .le. mm) then
ave_m44 = ave_m44 + am1
n44 = n44 + 1
call layers(z,costCM,bet,x1,x2,q,w44(i))
if(Sm44 .lt. w44(i)) then
Sm44 = w44(i)
endif
goto 4
endif
endif
ccccccccccccccccccc
c Fifth Layer
Ein7 = E44
call rangePb(Rg5,z,Ein7,mm,cs,Eout7)
Rg5 = Rg5 + Rg44
if(Eout7 .le. mm) then
ave_m5 = ave_m5 + am1
n5 = n5 + 1
call layers(z,costCM,bet,x1,x2,q,w5(i))
if(Sm5 .lt. w5(i)) then
Sm5 = w5(i)
endif
goto 4
else
call lossAlG10(Rg55,E55,z,Eout7,mm,cs)
```

```
Rg55 = Rg55 + Rg5
if(E55 .le. mm) then
ave_m55 = ave_m55 + am1
n55 = n55 + 1
call layers(z,costCM,bet,x1,x2,q,w55(i))
if(Sm55 .lt. w55(i)) then
Sm55 = w55(i)
endif
goto 4
endif
endif
c Sixth Layer
Ein8 = E55
call rangePb(Rg6,z,Ein8,mm,cs,Eout8)
Rg6 = Rg6 + Rg5
if(Eout8 .le. mm) then
ave_m6 = ave_m6 + am1
n6 = n6 + 1
call layers(z,costCM,bet,x1,x2,q,w6(i))
if(Sm6 .lt. w6(i)) then
Sm6 = w6(i)
endif
goto 4
else
goto 4
endif
4 continue
```

```
pmc = sqrt(Emc**2 - mm**2)
ccccccccccccccccccccccccccccccccccccc
c Cross Sections:
ccccccccccccccccccccccccccccccccccccc
c Drell-Yan Cross Section
call dS(ii,nd,x,Smd,wd,ave_md,m,nbind,j,Ld)
c First Layer
call dS(ii,n1,x,Sm1,w1,ave_m1,m,nbin1,j,L1)
call dS(ii,n11,x,Sm11,w11,ave_m11,m,nbin11,j,L11)
c Second Layer
call dS(ii,n2,x,Sm2,w2,ave_m2,m,nbin2,j,L2)
call dS(ii,n22,x,Sm22,w22,ave_m22,m,nbin22,j,L22)
c Third Layer
call dS(ii,n3,x,Sm3,w3,ave_m3,m,nbin3,j,L3)
call dS(ii,n33,x,Sm33,w33,ave_m33,m,nbin33,j,L33)
c Fourth Layer
call dS(ii,n4,x,Sm4,w4,ave_m4,m,nbin4,j,L4)
call dS(ii,n44,x,Sm44,w44,ave_m44,m,nbin44,j,L44)
c Fifth Layer
call dS(ii,n5,x,Sm5,w5,ave_m5,m,nbin5,j,L5)
call dS(ii,n55,x,Sm55,w55,ave_m55,m,nbin55,j,L55)
c Sixth Layer
call dS(ii,n6,x,Sm6,w6,ave_m6,m,nbin6,j,L6)
20 continue
return
end
ccccccccccccccccccccccccccccccccccccccccccccccccccccccccccccccccccccc
```

```
subroutine DYw(z,bet,x1,x2,q,w)
implicit double precision(a-h,o-z)
alpha = 1.0/137.0
pie = 4.0*atan(1.0)
rts = 1800.0
c get weight function based on the cross section integrand
call prot(x1,q,db1,ub1,u1,d1,s1)
call prot(x2,q,db2,ub2,u2,d2,s2)
A = 8.0*(137.0*z/2.0)**2*pie*alpha**2/(9.0*rts**2)
B=(4.0*(u1*u2+ub1*ub2) +
* d1*d2+db1*db2
* + 2.0*s1*s2)/(9.0*x1)
w = bet**3*A*B/sqrt(abs(q)) !m(j)
return
end
ccccccccccccccccccccccccccccccccccccccccccccccccccccccccccccccc
ccccccccccccccccccccccccccccccccccccccccccccccccccccccccccccccc
subroutine layers(z,csm,bet,x1,x2,q,w)
implicit double precision(a-h,o-z)
alpha = 1.0/137.0
pie = 4.0*atan(1.0)
rts = 1800.0
C = 2.0*(1.0 + csm**2)
c get weight function based on the cross section integrand
call prot(x1,q,db1,ub1,u1,d1,s1)
call prot(x2,q,db2,ub2,u2,d2,s2)
A = (137.0*z/2.0)**2*pie*alpha**2/(3.0*rts**2)
```

```
B=(4.0*(u1*u2+ub1*ub2)+d1*d2+db1*db2+2.0*s1*s2)/(9.0*x1)
w = bet**3*A*B*C/sqrt(abs(q)) !m(j)
return
end
ccccccccccccccccccccccccccccccccccccccccccccccccccccccccccccccc
subroutine dS(ij,n0,x,Sm,w,ave_m,m,nbin,j,L)
implicit double precision(a-h,o-z)
parameter (kk = 1300,k=600,n=1000)
double precision m,Ie
dimension f(n),w(n)
dimension nbin(kk),x(n)
Ie = 3.8935E+8
Emax = 1800.0
Rmax = 150.0
do 1 ii=1,n
f(ii) = 0.0
1 continue
do 2 jj= 1,kk
nbin(jj)=0
2 continue
Smax = Sm
if(n0 .ne. 0) then
m = ave_m/(1.0*n0)
endif
c accept-reject based on the weight w(j,i)
c rearrange the order of mass
Np=0
```

```
Nn=0
do 14 i=1,n-1
f(i) = rand(0)
if(Smax .gt. 0.0) then
w(i) = w(i)/Smax
endif
L1 = k*x(i) + 1
if(f(i) .lt. w(i)) then
nbin(L1) = nbin(L1) + 1
else
goto 14
endif
14 continue
Smax = Ie*Smax
aver1 = 0.0
aver2 = 0.0
sigma = 0.0
do 8 L1 = 1, k
sigma = sigma + 1.0*Smax*nbin(L1)/(1.0*n)
aver1 = aver1 + 1.0*Smax*nbin(L1)/(1.0*n*k)
aver2 = aver2 + (1.0*Smax*nbin(L1)/(1.0*n))**2/(1.0*k)
8 continue
del0 = sqrt(abs(aver2 - aver1**2)/(1.0*k))
del = sqrt(1.0/(1.0*n)*(sigma*abs((Smax-sigma))))
write(ij+10*L+200,12) m,sigma
12 format(3e14.4,3e14.4)
write(ij+10*L,11) j,Smax,sigma,m,del
```

```
11 format(i4,3e14.4,3e14.4,3e14.4,3e14.4)
return
end
ccccccccccccccccccccccccccccccccccccccccccccccccccccccccccccccccccccc
subroutine Eloss(R,cs,h,y,Eout,z,mm,E,cs0)
c Use S. Ahlen's formula, S.P. Ahlen, Monopole Energy Loss
c and Detector Excitation Mechanism, "Magnetic Monopoles"
c Edited by R. Carrigan,Jr and W.Trower, Plenum Press,1983
c use Simpson's rule
c energy loss in the D0 detector
implicit double precision(a-h,o-z)
double precision mm
R = 0.0
cs = cs0
Eout = E
if(E .le. mm) then
return
endif
call lossBe(R1,Ebe,z,E,mm,cs0,cs1,h1,y1)
if(Ebe.le.mm) then
h = h1
y = y1
cs = cs1
Eout = Ebe
R = R1
return
endif
```

```
E2 = Ebe
call lossSVX(R2,Esvx,z,E2,mm,cs1,cs2,h2,y2)
h2 = h2 + h1
y2 = y2 + y1
R2 = R2 + R1
if(Esvx.le.mm) then
h = h2
y = y2
cs = cs2
Eout = Esvx
R = R2
return
endif
E3 = Esvx
call lossVTPC(R3,Ev,z,E3,mm,cs2,cs3,h3,y3)
h3 = h3 + h2
y3 = y3 + y2
R3 = R3 + R2
if(Ev.le.mm) then
h = h3
y = y3
cs = cs3
Eout = Ev
R = R3
return
endif
E4 = Ev
```

```
call lossFTC(R4,Ef,z,E4,mm,cs3,cs4,h4,y4)
h = h4 + h3
y = y4 + y3
R = R4 + R3
cs = cs4
Eout = Ef
return
end
ccccccccccccccccccccccccccccccccccccccccccccccccccc
subroutine lossBe(Rn,E,z,E0,mm,cs0,cs,h,y)
implicit double precision(a-h,o-z)
double precision Im,m,Na,Im1,m1,Na1
double precision Ka,K1,K2,me,mm,Nc,Nmol
c Be:
Im = 63.7E-9
m = 2.4339
Na = 4
hbo = 26.098E-9
x0 = 0.0592
x1 = 1.6922
! cm
Za = 0.44384 ! Z/A
den = 1.848 ! g/cm^3
R1 = 0.05 ! cm
L1 = 1
call Solid(R1,Rn1,E1,z,E0,mm,cs0,Im,hbo,x0,x1,Na,m,den,Za,
* cs1,h1,y1,L1)
```

```
if(E1 .le. mm) then
E = E1
Rn = Rn1
h = h1
y = y1
cs = cs1
return
else
c C:
pi = 4.0*atan(1.0)
Im1 = 78.0E-9
m1 = 3.0036
Na1 = 6.0
hbo1 = 28.08E-9
x10 = -0.0351
x11 = 2.486
! cm
Za1 = 0.49954 ! Z/A
den1 = 2.00 ! g/cm^3
L2 = 2
yy1 = 10.0
yy2 = 28.0
ty1 = 180.0 - yy1
ty2 = 180.0 - yy2
xx = abs(acos(cs1))*180.0/pi
if((xx.gt.yy1) .and.(xx.lt.yy2)) then
R2 = -3.0*xx/4.0 + 24.0
```

```
else
if((xx.lt.ty1) .and.(xx.gt.ty2)) then
R2 = -3.0/4.0*(180.0-xx-32.0)
else
if((xx.gt.yy2) .or.(xx.lt.ty2)) then
R2 = 2.5
else
R2 = 0.0
endif
endif
endif
R2 = R2*18.8/100.0 ! cm
call Solid(R2,Rn2,E,z,E1,mm,cs1,Im1,hbo1,x10,x11,
* Na1,m1,den1,Za1,cs,h2,y2,L2)
Rn = Rn1 + Rn2
h = h1 + h2
y = y1 + y2
endif
return
end
ccccccccccccccccccccccccccccccccccccccccccccccccccccccccccc
ccccccccccccccccccccccccccccccccccccccccccccccccccccccccccc
subroutine lossAlG10(Rn,E,z,E0,mm,cs0)
implicit double precision(a-h,o-z)
double precision Im,m,Na,Im1,m1,Na1
double precision Ka,K1,K2,me,mm,Nc,Nmol
c Al:
```

```
Im = 164.0E-9
hbo = 32.86E-9
Na = 13
m = 3.6345
x0 = 0.1708
x1 = 3.0127
R1 = 0.22 ! cm
Za = 0.48181 ! Z/A
den = 2.7 ! g/cm^3
L3 = 30
call Solid(R1,Rn1,E1,z,E0,mm,cs0,Im,hbo,x0,x1,Na,m,den,Za,
* cs1,h1,y1,L3)
c print*,'Al,E1,E2:',E0,E1
if(E1 .le. mm) then
E = E1
Rn = Rn1
h = h1
y = y1
cs = cs1
return
else
c G10:
Im1 = 139.2E-9
hbo1 = 31.014E-9
x10 = 0.1385
x11 = 3.0025
Na1 = 30
```

```
m1 = 3.5064
R2 = 0.1 !cm
den1 = 2.32
Za1 = 0.4993
L7 = 7
call Solid(R2,Rn2,E,z,E1,mm,cs1,Im1,hbo1,x10,x11,
* Na1,m1,den1,Za1,cs,h2,y2,L7)
Rn = Rn1 + Rn2
h = h1 + h2
y = y1 + y2
endif
return
end
ccccccccccccccccccccccccccccccccccccccccccccccccccccccccc
subroutine Solid(R,Rn,Eout,z,Ein,mm,cs0,Im,hbo,x0,x1,
* Na,m,den,Za,cs,h,y,L)
implicit double precision(a-h,o-z)
double precision m,Ka,me,mm,Im,Nc,Ne,Na,Nmol,K1,K2,Nav
parameter (nn=201,n=4,n1=240)
dimension f(nn),v1(n),c1(n),v2(n1),c2(n1)
do 10 i3=1,nn
f(i3)=0.0
10 continue
rts = 1800.0
factor = z/2.0
ge = factor*1.97327E-14 ! Gev.cm n = 1
me = 0.511E-3 ! mass of electron Gev
```

```
hb = 6.582E-25 ! Gev s
pie = 4.0*atan(1.0)
Nav = 6.02E+23 ! Avogadro constant
C = -2.0*log(Im/hbo) -1.0
c ! number of electrons per
Ne = Nav*den*Za ! unit volume for gas
ccccccccccccccccccccccccc
B1 = 0.248 ! Bloch correction, n = 1
B2 = 0.672 ! Bloch correction, n = 2
B3 = 1.022 ! Bloch correction, n = 3
B6 = 1.685 ! Bloch correction, n = 6
if(z .eq. 1.0) then
B = B1
else if(z .eq. 2.0) then
B = B2
else if(z .eq. 3.0) then
B = B3
else if(z .eq. 6.0) then
B = B6
endif
K1 = 0.406
K2 = 0.346
if(z .lt. 2.0) then
Ka = K1
else if(z .ge. 2.0) then
Ka = K2
endif
```

```
ccccccccccccccccccccccccc
A2 = Ka/2.0 - 0.5
aa = -(C + 4.606*x0)/(x1 - x0)**m
D1 = 0.0
ee = Ein
Rn = 0.0
delE = 0.0
del1 = R/(1.0*nn)
dbeta = 1.0/(1.0*nn)
A = 4.0*pie*Ne*ge**2/(me)
do 50 i2=1,n
v1(i2) = 0.0
c1(i2) = 0.0
50 continue
beta3 = 0.00001+ 31*dbeta
ee3 = mm/sqrt(1.0-beta3**2)
A13 = Log(2*(ee3**2-mm**2)*me/(Im*mm**2))
X13 = Log10(sqrt(ee3**2-mm**2)/mm)
if(X13 .le. x0) then
A33 = D1
else if((X13 .gt. x0).and.(X13.lt.x1)) then
A33 = 4.606*X13+C+aa*(x1 - X13)**m
else if(X13 .ge. x1) then
A33 = 4.606*X13 + C
endif
beta4 = 0.00001+ 33*dbeta
ee4 = mm/sqrt(1.0-beta4**2)
```

```
A14 = Log(2*(ee4**2-mm**2)*me/(Im*mm**2))
X14 = Log10(sqrt(ee4**2-mm**2)/mm)
if(X14 .le. x0) then
A34 = D1
else if((X14 .gt. x0).and.(X14.lt.x1)) then
A34 = 4.606*X13+C+aa*(x1 - X14)**m
else if(X14 .ge. x1) then
A34 = 4.606*X14 + C
endif
v1(2) = 0.00001+ 3*dbeta
c1(2) = 180.0*v1(2)*(z/2.0)**2
v1(3) = beta3
c1(3) = A*(A13 + A2 - A33/2 - B)/den
v1(1) = 0.00001+ 2*dbeta
c1(1) = 180.0*v1(1)*(z/2.0)**2
v1(4) = beta4
c1(4) = A*(A14 + A2 - A34/2 - B)/den
v2(1) = v1(1)
v2(n1) = v1(n)
ccccccccccccccccccccccccccccccccccccccc
call coef(p0,p1,p2,p3,p4,p5,z,L)
ccccccccccccccccccccccccccccccccccccccccccccc
y = 0.0
cs = cs0
Rn = 0.0
h = 0.0
do 1 i = 1,nn
```

```
beta = sqrt(abs(1-(mm/ee)**2))
A1 = Log(2*(ee**2-mm**2)*me/(Im*mm**2))
X = Log10(sqrt(ee**2-mm**2)/mm)
if(X .le. x0) then
A3 = D1
else if((X .gt. x0).and.(X.lt.x1)) then
A3 = 4.606*X+C+aa*(x1 - X)**m
else if(X .ge. x1) then
A3 = 4.606*X + C
endif
if(beta .lt. v1(1)) then
f(i) = 180.0*beta*(z/2.0)**2
else if(beta .gt. v1(4)) then
f(i) = A*(A1 + A2 - A3/2 - B)/den
else
f(i) = g1(p0,p1,p2,p3,p4,p5,beta)
endif
if((cs .eq. 0.0).or.(cs .eq. 1.0)) then
exit
endif
sn = sqrt(abs(1.0-cs**2))
ctan = cs/sn
if((L .eq. 7) .or. (L .eq. 30)) then
delE = f(i)*del1*den/abs(cs)
else
call Bfield(z,ee,cs0,del1,mm,Eb,cs)
if(L .eq. 1) then
```

```
delE = f(i)*del1*den/sn
ee = Eb
else
delE = f(i)*del1*den
ee = Eb
endif
endif
ee = ee - delE
cs0 = cs
if((cs .eq. 0.0).or.(cs .eq. 1.0)) then
exit
endif
sn = sqrt(abs(1.0-cs**2))
ctan = cs/sn
y = del1 + y
h = del1*ctan + h
Eout = ee
if(ee .le. mm) then
Eout = mm
exit
endif
if((L .eq. 7) .or. (L .eq. 30)) then
Rn = Rn + del1*den/abs(cs)
else
if(L .eq. 1) then
Rn = Rn + del1*den/sn
else
```

```
Rn = Rn + del1*den
endif
endif
1 continue
return
end
ccccccccccccccccccccccccccccccccccccccccccccccccccccccc
subroutine Bfield(z,Ein,cosLb,del1,mm,Eout,cs)
implicit double precision(a-h,o-z)
double precision mm
c print*,'In Bfeild,Ein,cosLb:',Ein,cosLb
c Add B field B = 1.4 T, use SI units
pie = 4.0*atan(1.0)
GevJ = 1.6E-10 ! 1 GeV = 1.6E-10 J
g = z*3.29E-9 ! A.m
Bf = 1.4 !T
c Off B:
c Bf = 0.0
Elb = Ein
Eout = Ein
cs = cosLb
if(Ein .lt. mm) then
return
endif
del1 = del1/100.0 ! cm —> m
sinLb = sqrt(abs(1.0-cosLb**2))
p = sqrt(Elb**2-mm**2)
```

```
py = p*sinLb
if((cosLb .ge. 0.0) .and. (cosLb .lt. 1.0)) then
Elb = Elb + g*Bf*del1/GevJ
if(Elb .le. mm) then
return
endif
p = sqrt(Elb**2-mm**2)
if(p .lt. py) then
return
endif
px = sqrt(p**2 - py**2)
else
Elb = Elb - g*Bf*del1/GevJ
if(Elb .le. mm) then
return
endif
p = sqrt(Elb**2-mm**2)
if(p .lt. py) then
return
else
px = -sqrt(p**2 - py**2)
endif
endif
del1 = del1*100.0
cs = px/p
ss = sqrt(abs(1.0 - cs**2))
Eout = Elb
```

```
c print*,'In Bfeild,Eout,cs:',Eout,cs
return
end
ccccccccccccccccccccccccccccccccccccccccccccccccccccccccccccccccc
subroutine Bfield1(z,Ein,cosLb,mm,Eout,cs,h0,h,y0,y)
implicit double precision(a-h,o-z)
parameter(n = 100)
double precision mm
c Add B field B = 1.4 T, use SI units
pie = 4.0*atan(1.0)
GevJ = 1.6E-10 ! 1 GeV = 1.6E-10 J
g = z*3.29E-9 ! A.m
d1 = 1.4 ! m, region of constant field
Bf = 1.4 !T
c Bf = Bf*2.0/3.0
c Off B:
c Bf = 0.0
c cm -> m
eplugx = 240.0 !cm, distance between interaction and
! the iron
eplugy = 41.38 !cm, the height cut by the iron
Elb = Ein
Eout = Ein
h = h0
y = y0
cs = cosLb
if(Elb .lt. mm) then
```

```
return
endif
h0 = h0/100.0
y0 = y0/100.0
sinLb = sqrt(abs(1.0-cosLb**2))
ss = sinLb
if(cs .eq. 0.0) then
return
endif
t = abs(ss/cs)
dd = (d1 - h0)/(1.0*n)
if(dd .le. 0.0) then
return
endif
d2 = dd
hn0 = d1*100.0-dd*100.0
hneg = - hn0
p = sqrt(Elb**2-mm**2)
py = p*sinLb
if(p .lt. py) then
return
endif
do while((h .le. hn0).and.(h.ge.hneg))
if((cs .lt. 1.0).and.(cs.ge.0.0)) then
d2 = dd
Elb = Elb + g*Bf*d2/GevJ
if(Elb .lt. mm) then
```

```
cycle
endif
p = sqrt(Elb**2-mm**2)
if(p .lt. py) then
cycle
endif
px = sqrt(p**2 - py**2)
cs = px/p
ss = sqrt(abs(1.0 - cs**2))
else
d2 = -dd
Elb = Elb + g*Bf*d2/GevJ
if(Elb .lt. mm) then
d2 = dd
Elb = Elb + g*Bf*d2/GevJ
p = sqrt(Elb**2-mm**2)
if(p .lt. py) then
Elb = sqrt(py**2 + mm**2) + g*Bf*d2/GevJ
p = sqrt(Elb**2-mm**2)
endif
px = sqrt(p**2 - py**2)
cs = px/p
ss = sqrt(abs(1.0 - cs**2))
else
p = sqrt(Elb**2-mm**2)
if(p .lt. py) then
d2 = dd
```

```
Elb = sqrt(py**2 + mm**2) + g*Bf*d2/GevJ
p = sqrt(Elb**2-mm**2)
px = sqrt(p**2 - py**2)
cs = px/p
ss = sqrt(abs(1.0 - cs**2))
if(cs .eq. 0.0) then
return
endif
else
px = -sqrt(p**2 - py**2)
cs = px/p
ss = sqrt(abs(1.0 - cs**2))
if(cs .eq. 0.0) then
return
endif
endif
endif
endif
if(cs .eq. 0.0) then
return
endif
t = abs(ss/cs)
y2 = dd*t
h0 = h0 + d2
y0 = y0 + y2
y = y0*100.0
h = h0*100.0
```

```
if(y .gt. eplugy) then
exit
endif
enddo
Eout = Elb
return
end
ccccccccccccccccccccccccccccccccccccccccccccccccccccccccccccc
subroutine Bfield2(z,Ein,cosLb,mm,Eout,cs,h0,h,y0,y,L)
implicit double precision(a-h,o-z)
parameter(n = 100)
double precision mm
c Add B field B = 1.4 T, use SI units
pie = 4.0*atan(1.0)
GevJ = 1.6E-10 ! 1 GeV = 1.6E-10 J
B0 = 1.4 !T
c B0 = B0*2.0/3.0
c Off B:
c B0 = 0.0
rad = 1.5 !m
g = z*3.29E-9 ! A.m
hn = 4.0 ! m, region of unconstant field
eplugx = 240.0 !cm, distance between interaction and
! the iron
eplugy = 41.38 !cm, the height cut by the iron
c cm -> m
Elb = Ein
```

```
Eout = Ein
h = h0
y = y0
cs = cosLb
sinLb = sqrt(abs(1.0-cs**2))
ss = sinLb
if(cs .eq. 0.0) then
return
endif
t = abs(ss/cs)
if(Ein .lt. mm) then
return
endif
h0 = h0/100.0
y0 = y0/100.0
Lh = 2.5 ! half length of the solenoid
dd = (hn - h0)/(1.0*n)
d2 = dd
hn0 = hn*100.0-dd*100.0
hneg = - hn0
p = sqrt(Elb**2-mm**2)
py = p*sinLb
up0 = Lh
down0 = sqrt(rad**2 + up0**2)
fact = 2.0*up0/down0
do while((h .le. hn0).and.(h.ge.hneg))
den1 = sqrt(rad**2 + (Lh - h0)**2)
```

```
den2 = sqrt(rad**2 + (Lh + h0)**2)
Bf = B0*((Lh-h0)/den1 + (Lh+h0)/den2)/fact
if((Bf .lt. 0.0).or.(Elb .le. mm)) then
return
endif
p = sqrt(Elb**2-mm**2)
if(p .lt. py) then
return
endif
px = sqrt(p**2 - py**2)
if((cs .le. 1.0).and.(cs.ge.0.0)) then
d2 = dd
Elb = Elb + g*Bf*d2/GevJ
if(Elb .le. mm) then
return
endif
p = sqrt(Elb**2-mm**2)
if(p .lt. py) then
return
endif
px = sqrt(p**2 - py**2)
cs = px/p
ss = sqrt(abs(1.0 - cs**2))
if(cs .eq. 0.0) then
return
endif
else
```

```
d2 = -dd
Elb = Elb + g*Bf*d2/GevJ
if(Elb .lt. mm) then
d2 = dd
Elb = Elb + g*Bf*d2/GevJ
p = sqrt(Elb**2-mm**2)
if(p .lt. py) then
Elb = sqrt(py**2 + mm**2) + g*Bf*d2/GevJ
p = sqrt(Elb**2-mm**2)
endif
px = sqrt(p**2 - py**2)
cs = px/p
ss = sqrt(abs(1.0 - cs**2))
if(cs .eq. 0.0) then
return
endif
else
p = sqrt(Elb**2-mm**2)
if(p .lt. py) then
d2 = dd
Elb = sqrt(py**2 + mm**2) + g*Bf*d2/GevJ
p = sqrt(Elb**2-mm**2)
px = sqrt(p**2 - py**2)
cs = px/p
ss = sqrt(abs(1.0 - cs**2))
if(cs .eq. 0.0) then
return
```

```
endif
else
px = -sqrt(p**2 - py**2)
cs = px/p
ss = sqrt(abs(1.0 - cs**2))
if(cs .eq. 0.0) then
return
endif
endif
endif
endif
t = abs(ss/cs)
y2 = dd*t
h0 = h0 + d2
y0 = y0 + y2
y = y0*100.0
h = h0*100.0
c m —> cm
if((abs(h) .lt. eplugx) .and. (y .gt. eplugy)) then
L = 0
exit
else
L = 1
endif
enddo
Eout = Elb
c print*,'End B2,cs,h,y,Eout',cs,h,y,Eout
```

```
return
end
ccccccccccccccccccccccccccccccccccccccccccccccccccccccccccccccccccc
ccccccccccccccccccccccccccccccccccccccccccccccccccccccccccccccccccc
subroutine rangePb(Rn,z,E,mm,s,Eout)
implicit double precision(a-h,o-z)
double precision Im,m,Na
double precision Ka,K1,K2,me,mm,Nc,Nmol
Im = 823.0E-9
m = 3.1608
Na = 82
hbo = 61.072E-9
x0 = 0.3776
x1 = 3.8073
R = 0.5 ! cm
Za = 0.39575 ! Z/A
den = 11.35 ! g/cm^3
call SolidPb(R,Rn,Eout,z,E,mm,s,Im,hbo,x0,x1,Na,m,den,Za)
return
end
ccccccccccccccccccccccccccccccccccccccccccccccccccccccccccccccccccc
ccccccccccccccccccccccccccccccccccccccccccccccccccccccccccccccccccc
double precision function Spb(z,Na,Ne,vf,kf,a,tm,t,y)
implicit double precision(a-h,o-z)
double precision Ne,kf,me,Na
a0 = 5.3E-9
pi = 4*atan(1.0)
```

```
x = 1.0/3.0
me = 0.51E-3
factor = z/2.0
c = 3.0E+10
ge = factor*1.97327E-14
ge = factor*1.054E-34/1.602E-19*c*1.0E-9 !GeV.cm
pp =0.0025
Spb = pp*4*pi*c*Ne*ge**2/(vf*me)*Log(50*a*tm*kf/t)*y
return
end
ccccccccccccccccccccccccccccccccccccccccccccccccccccc
double precision function g1(p0,p1,p2,p3,p4,p5,x)
implicit double precision(a-h,o-z)
g1=p0+p1*x+p2*x**2+p3*x**3+p4*x**4+p5*x**5
return
end
ccccccccccccccccccccccccccccccccccccccccccccccccccccc
subroutine SolidPb(R,Rn,E2,z,E12,mm,ss,Im,hbo,
* x0,x1,Na,m,den,Za)
implicit double precision(a-h,o-z)
double precision m,Ka,me,mm,Im,Nc,Ne,Na,Nmol
double precision K1,K2,Nav,kf
parameter (k=201,n=4,n1=240)
dimension f(k),w(k),v1(n),c1(n),v2(n1),c2(n1)
dimension ran(12),En(12)
vf = 1.82E+8
kf = 1.57E+8
```

```
an = 3.5E-8
tm = 600.7 !K
t = 300.0
do 10 i=1,k
f(i)=0.0
10 continue
factor = z/2.0
ge = factor*1.97327E-14 ! Gev.cm n = 1
me = 0.511E-3 ! mass of electron Gev
nn = k
hb = 6.582E-25 ! Gev s
pie = 4*atan(1.0)
Nav = 6.02E+23 ! Avogadro constant
C = -2.0*log(Im/hbo) -1.0
c ! number of electrons per
Ne = Nav*den*Za ! unit volume for gas
ccccccccccccccccccccccccccccccc
B1 = 0.248 ! Bloch correction, n = 1
B2 = 0.672 ! Bloch correction, n = 2
B3 = 1.022 ! Bloch correction, n = 3
B6 = 1.685 ! Bloch correction, n = 6
if(z .eq. 1.0) then
B = B1
else if(z .eq. 2.0) then
B = B2
else if(z .eq. 3.0) then
B = B3
```

```
else if(z .eq. 6.0) then
B = B6
endif
K1 = 0.406
K2 = 0.346
if(z .lt. 2.0) then
Ka = K1
else if(z .ge. 2.0) then
Ka = K2
endif
ccccccccccccccccccccccccc
A2 = Ka/2.0 - 0.5
aa = -(C + 4.606*x0)/(x1 - x0)**m
D1 = 0.0
ee = E12
delE = 0.0
del1 = R/(1.0*nn)
A = 4.0*pie*Ne*ge**2/(me)
dbeta = 1.0/(1.0*k)
do 50 i2=1,n
v1(i2) = 0.0
c1(i2) = 0.0
50 continue
beta3 = 0.00001+ 31*dbeta
ee3 = mm/sqrt(1.0-beta3**2)
A13 = Log(2*(ee3**2-mm**2)*me/(Im*mm**2))
X13 = Log10(sqrt(ee3**2-mm**2)/mm)
```

```
if(X13 .le. x0) then
A33 = D1
else if((X13 .gt. x0).and.(X13.lt.x1)) then
A33 = 4.606*X13+C+aa*(x1 - X13)**m
else if(X13 .ge. x1) then
A33 = 4.606*X13 + C
endif
beta4 = 0.00001+ 33*dbeta
ee4 = mm/sqrt(1.0-beta4**2)
A14 = Log(2*(ee4**2-mm**2)*me/(Im*mm**2))
X14 = Log10(sqrt(ee4**2-mm**2)/mm)
if(X14 .le. x0) then
A34 = D1
else if((X14 .gt. x0).and.(X14.lt.x1)) then
A34 = 4.606*X13+C+aa*(x1 - X14)**m
else if(X14 .ge. x1) then
A34 = 4.606*X14 + C
endif
v1(2) = 0.00001+ 3*dbeta
c1(2) = Spb(z,Na,Ne,vf,kf,a,tm,t,v1(1))
v1(3) = beta3
c1(3) = A*(A13 + A2 - A33/2 - B)/den
v1(1) = 0.00001+ 2*dbeta
c1(1) = Spb(z,Na,Ne,vf,kf,a,tm,t,v1(1))
v1(4) = beta4
c1(4) = A*(A14 + A2 - A34/2 - B)/den
v2(1) = v1(1)
```

```
v2(n1) = v1(n)
ccccccccccccccccccccccccc
if(z .eq. 1) then
p0 = -0.0056944
p1 = 18.626
p2 = -126.36
p3 = 854.06
p4 = -3025.8
p5 = 4023.5
endif
if(z .eq. 2) then
p0 = -0.040523
p1 = 80.057
p2 = -924.57
p3 = 7537.9
p4 = -27782.0
p5 = 37233.0
endif
if(z .eq. 3) then
p0 = -0.092833
p1 = 180.6
p2 = -2112.0
p3 = 17382.0
p4 = -64548.0
p5 = 87105.0
endif
if(z .eq. 6) then
```

```
p0 = -0.36885
p1 = 721.56
p2 = -8390.5
p3 = 68702.0
p4 = -253850.0
p5 = 340730.0
endif
ccccccccccccccccccccccccccccccccccccccccccccccc
Rn = 0.0
do 1 i = 1,nn
if(ee .le. mm) then
E2 = ee
exit
endif
beta = sqrt(abs(1-(mm/ee)**2))
A1 = Log(2*(ee**2-mm**2)*me/(Im*mm**2))
X = Log10(sqrt(ee**2-mm**2)/mm)
if(X .le. x0) then
A3 = D1
else if((X .gt. x0).and.(X.lt.x1)) then
A3 = 4.606*X+C+aa*(x1 - X)**m
else if(X .ge. x1) then
A3 = 4.606*X + C
endif
if(beta .lt. v1(1)) then
f(i) = Spb(z,Na,Ne,vf,kf,an,tm,t,beta)
else if(beta .gt. v1(4)) then
```

```
f(i) = A*(A1 + A2 - A3/2 - B)/den
else
f(i) = g1(p0,p1,p2,p3,p4,p5,beta)
endif
if(ss .eq. 0.0) then
exit
endif
delE = f(i)*del1*den/abs(ss)
ee = ee - delE
E2 = ee
if(E2 .le. mm) then
E2 = mm
exit
endif
Rn = Rn + del1*den/abs(ss)
1 continue
if(E2 .gt. mm) then
Rn = R*den/abs(ss)
endif
return
end
ccccccccccccccccccccccccccccccccccccccccccccccccccccccc
double precision function g(p0,p1,p2,p3,x)
implicit double precision(a-h,o-z)
g=p0+p1*x+p2*x**2+p3*x**3
return
end
```

```
ccccccccccccccccccccccccccccccccccccccccccccccccccccccccccccc
ccccccccccccccccccccccccccccccccccccccccccccccccccccccccccccc
subroutine lossSVX(Rn,E,z,E0,mm,s,cs,h,y)
implicit double precision(a-h,o-z)
double precision Im,m,Na
double precision Ka,K1,K2,me,mm,Nc,Nmol
h0 = 0.0
y0 = 0.0
Rn0 = 0.0
cs0 = 1.0
c Al :
Im = 164.0E-9
hbo = 32.86E-9
Na = 13
m = 3.6345
x0 = 0.1708
x1 = 3.0127
R0 = 0.0046 ! cm
Za = 0.48181 ! Z/A
den = 2.7 ! g/cm^3
L3 = 3
pi = 4.0*atan(1.0)
yy1 = 4.76
yy2 = 7.6
yy3 = 15.0
ty1 = 180.0 - yy1
ty2 = 180.0 - yy2
```

```
ty3 = 180.0 - yy3
xx = abs(acos(s))*180.0/pi
if(((xx.gt.yy2).and.(xx.lt.yy3)).or.
* ((xx.lt.ty2).and.(xx.gt.ty3))) then
R1 = 5.0
else
if((xx .gt. yy3) .or. (xx.lt.ty3)) then
R1 = 2.5
else
R1 = 0.0
endif
endif
R1 = R1*8.9/100.0 ! cm
call Solid(R1,Rn1,E1,z,E0,mm,s,Im,hbo,x0,x1,Na,m,den,Za,
* cs1,h1,y1,L3)
if(E1 .le. mm) then
E = E1
Rn = Rn1
h = h1
y = y1
cs = cs1
return
else
if((xx .lt. yy2) .or. (xx.gt.ty2)) then
R2 = 0.0
else
if(((xx.gt.yy2).and.(xx.lt.yy3)).or.
```

```
* ((xx.lt.ty2).and.(xx.gt.ty3))) then
R2 = 5.0
else
if((xx .gt. yy3) .or. (xx.lt.ty3)) then
R2 = 2.5
else
R2 = 0.0
endif
endif
endif
R2 = R2*42.5/100.0 !
Im = 74.0E-9
m = 3.3836
Na = 64
hbo = 23.086E-9
x0 = 0.1824
x1 = 2.6681
! cm
Za = 0.53937 ! Z/A
den = 0.075 ! g/cm^3
L4 = 4
call Solid(R2,Rn2,E2,z,E1,mm,cs1,Im,hbo,x0,x1,Na,m,den,Za,
* cs2,h2,y2,L4)
Rn2 = Rn2 + Rn1
h2 = h1 + h2
y2 = y1 + y2
if(E2 .le. mm) then
```

```
E = E2
Rn = Rn2
h = h2
y = y2
cs = cs2
return
else
Im1 = 173.0E-9
m1 = 3.2546
Na1 = 14
hbo1 = 31.055E-9
x10 = 0.2014
x11 = 2.8715
Za1 = 0.49848 ! Z/A
den1 = 2.33 ! g/cm^3
L5 = 5
yy4 = 7.0
ty4 = 180.0 - 7.0
if(((xx.gt.yy4).and.(xx.lt.yy3))
* .or.((xx.lt.ty4).and.(xx.gt.ty3))) then
R3 = 3.3
else
if((xx.gt.yy3).or.(xx.lt.ty3)) then
R3 = 2.0
else
R3 = 0.0
endif
```

```
endif
R3 = R3*9.36/100.0 !
call Solid(R3,Rn3,E3,z,E2,mm,cs2,Im,hbo,x0,x1,Na,m,den,Za
* ,cs3,h3,y3,L5)
Rn3 = Rn3 + Rn2
h3 = h2 + h3
y3 = y2 + y3
if(E3 .le. mm) then
E = E3
Rn = Rn3
h = h3
y = y3
cs = cs3
return
else
Im = 145.2E-9
m = 3.5458
Na = 50
hbo = 40.206E-9
x0 = 0.0402
x1 = 2.8665
! cm
Za = 0.49038 ! Z/A
den = 3.97 ! g/cm^3
L6 = 6
if((xx .lt. yy1) .or. (xx.gt.ty1)) then
R4 = 0.0
```

```
else
if(((xx.gt.yy1).and.(xx.lt.yy3)).or.
* ((xx.lt.ty1).and.(xx.gt.ty3))) then
R4 = 5.0
else
if((xx .gt. yy3) .or. (xx.lt.ty3)) then
R4 = 2.5
else
R4 = 0.0
endif
endif
endif
R4 = R4*4.85/100.0 !
call Solid(R4,Rn4,E4,z,E3,mm,cs3,Im,hbo,x0,x1,Na,m,den,Za
* ,cs,h,y,L6)
E = E4
Rn = Rn3 + Rn4
h = h3 + h
y = y3 + y
endif
endif
endif
return
end
ccccccccccccccccccccccccccccccccccccccccccccccccccccccccccccc
ccccccccccccccccccccccccccccccccccccccccccccccccccccccccccccc
subroutine lossVTPC(Rn,E,z,E0,mm,s,cs,h,y)
```

```
implicit double precision(a-h,o-z)
double precision Im,m,Na
double precision Ka,K1,K2,me,mm,Nc,Nmol
c C :
pi = 4.0*atan(1.0)
Im = 78.0E-9
m = 3.0036
Na = 6.0
hbo = 28.08E-9
x0 = -0.0351
x1 = 2.486
! cm
Za = 0.49954 ! Z/A
den = 2.00 ! g/cm^3
L2 = 2
y1 = 3.0
y2 = 16.0
ty1 = 180.0 - y1
ty2 = 180.0 - y2
xx = abs(acos(s))*180.0/pi
if((xx.gt.y1) .and.(xx.lt.y2)) then
R = -5.0*xx/9.0 + 10.0
else
if((xx.lt.ty1) .and.(xx.gt.ty2)) then
R = -5.0/9.0*(180.0-xx-18.0)
else
if((xx.gt.y2) .or.(xx.lt.ty2)) then
```

```
R = 1.0
else
R = 0.0
endif
endif
endif
R = R*18.8/100.0 ! cm
call Solid(R,Rn,E,z,E0,mm,s,Im,hbo,x0,x1,Na,m,den,Za
* ,cs,h,y,L2)
return
end
ccccccccccccccccccccccccccccccccccccccccccccccccccccccc
subroutine lossFTC(Rn,E,z,E0,mm,s,cs,h,y)
implicit double precision(a-h,o-z)
double precision Im,m,Na
double precision Ka,K1,K2,me,mm,Nc,Nmol
c Al :
c print*,'Start FTC,E0,s:',E0,s
Im = 164.0E-9
hbo = 32.86E-9
Na = 13
m = 3.6345
x0 = 0.1708
x1 = 3.0127
R0 = 0.0046 ! cm
Za = 0.48181 ! Z/A
den = 2.7 ! g/cm^3
```

```
L3 = 3
pi = 4.0*atan(1.0)
y1 = 3.0
y2 = 9.0
y3 = 10.0
y4 = 32.0
ty1 = 180.0 - y1
ty2 = 180.0 - y2
ty3 = 180.0 - y3
ty4 = 180.0 - y4
xx = abs(acos(s))*180.0/pi
if((xx.ge.y1) .and.(xx.lt.y2)) then
R = -0.87*xx + 13.05
else
if((xx.le.ty1) .and.(xx.gt.ty2)) then
R = -0.87*(180.0-xx - 13.05/0.87)
else
if((xx.ge.y2) .and.(xx.lt.y3)) then
R = 0.96*xx - 2.88
else
if((xx.le.ty2) .and.(xx.gt.ty3)) then
R = 0.96*(180.0 -xx - 2.88/0.96)
else
if((xx.ge.y3) .and.(xx.lt.y4)) then
R = -25.0*xx/38.0 + 25.0
else
if((xx.le.ty3) .and.(xx.gt.ty4)) then
```

```
R = -25.0/38.0*(180.0-xx - 25.0*38.0)
else
if((xx.gt.y4).or. (xx.lt.ty4)) then
R = 4.0
else
R = 0.0
endif
endif
endif
endif
endif
endif
endif
R = R*8.9/100.0 ! cm
call Solid(R,Rn,E,z,E0,mm,s,Im,hbo,x0,x1,Na,m,den,Za,
* cs,h,y,L3)
return
end
ccccccccccccccccccccccccccccccccccccccccccccccccccccccccc
subroutine coef(p0,p1,p2,p3,p4,p5,z,L)
implicit double precision(a-h,o-z)
c Be: L = 1
if(L .eq. 1) then
if(z .eq. 1) then
p0 = -0.013061
p1 = 48.961
p2 = -274.09
```

```
p3 = 816.48
p4 = -970.7
p5 = 51.719
endif
if(z .eq. 2) then
p0 = -0.071284
p1 = 201.8
p2 = -1540.5
p3 = 7508.0
p4 = -19489.0
p5 = 20486.0
endif
if(z .eq. 3) then
p0 = -0.19373
p1 = 464.49
p2 = -4256.6
p3 = 24646.0
p4 = -73435.0
p5 = 86288.0
endif
if(z .eq. 6) then
p0 = -1.0386
p1 = 1939.7
p2 = -23101.0
p3 = 157640.0
p4 = -515570.0
p5 = 640110.0
```

```
endif
endif
ccccccccccccccccccccccccccccccccc
c C: L = 2
if(L .eq. 2) then
if(z .eq. 1) then
p0 = -0.0095844
p1 = 47.881
p2 = -193.79
p3 = 99.217
p4 = 1629.9
p5 = -3362.8
endif
if(z .eq. 2) then
p0 = -0.059967
p1 = 198.28
p2 = -1280.2
p3 = 5247.9
p4 = -11455.0
p5 = 10107.0
endif
if(z .eq. 3) then
p0 = -0.17496
p1 = 458.68
p2 = -3830.2
p3 = 21286.0
p4 = -62369.0
```

```
p5 = 72771.0
endif
if(z .eq. 6) then
p0 = -0.99354
p1 = 1925.8
p2 = -22098.0
p3 = 151060.0
p4 = -497810.0
p5 = 623070.0
endif
endif
ccccccccccccccccccccccccccccccccccc
c Al: L = 3
if(L .eq. 3) then
if(z .eq. 1) then
p0 = -0.019902
p1 = 51.095
p2 = -434.65
p3 = 2409.7
p4 = -6997.5
p5 = 8094.0
endif
if(z .eq. 2) then
p0 = -0.10207
p1 = 211.4
p2 = -2265.2
p3 = 14833.0
```

```
p4 = -47697.0
p5 = 58728.0
endif
if(z .eq. 3) then
p0 = -0.26623
p1 = 487.12
p2 = -5962.6
p3 = 41854.0
p4 = -139530.0
p5 = 175630.0
endif
if(z .eq. 6) then
p0 = -1.3447
p1 = 2035.2
p2 = -30295.0
p3 = 229730.0
p4 = -791530.0
p5 = 1012800.0
endif
endif
ccccccccccccccccccccccccccc
c Al: L = 30, for the materials between Pb layers
if(L .eq. 30) then
if(z .eq. 1) then
p0 = -0.019902
p1 = 51.095
p2 = -434.65
```

```
p3 = 2409.7
p4 = -6997.5
p5 = 8094.0
endif
if(z .eq. 2) then
p0 = -0.10207
p1 = 211.4
p2 = -2265.2
p3 = 14833.0
p4 = -47697.0
p5 = 58728.0
endif
if(z .eq. 3) then
p0 = -0.26623
p1 = 487.12
p2 = -5962.6
p3 = 41854.0
p4 = -139530.0
p5 = 175630.0
endif
if(z .eq. 6) then
p0 = -1.3447
p1 = 2035.2
p2 = -30295.0
p3 = 229730.0
p4 = -791530.0
p5 = 1012800.0
```

```
endif
endif
ccccccccccccccccccccccccccc
c Rohacell: L = 4
if(L .eq. 4) then
if(z .eq. 1) then
p0 = -0.0051014
p1 = 46.487
p2 = -90.012
p3 = -842.03
p4 = 5022.7
p5 = -7757.2
endif
if(z .eq. 2) then
p0 = -0.04405
p1 = 193.34
p2 = -913.3
p3 = 2021.0
p4 = -272.33
p5 = -3693.0
endif
if(z .eq. 3) then
p0 = -0.13767
p1 = 447.08
p2 = -2962.3
p3 = 13110.0
p4 = -31695.0
```

```
p5 = 31506.0
endif
if(z .eq. 6) then
p0 = -0.87904
p1 = 1890.3
p2 = -19453.0
p3 = 127370.0
p4 = -412720.0
p5 = 512980.0
endif
endif
ccccccccccccccccccccccccccc
c Si, L = 5
if(L .eq. 5) then
if(z .eq. 1) then
p0 = -0.019441
p1 = 50.953
p2 = -424.52
p3 = 2353.1
p4 = -6889.8
p5 = 8052.7
endif
if(z .eq. 2) then
p0 = -0.10017
p1 = 210.82
p2 = -2223.2
p3 = 14577.0
```

```
p4 = -47248.0
p5 = 58843.0
endif
if(z .eq. 3) then
p0 = -0.26327
p1 = 486.21
p2 = -5897.3
p3 = 41453.0
p4 = -138500.0
p5 = 174630.0
endif
if(z .eq. 6) then
p0 = -1.3413
p1 = 2034.2
p2 = -30229.0
p3 = 229880.0
p4 = -793290.0
p5 = 1015500.0
endif
endif
ccccccccccccccccccccccccccc
c AL2O3: L = 6
if(L .eq. 6) then
if(z .eq. 1) then
p0 = -0.018152
p1 = 50.552
p2 = -394.4
```

p3 = 2062.0

p4 = -5818.8

p5 = 6661.3

endif

if(z .eq. 2) then

p0 = -0.08505

p1 = 206.05

p2 = -1851.1

p3 = 9792.3

p4 = -24094.0

p5 = 20191.0

endif

if(z .eq. 3) then

p0 = -0.24994

p1 = 482.06

p2 = -5585.2

p3 = 38404.0

p4 = -127130.0

p5 = 59670.0

endif

if(z .eq. 6) then

p0 = -1.2785

p1 = 2014.6

p2 = -28752.0

p3 = 214980.0

p4 = -735790.0

p5 = 37090.0

```
endif
endif
c G10, L = 7
if(L .eq. 7) then
if(z .eq. 1.0) then
p0 = -0.016676
p1 = 50.091
p2 = -359.77
p3 = 1719.2
p4 = -4487.7
p5 = 4826.4
endif
if(z .eq. 2.0) then
p0 = -0.08908
p1 = 207.36
p2 = -1963.2
p3 = 12013.0
p4 = -37450.0
p5 = 45579.0
endif
if(z .eq. 3.0) then
p0 = -0.23877
p1 = 478.58
p2 = -5323.9
p3 = 35868.0
p4 = -117450.0
p5 = 146520.0
```

```
endif
if(z .eq. 6.0) then
p0 = -1.2492
p1 = 2005.5
p2 = -28084.0
p3 = 209520.0
p4 = -718780.0
p5 = 919110.0
endif
endif
return
end
ccccccccccccccccccccccccccccccccccccccccccccccccccc
ccccccccccccccccccccccccccccccccccccccccccccccccccc
ccccccccccccccccccccccccccccccccccccccccccccccccccccccccccccccccccccccccccccccccc
subroutine prot(x,q2,db,ub,u,d,s)
c PDF5(-2),PDF5(-1),PDF5(1),PDF5(2),PDF5(3)
C=============================================================
C Trivial test program for CTEQ PDFs: Fred Olness 6/20/96
C
C Revised 12 March 1999 by Randall J. Scalise (scalise@phys.psu.edu)
C for CTEQ5
C=============================================================
Implicit Double Precision (A-H, O-Z)
Dimension PDF5 (-5:5)
DATA ISET, Q /1,10./
ISET = 1
```

```
Q = sqrt(q2)
c print *, 'DBAR , UBAR , U , D, S'
Call SetCtq5(Iset)
DO 11 Iparton=-5,5
PDF5(Iparton) = Ctq5Pdf (Iparton, X, Q)
11 CONTINUE
DO 21 Iparton=3,5
If(PDF5(Iparton) .ne. PDF5(-Iparton))
> Write(6,*) ' Error: Sea not symmetric. iparton= ',iparton
21 CONTINUE
db = PDF5(-2)
ub = PDF5(-1)
u = PDF5(1)
d = PDF5(2)
s = PDF5(3)
return
END
c=============================================================================
Function Ctq5Pdf (Iparton, X, Q)
Implicit Double Precision (A-H,O-Z)
Logical Warn
Common
> / CtqPar2 / Nx, Nt, NfMx
> / QCDtable / Alambda, Nfl, Iorder
Data Warn /.true./
save Warn
If (X .lt. 0D0 .or. X .gt. 1D0) Then
```

```
Print *, 'X out of range in Ctq5Pdf: ', X
Stop
Endif
If (Q .lt. Alambda) Then
Print *, 'Q out of range in Ctq5Pdf: ', Q
Stop
Endif
If ((Iparton .lt. -NfMx .or. Iparton .gt. NfMx) .or.
* (Iparton .eq. 0 .and. NfMx .eq. 0)) Then
If (Warn) Then
C put a warning for calling extra flavor.
Warn = .false.
Print *, 'Warning: Iparton out of range in Ctq5Pdf: '
> , Iparton
Endif
Ctq5Pdf = 0D0
Return
Endif
Ctq5Pdf = PartonX (Iparton, X, Q)
if(Ctq5Pdf.lt.0.D0) Ctq5Pdf = 0.D0
Return
End
ccccccccccccccccccccccccccccccccccccccccccccccccccccccccccc
FUNCTION PartonX (IPRTN, X, Q)
C
C Given the parton distribution function in the array Upd in
C COMMON / CtqPar1 / , this routine fetches u(fl, x, q) at any value of
```

```
C x and q using Mth-order polynomial interpolation for x and Ln(Q/Lambda).
C
IMPLICIT DOUBLE PRECISION (A-H, O-Z)
C
PARAMETER (MXX = 105, MXQ = 25, MXF = 6)
PARAMETER (MXPQX = (MXF *2 +2) * MXQ * MXX)
PARAMETER (M= 2, M1 = M + 1)
C
Logical First
Common
> / CtqPar1 / Al, XV(0:MXX), QL(0:MXQ), UPD(MXPQX)
> / CtqPar2 / Nx, Nt, NfMx
> / XQrange / Qini, Qmax, Xmin
C
Dimension Fq(M1), Df(M1)
Data First /.true./
save First
C Work with Log (Q)
QG = LOG (Q/AL)
C Find lower end of interval containing X
JL = -1
JU = Nx+1
11 If (JU-JL .GT. 1) Then
JM = (JU+JL) / 2
If (X .GT. XV(JM)) Then
JL = JM
Else
```

```
JU = JM
Endif
Goto 11
Endif
Jx = JL - (M-1)/2
If (X .lt. Xmin .and. First ) Then
First = .false.
Print '(A, 2(1pE12.4))',
> ' WARNING: X << Xmin, extrapolation used; X, Xmin =', X, Xmin
If (Jx .LT. 0) Jx = 0
Elseif (Jx .GT. Nx-M) Then
Jx = Nx - M
Endif
C Find the interval where Q lies
JL = -1
JU = NT+1
12 If (JU-JL .GT. 1) Then
JM = (JU+JL) / 2
If (QG .GT. QL(JM)) Then
JL = JM
Else
JU = JM
Endif
Goto 12
Endif
Jq = JL - (M-1)/2
If (Jq .LT. 0) Then
```

```
Jq = 0
If (Q .lt. Qini) Print '(A, 2(1pE12.4))',
> ' WARNING: Q << Qini, extrapolation used; Q, Qini =', Q, Qini
Elseif (Jq .GT. Nt-M) Then
Jq = Nt - M
If (Q .gt. Qmax) Print '(A, 2(1pE12.4))',
> ' WARNING: Q > Qmax, extrapolation used; Q, Qmax =', Q, Qmax
Endif
If (Iprtn .GE. 3) Then
Ip = - Iprtn
Else
Ip = Iprtn
EndIf
C Find the off-set in the linear array Upd
JFL = Ip + NfMx
J0 = (JFL * (NT+1) + Jq) * (NX+1) + Jx
C
C Now interpolate in x for M1 Q's
Do 21 Iq = 1, M1
J1 = J0 + (Nx+1)*(Iq-1) + 1
Call Polint (XV(Jx), Upd(J1), M1, X, Fq(Iq), Df(Iq))
21 Continue
C Finish off by interpolating in Q
Call Polint (QL(Jq), Fq(1), M1, QG, Ftmp, Ddf)
PartonX = Ftmp
C
RETURN
```

```
C ****************************
END
Subroutine SetCtq5 (Iset)
Implicit Double Precision (A-H,O-Z)
Parameter (Isetmax=9)
Character Flnm(Isetmax)*12, Tablefile*40
Data (Flnm(I), I=1,Isetmax)
> / 'cteq5m.tbl', 'cteq5d.tbl', 'cteq5l.tbl', 'cteq5hj.tbl'
> , 'cteq5hq.tbl', 'cteq5f3.tbl', 'cteq5f4.tbl'
> , 'cteq5m1.tbl', 'ctq5hq1.tbl' /
Data Tablefile / 'test.tbl' /
Data Isetold, Isetmin, Isettest / -987, 1, 911 /
save
C If data file not initialized, do so.
If(Iset.ne.Isetold) then
IU= NextUn()
If (Iset .eq. Isettest) then
Print* ,'Opening ', Tablefile
21 Open(IU, File=Tablefile, Status='OLD', Err=101)
GoTo 22
101 Print*, Tablefile, ' cannot be opened '
Print*, 'Please input the .tbl file:'
Read (*,'(A)') Tablefile
Goto 21
22 Continue
ElseIf (Iset.lt.Isetmin .or. Iset.gt.Isetmax) Then
Print *, 'Invalid Iset number in SetCtq5 :', Iset
```

```
Stop
Else
Tablefile=Flnm(Iset)
Open(IU, File=Tablefile, Status='OLD', Err=100)
Endif
Call ReadTbl (IU)
Close (IU)
Isetold=Iset
Endif
Return
100 Print *, ' Data file ', Tablefile, ' cannot be opened '
>//'in SetCtq5!!'
Stop
C ********************
End
Subroutine ReadTbl (Nu)
Implicit Double Precision (A-H,O-Z)
Character Line*80
PARAMETER (MXX = 105, MXQ = 25, MXF = 6)
PARAMETER (MXPQX = (MXF *2 +2) * MXQ * MXX)
Common
> / CtqPar1 / Al, XV(0:MXX), QL(0:MXQ), UPD(MXPQX)
> / CtqPar2 / Nx, Nt, NfMx
> / XQrange / Qini, Qmax, Xmin
> / QCDtable / Alambda, Nfl, Iorder
> / Masstbl / Amass(6)
Read (Nu, '(A)') Line
```

```
Read (Nu, '(A)') Line
Read (Nu, *) Dr, Fl, Al, (Amass(I),I=1,6)
Iorder = Nint(Dr)
Nfl = Nint(Fl)
Alambda = Al
Read (Nu, '(A)') Line
Read (Nu, *) NX, NT, NfMx
Read (Nu, '(A)') Line
Read (Nu, *) QINI, QMAX, (QL(I), I =0, NT)
Read (Nu, '(A)') Line
Read (Nu, *) XMIN, (XV(I), I =0, NX)
Do 11 Iq = 0, NT
QL(Iq) = Log (QL(Iq) /Al)
11 Continue
C
C Since quark = anti-quark for nfl>2 at this stage,
C we Read out only the non-redundent data points
C No of flavors = NfMx (sea) + 1 (gluon) + 2 (valence)
Nblk = (NX+1) * (NT+1)
Npts = Nblk * (NfMx+3)
Read (Nu, '(A)') Line
Read (Nu, *, IOSTAT=IRET) (UPD(I), I=1,Npts)
Return
C ****************************
End
Function NextUn()
C Returns an unallocated FORTRAN i/o unit.
```

```
Logical EX
C
Do 10 N = 10, 300
INQUIRE (UNIT=N, OPENED=EX)
If (.NOT. EX) then
NextUn = N
Return
Endif
10 Continue
Stop ' There is no available I/O unit. '
C ************************
End
SUBROUTINE POLINT (XA,YA,N,X,Y,DY)
IMPLICIT DOUBLE PRECISION (A-H, O-Z)
C Adapted from "Numerical Recipes"
PARAMETER (NMAX=10)
DIMENSION XA(N),YA(N),C(NMAX),D(NMAX)
NS=1
DIF=ABS(X-XA(1))
DO 11 I=1,N
DIFT=ABS(X-XA(I))
IF (DIFT.LT.DIF) THEN
NS=I
DIF=DIFT
ENDIF
C(I)=YA(I)
D(I)=YA(I)
```

```
11 CONTINUE
Y=YA(NS)
NS=NS-1
DO 13 M=1,N-1
DO 12 I=1,N-M
HO=XA(I)-X
HP=XA(I+M)-X
W=C(I+1)-D(I)
DEN=HO-HP
IF(DEN.EQ.0.) PAUSE
DEN=W/DEN
D(I)=HP*DEN
C(I)=HO*DEN
12 CONTINUE
IF (2*NS.LT.N-M)THEN
DY=C(NS+1)
ELSE
DY=D(NS)
NS=NS-1
ENDIF
Y=Y+DY
13 CONTINUE
RETURN
ENd
ccccccccccccccccccccccccccccccccccccccccccccccccccccccccccc
```